STUDY OF INHOMOGENEITIES IN THE SOLAR ATMOSPHERE

By
R. KARIYAPPA

DECLARATION

I hereby declare that the matter contained in this thesis is the result of the investigations carried out by me in the Indian Institute of Astrophysics, Bangalore and The Department of Physics, Bangalore University, Bangalore, under the supervision of Prof. K. R. Sivaraman and Dr. M. N. Anandaram. This work has not been submitted for the award of any Degree, Diploma, Associateship, Fellowship, etc. of any university or Institute.

(R. KARIYAPPA)

Candidate
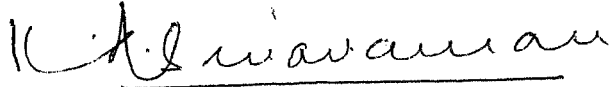
(K. R. Sivaraman)

Supervisor

(M. N. Anandaram)

Supervisor

Bangalore-34

Feb. 19 , 1992

To

my beloved Parents

and Teachers

Acknowledgements

I owe an immense debt of gratitude to Prof. K. R. Sivaraman, who initiated me into the study of the Solar Physics. It was his deep interest and direction that have made this investigation possible at all. The inspiration and the emphasis he provided, are behind every aspect of the work connected with this investigation. Without his willingness and great patience in going over the manuscript, this thesis would not be readable. Also I am extremely grateful to Dr. M. N. Anandaram for the invaluable guidence and help rendered for the successful completion of the thesis.

The data that I have used for this study were obtained by Prof. K. R. Sivaraman and Dr. J. Beckers at the Vacuum Tower Telescope (VTT) of the Sacramento Peak Observatory, New Mexico. I am extremely thankful to them and to the Sacramento Peak Observatory for allowing me to use this data for this study.

I am grateful to Prof. J. C. Bhattacharyya for his kind encouragement and support. I thankfully acknowledge the keen interests shown by Prof. N. G. Puttaswamy and Prof. K. H. Chennappa in the progress of the work.

I am indebted to Prof. W. Kalkofen and Prof. Vinod Kishan for their stimulating discussions. I have great pleasure in expressing my sincere thanks to Mr. Baba Verghese for helping me at various stages during the reduction of the data at the computer even at the late evenings. Dr. A. V. Raveendran is allowed me to use his FFT program and I am grateful to him for his kind help.

I am extremely thankful to Dr. R. Srinivasan, Prof. R. Rajamohan and Prof. Ramasagar for their kind help in allotting the PDS scanning time. I am thankful to Mr. S. S. Gupta for his kind help at the PDS while scanning the first few frames of the sequence. Also my grateful thanks are due to Mr. Ramaswamy and Mrs. S. Savithri for their help while scanning the spectra at the PDS. I am thankful to Mrs. K. Padmavathi for her help in editing the first draft of the thesis. I am thankful to

iv

SUMMARY

It has been recognised that the two resonance lines of singly ionized calcium viz. the H and K lines (3968A and 3934A) can be used as the most reliable diagnostic indicators in the visible region of the spectrum to identify regions of chromospheric activity in the solar atmosphere. Since then they have been used extensively as a tool to study both the spatial and dynamical properties of the inhomogeneities in the solar chromosphere. Among the chromospheric inhomogeneities, the network, the bright points and the regions in between them characterize the quiet solar chromosphere. These regions are seen in emission and they have a one to one correspondence with the underlying photospheric magnetic fields.

In this thesis work a study of the dynamical evolution of the CaII H line profiles both at the sites of the arc sec structures namely the bright points and the network boundary regions and the main role of 3-min oscillations in the heating of the quiet solar chromosphere has been made. The basic data for this study is the time series spectra of 35 minute duration in the CaII H line. This sequence spectra was obtained at the Vacuum Tower Telescope (VTT) of the Sacramento Peak Observatory,New Mexico on September 13, 1971 under exceptionally good seeing conditions, on a quiet region around the centre of the solar disc. The spectra are of high spatial, spectral and temporal resolution.

Chapter I contains a general introduction to the field ,a summary of the earlier work in the area relevant to this thesis and the main problems that remain unresolved.

Chapter II describes briefly the telescope and the echelle spectrograph and the observations obtained with these. The procedure adopted for the reduction of this data are also described.

In Chapter III, results of this study of the dynamical evolution of the bright points has been presented. It is found that the seemingly large variety of profiles describing the evolution of the many bright points can be broadly classified into three classes. This classification (class I, class II and class III) was done on the basis of the light curves of the bright points during the 35-minute duration of the time sequence. The most striking feature of all these light curves is that there is a strong pulse (designated here as the "Main Impulse") which is followed by 8-10 smaller pulses decreasing in their brightness exponentially. In class II and class III the number of follower pulses are 4-6. The period of the brightness oscillations is 190 $^+_-$10 sec sec in all the three classes and thus seems to be independent of the brightness enhancement. The period of the main impulse and the follower pulses are same. It is hypothesised that the magnitudes of the enhancements in brightness of the main impulses of each of the 3 classes are closely related with magnetic field associated with the bright point location.

The intensity oscillations at the network boundary regions was studied. The network boundary regions exhibit oscillations of longer periods of the order of 5-7 minutes. Thus the network boundaries also exhibit intensity oscillations but unlike the bright points have longer periods. This itself could be taken as an evidence to argue that the mechanism of heating in the two cases are dissimilar.

The properties of the main impulses and their follower pulses and the energy budget required to heat the chromosphere are discussed in

Chapter IV. The total energy contained in the bright points over the sun is estimated. This energy flux together with that contributed by the network regions $(3.46 \times 10^7 \text{ergs/cm}^2/\text{sec})$ match well with the energy estimated by Anderson and Athay , 1981 as $3.8 \times 10^7 \text{ergs/cm}^2/\text{sec}$. Thus the bright points are the sites where substantial heating takes place and the main impulses transport this energy. It is concluded that inside the class I bright point where the magnetic fields are high the energy propagation is by a combination of Alfven' and acoustic waves with a predominance of the Alfven' wave whereas when the magnetic fields become weaker (as in class II and particularly class III bright points) the propagation is mainly by acoustic waves.

The results and the conclusions of the study are summarized in Chapter V.

CONTENTS

LIST OF FIGURES

xii

CHAPTER I

INTRODUCTION

The solar limb presents a colourful view ("chromosphere" or the "coloured sphere") for a few seconds immediately following the second contact and before the third contact during a total solar eclipse. The spectrograph reveals the "flash spectrum" which shows a large number of the lines in emission which are otherwise seen as absorption lines in the normal solar spectrum. The most prominent of these emission lines are the H_α line ($\lambda 6563 \text{Å}$) and the CaII H & K lines ($\lambda 3968 \text{Å}$ and $\lambda 3934 \text{Å}$ respectively) which extend over several scale heights. These lines are seen in emission because at their frequencies the solar atmosphere is still opaque at a level where, even for a tangential line of sight, it is transparent in the continuum. The flash spectrum of the chromosphere was first observed during the total solar eclipse in 1870 by C.A.Young (Mitchell,1935). From then on many astronomers have organized expeditions to hunt for the very brief but most exciting moments of the total solar eclipses travelling to remote and uninhabited corners of the world. In spite of many odds, flash spectra have been obtained at many eclipses and these contain a wealth of information pertaining to the solar chromosphere. A very good example is the comprehensive analysis of the flash spectrum obtained during the eclipse on February 25,1952 observed at Khartoum (Athay 1963). This exhaustive study of the excellent spectra of the chromosphere opened up a new era in the physics of the chromosphere and following this, models of the chromosphere based on observations became available for the first time. The steep temperature rise in the chromosphere and the

1

consequent abnormal increase in the scale height became clear from their studies. This increase in the temperature was explained as the result of the non-radiative heating and this led to the concept of the non-LTE in the solar and stellar atmospheres. Since then, one of the important aspects of study has been to identify the precise mechanism of heating, the source of energy for this heating and mode of propagation of energy in the chromosphere.

Biermann(1946, 1948) and Schwarzchild (1948) suggested that the acoustic waves generated by the granulation provide the heat input for the upper chromosphere and the corona. Schatzman (1949) showed that the amplitudes of these waves steadily increase as the waves propagate upward through regions of decreasing density, ultimately forming a sequence of shock waves. The outer solar atmosphere is heated by the dissipation of the shock waves. In the earlier investigations of Biermann and Schwarzchild, the computed energy brought up by the granules was far in excess of the amount required for maintaining the temperature of the corona. Subsequent work has shown that, only a small part of the turbulent energy, which is later converted into acoustic energy, escapes dissipation as heat at the source itself. Lighthill (1952, 1954) developed a theory of the aerodynamic generation of acoustic noise by isotropic turbulence, in a compressible medium. The turbulent regions act as sources of sound, radiating like a quadrupole. Proudman (1952) derived a numerical expression for the acoustic power so generated. The uppermost layers of the convection zone, confined to a thickness of about 60 km characterised by high

Reynolds number, are supposed to be the source of flux of acoustic energy. Lighthill's theory has been applied to this turbulent zone by many workers like de Jager and Kuperus (1961), Osterbrock (1961), Moore and Spiegel (1964), Kuperus (1965), to derive an order of magnitude for the acoustic flux, which approximately balances the energy necessary for the coronal heating.

Under the combined influence of gravitational forces and a magnetic field, three modes of wave propagation are possible in a compressible medium:

i) Ordinary sound waves controlled by compressibility, can propagate in all directions.

ii) Internal gravity waves, also play a vital role in the transport of mechanical energy in the photosphere and chromosphere. Lighthill (1967) has shown that these waves generated in the stable layers above the convection zone, by 'tongues of turbulence' penetrate into the stable layers above. Whitaker (1963) has worked out the propagation and dissipation of these waves.

iii) The Alfven's waves, which propagate along the magnetic lines of force.

Osterbrock (1961) and Lighthill (1967) following Alfven considered the propagation in the presence of a magnetic field, consisting of the fast, slow, and Alfven-mode magnetohydrodynamic waves. The fast-mode disturbances generated in the hydrogen convection zone are sound waves to a good approximation. These travel through the photosphere and their dissipation is the main source of chromospheric heating, while the corona is heated by Alfven waves.

~~the wave generation in the convection zone is larger leading to more heating.~~

In the photosphere, the five minute oscillations are believed to be the visible manifestation of these mechanical waves. There have been several detailed investigations trying to study the various properties of the five minute oscillations in the photosphere and the energy they transport upwards into the chromosphere and the corona (Evans and Michard 1962;Leighton, Noyes and Simon 1962 ; Edmonds et al 1965 ; and Sivaraman 1973). Studies by Evans and Michard (1962), and Noyes and Leighton (1963) brought out many of the properties of the five-minute oscillations, leading to a flurry of theoretical investigations of wave propagation in compressible gravitational atmospheres and their main role in transporting the mechanical energy to heat the higher layers in the solar atmosphere. In particular, Simon and Leighton (1964) established the relationships between supergranulation , the photospheric magnetic fields and the chromospheric network. Their work laid the foundation for subsequent investigations of the structuring of photospheric magnetic fields by convection and of the chromospheric and coronal heating and the dynamics associated with them in the presence of inhomogeneous magnetic fields.

This thesis work, concentrates on the study of the role of fine structures in the quiet regions in the heating of the solar chromosphere. The chromosphere can be viewed against the solar disc in

4

the strong Fraunhofer lines, UV lines, and millimeter and centimeter radio emission. However, UV lines are not observable with ground-based telescopes and the spatial resolution obtainable presently with radio telescopes is not high enough for studying the fine structures. The strong Fraunhofer lines, such as the NaI D lines, the MgI b group and the CaII infrared triplets are formed just above the temperature minimum which corresponds to the lower chromosphere. For the observation of the middle and higher chromosphere one generally chooses H_α or the CaII H and K lines. A monochromatic picture of the chromosphere on the solar disk is obtained by using a polarising filter or spectroheliograph with the passband centered on the core of one of these lines. The spectroheliograms obtained in some of the strong lines (H_α , CaII H and K , Mg b_1 etc.) show a wealth of details and have been the subject of study of both quiet and active chromospheres since the time of Hale and Ellerman (1904) and D'Azambuja (1930). In recent times high quality spectroheliograms have been obtained by Alan Title et al. (1966). From the studies over the years from examination of the spectroheliograms it has been recognised that the two resonance lines of singly ionized calcium viz. the H and K lines (3968Å and 3934Å) could be used as the most reliable diagnostic indicators in the visible region of the spectrum to identify regions of chromospheric activity on the solar surface. Since then they have been used extensively as a tool to study both the spatial and dynamical properties of the inhomogeneities in the solar chromosphere.

A two dimensional scan of the sun in the H or the K line reveal the following chromospheric features (inhomogeneities) in emission:

i. plages, which are most conspicuous by virtue of the emission that far exceed the emission from other features and represent the active regions on the sun,

ii. the network which are cospatial with the supergranular cells in the underlying photospheric levels,

iii. the bright points (of the dimensions of 1-2 arc sec.) that populate the interior of the network. These are named as 'minute bright calcium flocculi' by Hale and Ellerman (1904) to distinguish them from the coarser flocculi. Beckers (1968) has designated them as 'grains'. From their apparent roundish shape and their occurrence inside the cell, Leighton (1961), Bappu and Sivaraman (1971) and Liu (1974) have used the term 'cell points' or 'bright points' to describe these features. These are most conspicuous in H_{2v} emission peak and so are also referred to as 'H_2 grains' and

iv. the regions in between the bright points within the network which form the unresolved 'truly quiet chromosphere' and which show up in weak emission and the dark condensations (Bappu and Sivaraman ,1971).

Among these chromospheric inhomogeneities, the network, the bright points and the regions inbetween them characterize the quiet solar chromosphere. Babcock and Babcock(1955) noticed for the first time that the regions of excess emission in the K-line spectroheliograms namely the plages, showed a one to one correspondence with regions of enhanced magnetic fields (active regions) at the photosphere. This was put on a firm basis by Leighton and his co workers (Leighton ,Noyes and

6

Simon, 1962) from their detailed study using the photospheric subtraction technique developed by them. A similar correlation was established in quantitative terms for the network boundaries by Skumanich et al (1975) and for the bright points that populate the interior of the network by Sivaraman and Livingston (1982). Thus the correlation between regions of excess emission in the K or H line with regions of excess magnetic fields at the photospheric level seems to hold good for the full range of size scale ranging from extensive plage regions to sub arc sec features such as the bright points . This has naturally led to the interpretation that non-radiative heating seen as excess emission occurs only in regions associated with magnetic fields, irrespective of the size of the chromospheric structures.

The K line (or H line) profiles exhibit variety of forms and shapes corresponding to the various inhomogeneities in the chromosphere. A detailed study of the spatial variation in the K line profiles over plages was done by Smith (1960) and over the network boundaries and the bright points by Bappu and Sivaraman (1971). Among the earliest studies using time sequence spectra to look for intensity oscillations in the chromosphere corresponding to the 5-min oscillations in the photosphere are those by Jensen and Orrall (1963) and Orrall (1966). They identified for the first time the oscillatory nature of the K line variability. Orrall (1966) noticed that the velocity fluctuations observed in K_3 core are oscillatory. By power spectral analysis he showed that this period is around 180 sec. He also measured the period of the velocity oscillations in K_3 using the

7

brightness of K_2 as the guiding factor. Thus for regions where K_2 was faint (weak emission in the violet peak, K_{2v}) the period of oscillations ranged from 180 to 400 sec; and in regions where K_2 was bright (strong K_{2v} emission) the period of the oscillations extended up to 600 sec. He postulated a significant positive correlation between the period of velocity oscillations in K_3 and the K_{2v} intensity. Also Jensen and Orrall (1963) noticed the phase lag in the intensity of the K line wings with reference to the neighbouring FeI lines and interpreted this as an indication of an upward-transport of energy by these oscillations. About ten years later a major progress in this field was made by Punetha (1974) ,Liu (1974) and Cram and Dame (1983). Punetha and Liu independently observed the K line at high spatial and temporal resolution in quiet regions around the centre of the solar disk. The intensity perturbations first visible in the far line wings were seen to travel towards the line core in the course of a tens of seconds. These occured at the sites of the bright points in the interior of the network. Liu observed that there was a time lag between the intensity enhancement maxima at the K_2 and K_1 levels which he interpreted as an evidence for an upward-propagating disturbance causing local heating in the chromosphere. Cram and Dame (1983) with their high spatial and temporal resolution spectra in the CaII H line, studied the dynamical evolution of the H line profiles at the sites of the bright points. The dynamical event of the passage of the impulse is seen as the waxing and waning in brightness of bright point in a sinusoidal fashion and takes nearly 180 seconds. A series of such events following one after the other due to the passage of the impulses

give rise to the impression of a 3-minute (180sec) oscillation in brightness. Cram and Dame (1983) confirmed the findings of Liu (1974) that the three-minute chromospheric oscillation is the visible manifestation of the upward-propagating excitation and suggested that the three-minute oscillations are responsible for the heating of the quiet chromosphere at the sites of the bright points. Also they suggested that the extra radiative emission loss they saw from the chromospheric fine structures, when averaged over space and time, compared with the H line emission in the empirical model of the average chromosphere, Vernazza, Avrett and Loeser(1981):VAL model C. Finally they concluded that the heating of the layers in the H line level is consistent with the heating by the long period acoustic waves. Although these observational work provides an overall understanding of the heating mechanism , some of the important questions which remain unanswered are:

i.   Do all bright points behave in the same way when the impulses pass through them ?

ii.   Do the brightness enhancement occur in a random fashion or whether there is any organisation in their behaviour ?

iii.   Is there any spatial and temporal coherence in their behaviour?

iv.   What is the role of the magnetic fields in this dynamical process ?

v.   What is the physical nature of the impulse and the nature of wave that carries the energy and dissipate at the chromospheric level?

In this thesis work, an attempt has been made to answer these questions.

Parallely there have been attempts made to understand the mechanism of heating of the solar chromosphere and several scenarios are available in the literature. In a highly turbulent convection zone the physical arguments suggested that the period of the waves is of the order of the time scale of the turbulent motions. The power spectrum of this kind of a system shows a broad noise spectrum with time scales ranging from short periods (less than a minute), the time required for sound waves to travel the distance of one scale height in the upper convection zone, to eight minutes, the life time of a typical granule. The wave generation theory suggested that the power spectrum of acoustic waves, which are generated in the hydrogen convection zone grows linearly at the acoustic cutoff period from zero towards shorter periods and attains a high value below one minute (Stein 1967, 1968 and Stein and Leibacher 1981). The wave propagation theory in a linear system (Bray and Loughhead 1974, and Priest 1982)showed that if the period of the acoustic waves is below the cutoff, which is equal to 3-min in the lower chromosphere, the acoustic waves may travel in the vertical direction. If the period of the acoustic waves is less than the cutoff period, then the waves travel with a speed equal to the sound speed. When the period of the acoustic waves is greater than the cutoff period, the waves are evanescent or not propagating. Thus, the acoustic waves can transport mechanical energy from the convection zone into the chromosphere, only if the period is less than the acoustic

10

cutoff period which is 3-min. The heating of the solar chromosphere has been discussed and reviewed by many workers (e.g. Kuperus 1969; Ulmschneider 1986, 1989; Athay 1985; Kalkofen 1989). Kalkofen (1989a, 1989b) has brought together all the facts known so far (both observational and theoretical) and has argued that the inner network bright points are the sites where major chromospheric heating takes place and that the heating is by long period acoustic waves. These bright points have magnetic fields associated with them and so can be considered as flux tubes. Although these earlier attempts provide an overall understanding of the phenomena, many details of the physical processes remain unclear and some of them are listed below:

i. Are these waves purely compressional in nature ?

ii. Do all the bright points have magnetic fields associated with them?

iii. If these are different for different bright points are these not reflected in the nature of the wave propagation ? or

iv. Is it that the magnetic fields have no influence at all in the wave propagation ?

v. Are there periods other than the 3-min for the propagating waves ?

The present study was undertaken with the goal of understanding the dynamical processes associated with the bright points and the network regions using high quality observations which would answer some of these questions.

In Chapter II, the methods of observations and the reductions of the data have been described.

11

In Chapter III, the following aspects have been studied and discussed in great detail:

i. The possible classification based on the evolution of the bright points.

ii. The plausible relation between these classifications of the bright points and the photospheric magnetic fields.

iii. The dynamical processes associated with the evolution of the bright points.

iv. The main contribution to the heating of the chromosphere at the sites of the bright points by 3-min oscillations.

v. The spatial scale length over which the 3-minute intensity oscillations associated with the bright points show a phase coherence.

vi. The properties of the intensity oscillations on the network boundaries.

In Chapter IV the properties of the main impulse, the follower pulses and energy budget for the heating of the quiet chromosphere at the sites of the bright points have been discussed.

Finally in Chapter V the results from the present study and the conclusions made in Chapters III and IV are summarized.

CHAPTER II

OBSERVATIONS AND DATA REDUCTION

2.1 The suitability of H and K lines of CaII as diagnostic tools for the study of the chromosphere

The H and K lines arise from a transition 4^2S to 4^2P (shown in Fig. II.1)of the singly ionized calcium ion. These are resonance lines and hence are collisionally controlled (Thomas 1957) unlike the H_α line which has a photoelectrically controlled source function. Thus the intensity of the lines in the core of H and K lines will reflect the local physical conditions and are thus the best probes for studying the local conditions within the chromosphere. It is known since the time of Hale and Ellerman (1904) and D'Azambuja (1930) that these lines are reliable indicators of chromospheric inhomogeneities on the sun. Over the years their potential as diagnostic tool in probing the chromospheric behaviour both of the quiet as well as of the active sun has been established so well that in recent years this has been used to look for chromospheric features and infer the chromospheric heating in sun like stars. In this thesis, the intensity variations in the CaII H line is chosen as a parameter to study the chromospheric inhomogeneities.

2.2 Features of the H-line profile

The CaII H line is basically an absorption line with emission reversals on either sides of the core of the line. A high dispersion

13

CONTINUUM
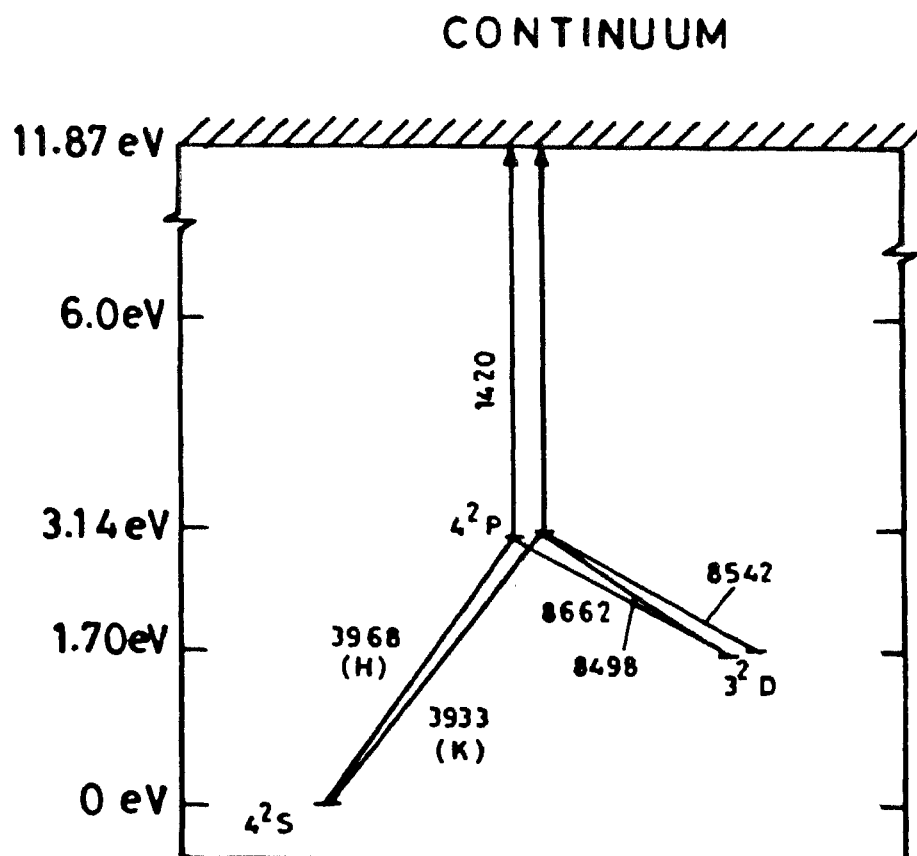
Fig. II.1 Energy-level diagram for the lower states of CaII showing the resonance doublet transitions H(3968A) and K(3933A) and the transitions for the infrared lines at 8498A, 8542A and 8662A.

spectrum (~1mm/Å) shows the double reversal with two emission peaks; one on the violet edge and the other on the red edge of the central absorption. FigureII.2 shows the spatially averaged line profile of the H line in quiet regions of the sun (Hale and Ellerman, 1904),where H_3 is the central absorption core,

H_{2V} and H_{2R} are the self reversed emission peaks on the violet and the red wings, and

H_{1V} and H_{1R} are the dips at the violet and the red wings.

2.3 Description of the Instruments

The observations made on September 13,1971 at the Vacuum Tower Telescope (VTT) of the Sacramento Peak Observatory, New Mexico based on the observing proposal by Sivaraman and J& Beckers have been used for this study. In the VTT the 44-inch two mirror coelostat mounted on the top of a tower nearly 130 feet above the ground collects the sunlight and sends the beam downwards. The telescope is evacuated and the entrance aperture is sealed with a quartz window of size 30 inches. The sunlight enters through this window and falls on the first mirror of the coelostat. The reflected light falls on a second mirror which reflects the beam of sunlight downwards to the main spherical mirror (or objective) 64-inch aperture and located 50 feet below the ground level. The objective has a focal length of 180 feet and forms a 20-inch image of the sun at the ground level, where the observing table is located. The image has a scale of about 3.48 arc sec/mm. The focussed image of the sun falls on the slit of an Echelle Spectrograph which is an all-mirror system of 36 feet focal length. The light

15
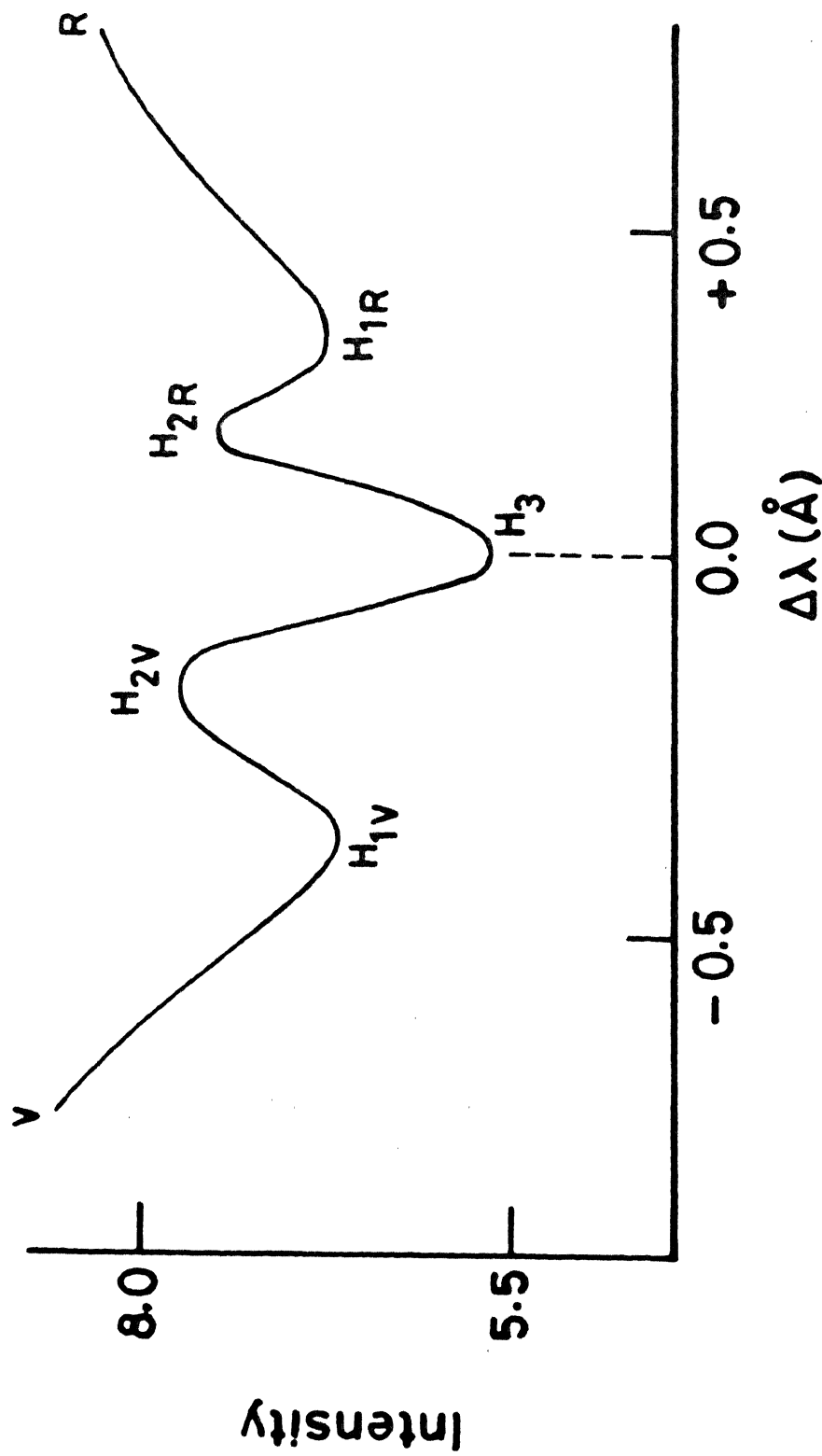
Fig.II.2 CaII H line profile of a typical bright point. The intensity is in percent of the continuum. The five parameters of the line profile used in this study are shown (See text para 2.2 and page 15 for definitions of these parameters).

entering the spectrograph is first dispersed by a prism monochromator. Through a multiple slit system in the focal plane of the monochromator the light is admitted into the echelle grating with 300 grooves mm^{-1}. In one of the modes of operation of the echelle spectrograph, it is possible to obtain simultaneously spectra of the H and K lines, the calcium infrared lines 8498Å and 8542Å, the H$_\alpha$ line and the sodium D lines. The code name for this mode is HIRKHAD (Beckers et al. 1972)which stands for the five wavelength regions that can be photographed simultaneously (H for the CaII H line; IR for the calcium infrared lines; K for the CaII K line; HA for the H$_\alpha$ line and D for the NaI D$_1$ & D$_2$ lines). The work reported in this thesis is based on the study of the H line of CaII from a HIRKHAD run.

2.4 Method of Observations

A beam spliter placed before the entrance slit of the spectrograph divides the incoming beam into two parts. The first part feeds the slit of the spectrograph and the other is split further into two, to feed two slit jaw cameras: one for solar granulation pictures through a broad band filter and the second for H$_\alpha$ images (using a Halle filter with a pass band of 0.3Å) or K line images (using a CaII K line filter with a pass band of 0.6Å).

Table 1. lists the wavelengths, the orders of the spectrum , the dispersion and the emulsion that were used for recording the spectra.

17

Table 1

Parameters of the Echelle Spectrograph for the 'HIRKHAD' mode

wavelength of line: λ(Å)	Element	Order	Dispersion mm/Å	Emulsion (Kodak)
3933.68	Ca^+	15	11.67	5375
3968.49	Ca^+	15	12.10	5375
5889.97	Na	10	7.54	2498
5895.94	Na	10	7.54	2498
6562.81	H	9	7.02	S0392
8498.06	Ca^+	7	5.60	2424
8542.14	Ca^+	7	5.71	2424

The scheme of observations used Program B of the HIRKHAD mode which takes spectra at the repetition rate of 12 sec (Beckers et al 1972). The exposure time for each frame was about 3 sec. The entrance slit was set to have a width of 144µ or 0.5 arc sec and the length of the slit was 80mm corresponding to about 280 arc sec on the sun. The slit was positioned in the north-south direction in the sky and was set over a quiet region on the sun around the centre of the disc and the solar rotation was compensated for. Two hair lines stretched across the slit provided the local fiducial references against which all features on the spectra were identified and referred to in the analysis of the spectra. The spectra were obtained on Kodak emulsion 70mm format (see

18

Table 1.). The sequence has a duration of 35 minutes and the seeing was exceptionally good for most of the duration of the sequence. Thus in all there are 177 frames within the 35 minutes of observations. Photometric calibration of the emulsion was done for the H line by placing in turn three neutral density filters with transmission values Log T= -0.689, -1.320, -2.009 in front of the slit over and above the step wedge. The time sequence spectra contains the step wedge calibration both at the beginning and at the end of the observations and the mean of these two curves (the measured densities versus the step wedge with neutral density transmission) was adopted as the final photometric calibration curve for the photometric reduction of the spectra. The transmission values of the steps with and without the neutral density filters are shown in Table.2.

Table 2.

Transmission values of the step wedge with and without Neutral density filters

Step Wedge No.	Log T	Log T values for Neutral Density Filter		
		-0.689	-1.320	-2.009
		Log T (Step wedge + N.D. Filter)		
1	1.95	1.26	0.63	-0.06
2	1.71	1.02	0.39	-0.30
3	1.47	0.78	0.15	-0.54
4	1.18	0.49	-0.14	-0.83
5	0.86	0.17	-0.46	-1.15
6	0.56	-0.13	-0.76	-1.45

2.5 Reduction of the Data

The spectra are of high quality and show the individual bright points well resolved and the time varying brightness of the individual bright points in excellent detail. An enlarged print of one of the frames is shown in Fig. II.3. The 177 frames constituting the 35 minutes long time sequence were visually examined frame by frame in detail to follow the evolution of the H line profile of the bright points by placing the film over an illuminated viewer. The visual examination revealed that there are many bright points along the slit in addition to the network elements. Their identity was confirmed through the slit jaw pictures in the K line. It is possible to follow any one bright point from frame to frame using the hair line as the reference. When this is done, it is seen that the bright point oscillates in brightness i.e. the brightness increases, reaches a maximum and decreases and finally touches a minimum. This cycle repeats many times. Also it was clear that all the bright points do not brighten up to the same level in their life cycle. Some of them appear very bright, some less and still some others brighten up much less. The selection of the sites for detailed study cover all these varieties of bright points as well as regions on the network boundaries. A sample of 28 features were chosen for detailed analysis and these are designated as $B_1, B_2, B_3, \ldots \ldots B_{28}$. The locations of these 28 features $(B_1, B_2, B_3, \ldots \ldots B_{28})$ marked in Fig. II.3 , were fixed using to the two hair lines as the local references (shown as W_1 and W_2

20

Violet   Red

W_1

$14.3''$

W_2

↑ 3966.07 Å
FeI

↑ 3967.4 Å
FeI

↑ 3968 Å
CaII H

↑ 3969.3 Å
FeI
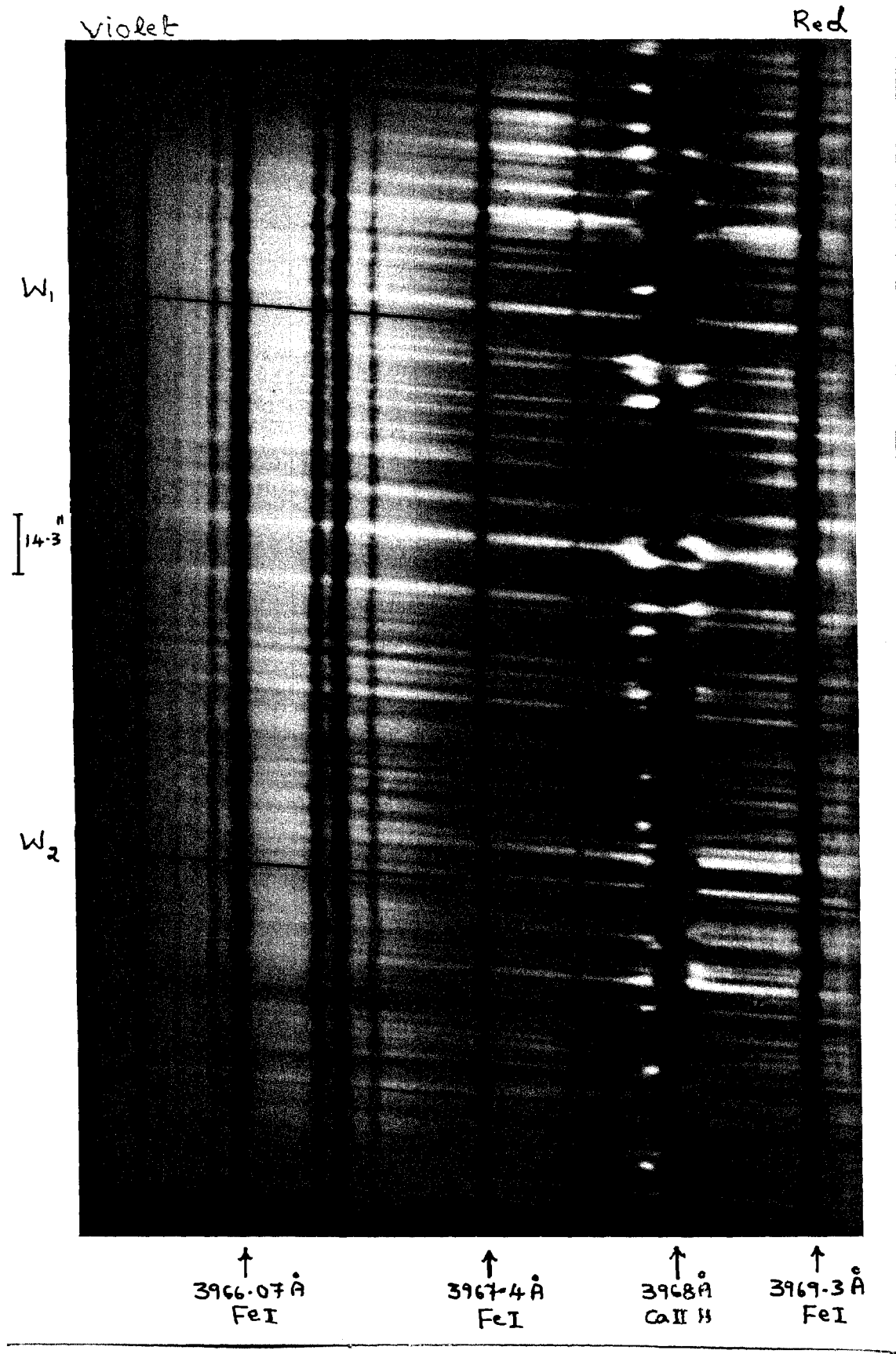
Fig. II.3   Enlarged photographic print of frame no.209 of the CaII H-spectra from the 35-minute long sequence. W_1 and W_2 are the images of the two hair lines used as the local reference for positions.   The features $B_1, B_2, \ldots \ldots \ldots, B_{32}$ are marked for identification.

21

in Fig. II.3.). Of these 26 are on bright points and 2 are on network regions (B$_4$and B$_{18}$). The spectra were scanned along the direction of dispersion at these 28 positions using the PDS micro densitometer of the Indian Institute of Astrophysics and the density profiles were obtained frame by frame for the 177 frames. The projected size of the scanning aperture at the PDS was 50μ x 200μ, which corresponds to 0.004132A x 500 km. The images of the hair lines in each frame was used to precisely position each frame on the microphotometer table. The step wedge calibration spectra were also scanned with the same setting. Then using the measured density values and the standard transmission values for each step, the photometric calibration curve for the emulsion was constructed. The density profiles were then converted to relative intensity units through this photometric calibration curve. These profiles were then further converted to units of intensity of the continuum, adopting the residual intensity at λ3966.250Å on the violet wing of the H-line as 23% of the continuum from the photometrically calibrated H-line profiles of White and Suemoto (1968). Thus in all 5664 line profiles calibrated in units of the continuum were derived from the time sequence spectra consisting of 177 frames for further analysis.

CHAPTER III

THE DYNAMICAL PROCESSES IN THE EVOLUTION OF A BRIGHT POINT, THE CHROMOSPHERIC 3-MINUTE OSCILLATIONS AND TEMPORAL BEHAVIOUR OF NETWORK BOUNDARIES

3.1 Introduction

In this chapter, the results of the analysis of the H-line profiles derived from the reduction of the 35-minutes long time sequence will be narrated. In all there are 5664 profiles. A detailed description of the dynamical evolution of the line profiles both at the sites of the bright points and the network boundary regions and the role of the 3-minute intensity oscillations in the heating of the chromosphere at these levels are presented. It is found that the bright points can be categorised into three classes in terms of their evolutionary behaviour. The differing strengths of the intensity oscillations seen in the bright points in the three classes are interpreted to be related to the differing strengths of the inner network magnetic fields to which these bright points of the three classes correspond to.

23

3.2. **The dynamical evolution of the bright points inferred from the H-line profiles**

To study the dynamical evolution of the H line profile of a bright point, the initial time of start is arbitrarily set to zero, when the profile at this site is in an undisturbed condition. Even in the undisturbed condition the profile shows weak emission in H_{2V} and H_{2R} and slight asymmetry (Bappu and Sivaraman,1971, Grossmann-Doerth,Kneer and Uexkull,1974 and Liu,1974) and this can be taken as the reference profile. The dynamical changes in the line profiles can now be described with respect to this reference profile as follows: At the outset, the perturbation appears as a brightening in the far wings on the red and violet sides, whereas the H_{2V} and H_{2R} show the same emission as in the quiet reference profile. The brightenings in the far wings appear as bright threads and correspond to red shifted wiggles in the FeI lines that lie in the wings of the H line profile. With the progress of time the intensity enhancement propagates simultaneously towards the core of the H line. When the brightening reaches the level of formation of H_2 (i.e. level of H_{2V} and H_{2R}) one would expect that both H_{2V} and H_{2R} would brighten simultaneously and following this H_3 would also brighten. Whereas H_{2V} alone shows a large increase in brightness but not H_{2R}. This increase in brightness which is nearly 4-5 times the normal value makes the profile appear highly asymmetric. By the time the intensity of H_{2V} reaches a maximum, the brightness in the wings is on the decline. Eventually the profile returns to the original undisturbed condition which is the reference profile. This process constitutes one cycle of evolution and takes about 180 secs. This is the general pattern of evolution of a bright

24

point. The brightening travelling from the wings towards the core of the H line represents an observational evidence for the upward transport of the non-radiative energy and the bright points are the sites where this takes place in the chromosphere.

3.3 Time dependent properties of the H line profile parameters

To estimate quantitatively the changes in the profile narrated above during the evolution of a bright point, the following parameters were employed:

i. Intensity of the H_{2V} emission peak , (I_{H2V})

ii. Intensity of the H_{2R} emission peak , (I_{H2R})

iii. Intensity of the H_3 absorption core , (I_{H3})

iv. Intensity ratio of the H_{2V} and H_{2R} emission peaks , (I_{H2V}/I_{H2R})

v. Doppler shift of H_3 core , $(\Delta\lambda_{H3})$

For every one of the profiles, the above five parameters were derived. These parameters were plotted versus time covering the 35-minutes duration of the sequence and these are shown in Figs. III.1 to III.16. Among the five parameters, plots of I_{H2V} show the intensity oscillations most convincingly. An examination of these plots shows that the bright points show a variety of profiles during the evolution and the term 'typical' bright point used by Liu (1974) and Durrant ,Grossmann-Doerth and Kneer (1976) is no longer valid. It is seen that these profiles can be classified into three classes in terms of their evolutionary behaviour. In Table 3 the features associated with the evolution of the bright points of the three classes are presented.

25

Table 3.
Properties of the three Classes of the Bright points

| Bright Point | | No. of wave pulses preceding /following the main impulse | | Remarks |
Class	designation	Preceding	Following	
	B_1	6	7	
	B_2	1	9	
Class I	B_3	7	3	
(No. of samples: 11)	B_5	8	2	
	B_{17}	0	10 *	Main impulse at
Max. brightness(I_{H2V})	B_{19}	0	11 *	the beginning of
of the main pulse is	B_{20}	2	8	the obsn.
4-5 times the	B_{22}	9	2	
normal value	B_{27}	4	6	
	B_{28}	8	1	
	B_{25}	7	2	
	B_{29}	10	2	
	B_{31}	6	4	
	B_{32}	6	5	
	B_6	3	4	
Class II	B_{12}	0	8	
(No. of samples: 8)	B_{13}	3	6	
	B_{14}	4	4	
Max. brightness(I_{H2V})	B_{15}	5	5	
of the main pulse is	B_{16}	5	5	
2-3 times the	B_{21}	5	4	
normal value	B_{26}	7	0	
	B_{30}	3	5	

Table 3 (continued)

| Bright point | | No. of wave pulses preceding /following the main impulse | | Remarks |
Class	Designation	Preceding	Following	
	B_7	3	2	
Class III	B_8	Main impulse not easily identifie
(No. of samples: 7	B_9	4	6	
Max. brightness (I_{H2V})	B_{10}	5^+	0 main impulse	
of the main pulse is	B_{11}	0	7 at the end of	
1.1-2.0 times the	B_{23}	7	1 the obsn.	
normal value	B_{24}	6	2	

Note: B_4 and B_{18} are on the network boundary regions and hence are separately dicussed.

26a

Class I.   Those bright points that show very large intensity enhancements in H_{2v} (I_{H2v}) at their brightest phase as high as 4 times or more the normal value.   Of the 14 samples in this class , the light curves of B_{17}, B_{19}, B_{22} and B_{28} and B_1, B_2, B_3 and B_5 are shown in Figs. III.1 and III.2.   The light curves of the remaining 6 bright points look similar to these.

Class II.   Those bright points that show moderate (about 2 times the normal value) intensity enhancement in H_{2v} (I_{H2v}) at the maximum brightness phase.   Of the 9 samples in this class, the light curves of B_{12}, B_{13} and B_{14} are shown in Fig. III.3.   The light curves of the remaining 5 bright points look similar to these.

Class III.   Those bright points that show only a marginal increase in intensity in H_{2v} (I_{H2v}) at the brightest phase.   Of the 7 samples in this class, the light curves of B_8, B_9, B_{10}, and B_{11} are shown in Fig. III.4.   The light curves of the remaining 3 bright points are similar to these.

The plots of the remaining parameters I_{H2R}, I_{H3}, I_{H2v}/I_{H2R} and $\Delta\lambda_{H3}$ for the three classes are shown in Figs. III.5 to III.16.   (Kindly see Appendix I page No.87 to 98 for these figures).   These also show the differences in the behaviour from one class to the other and also exhibit the brightness oscillations that resemble those of I_{H2v} except that these are of smaller amplitudes.

27
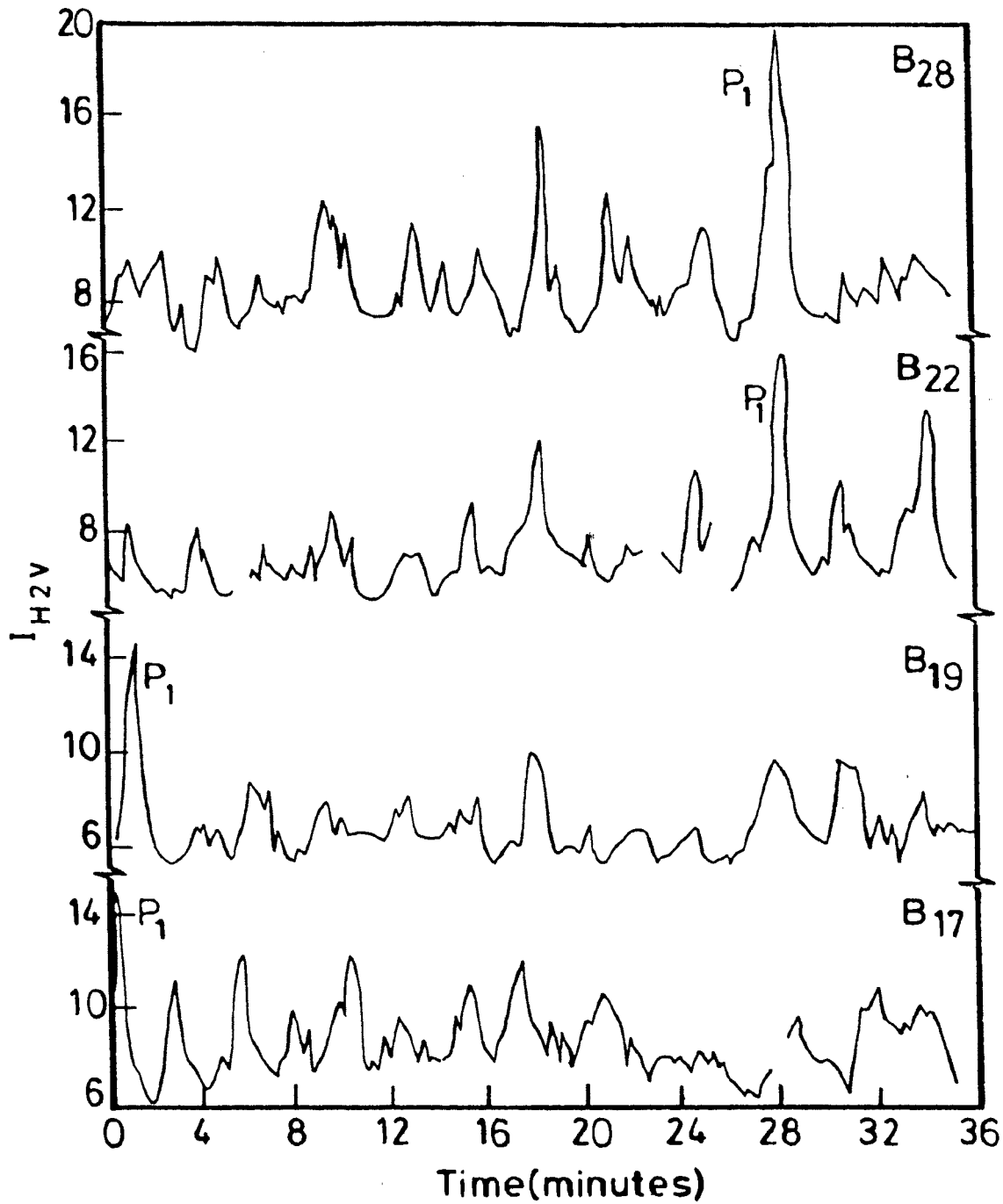
Fig. III.1 The variations in the intensity of H_{2v} emission peak (I_{H2v}) of the four bright points $(B_{17}, B_{19}, B_{22}$ and $B_{28})$ during the 35-minute of observations (i.e. the light curve of the bright point in H_{2v} emission). These samples belong to Class I. The main impulse designated as P_1 is 4 to 5 times the normal brightness value and is followed by smaller pulses.
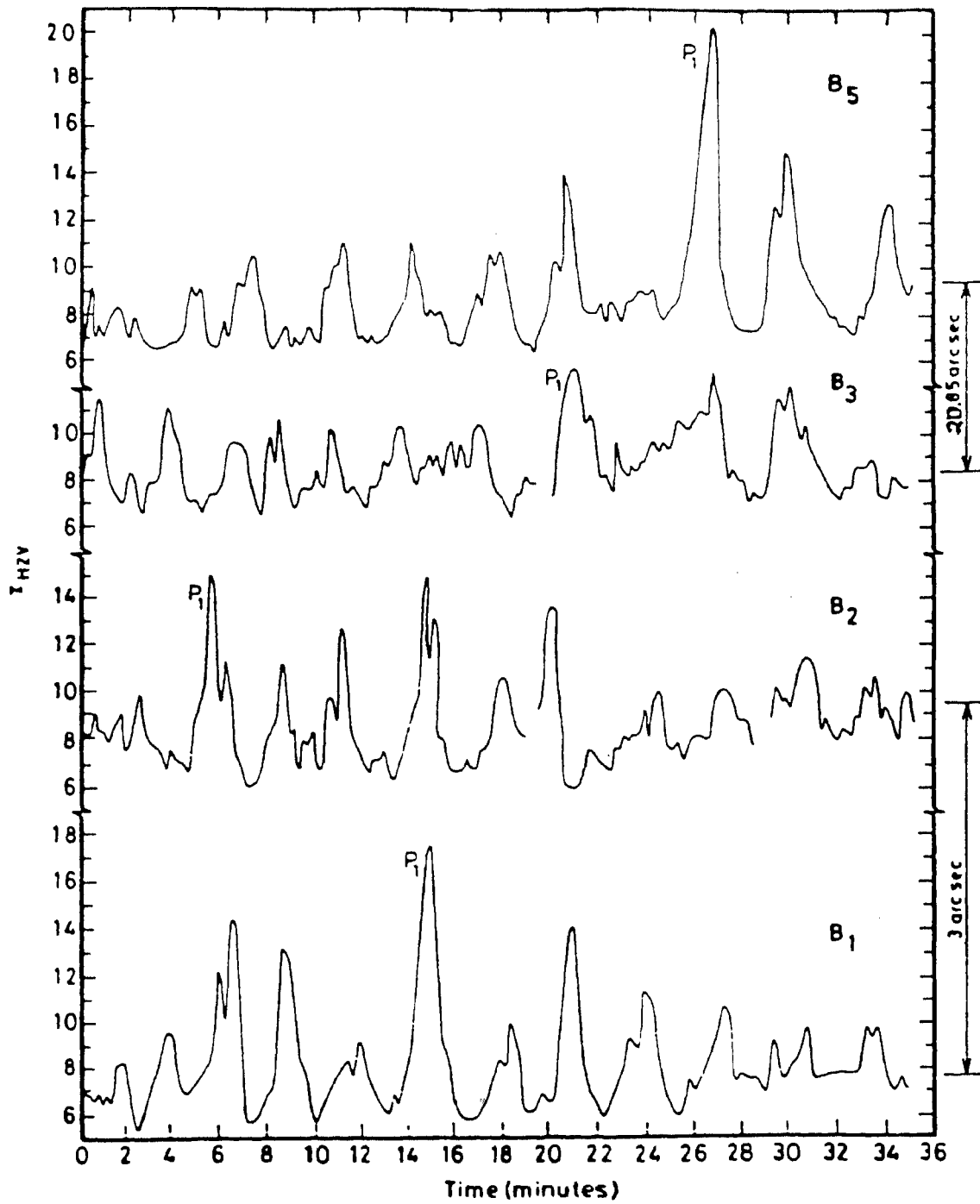
Fig. III.2 Additional samples of light curves of bright points (B_1, B_2, B_3 and B_5) of Class I. The main impulse is designated by P_1 in each case.
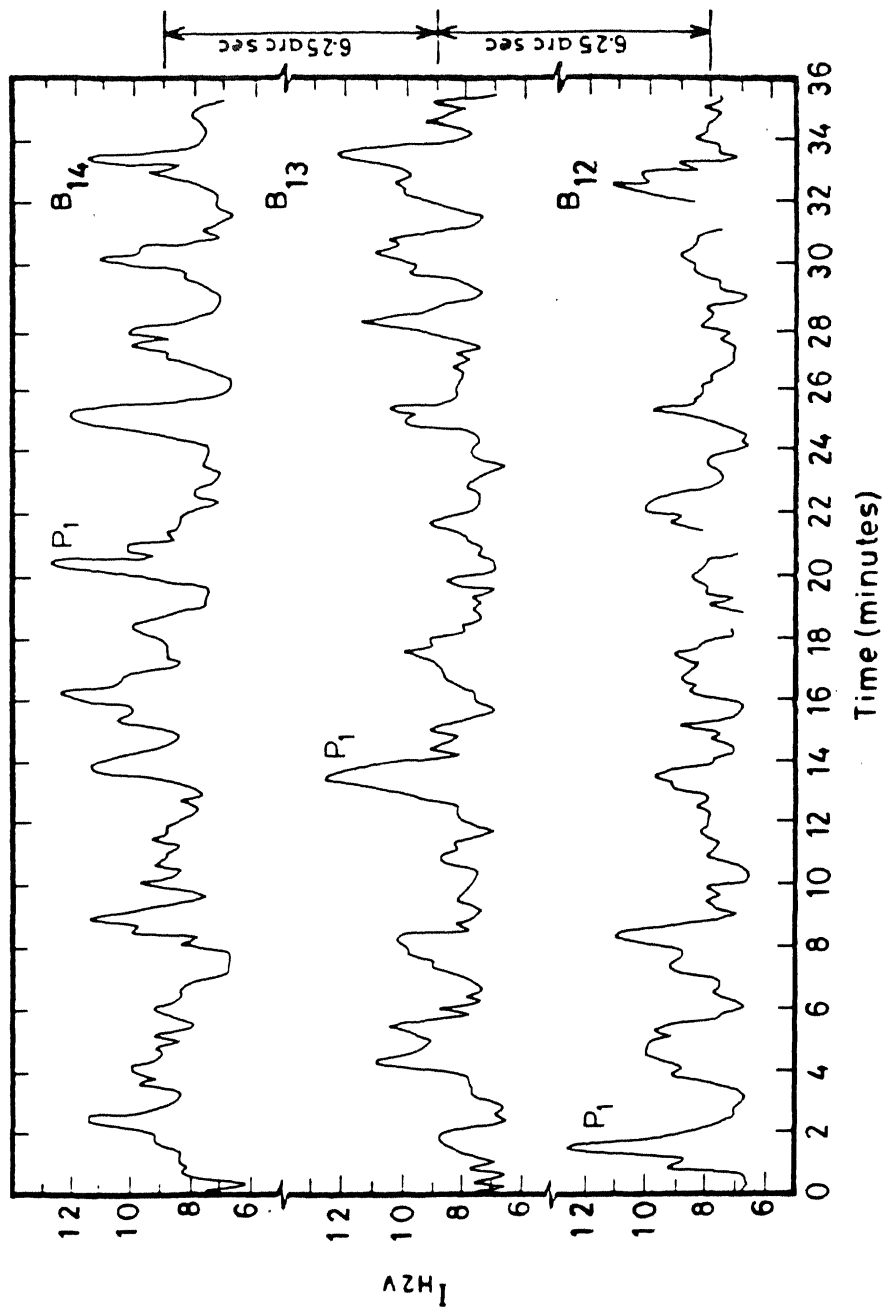
Fig.III.3 Light curves of the bright points B_{12}, B_{13}, and B_{14}. The main impulse (P_1) is only 2 to 3 times the normal value in brightness. These belong to Class II. B_{12} and B_{14} are 12.5 arc sec apart on the sun and show a weak phase coherence in their light curves.
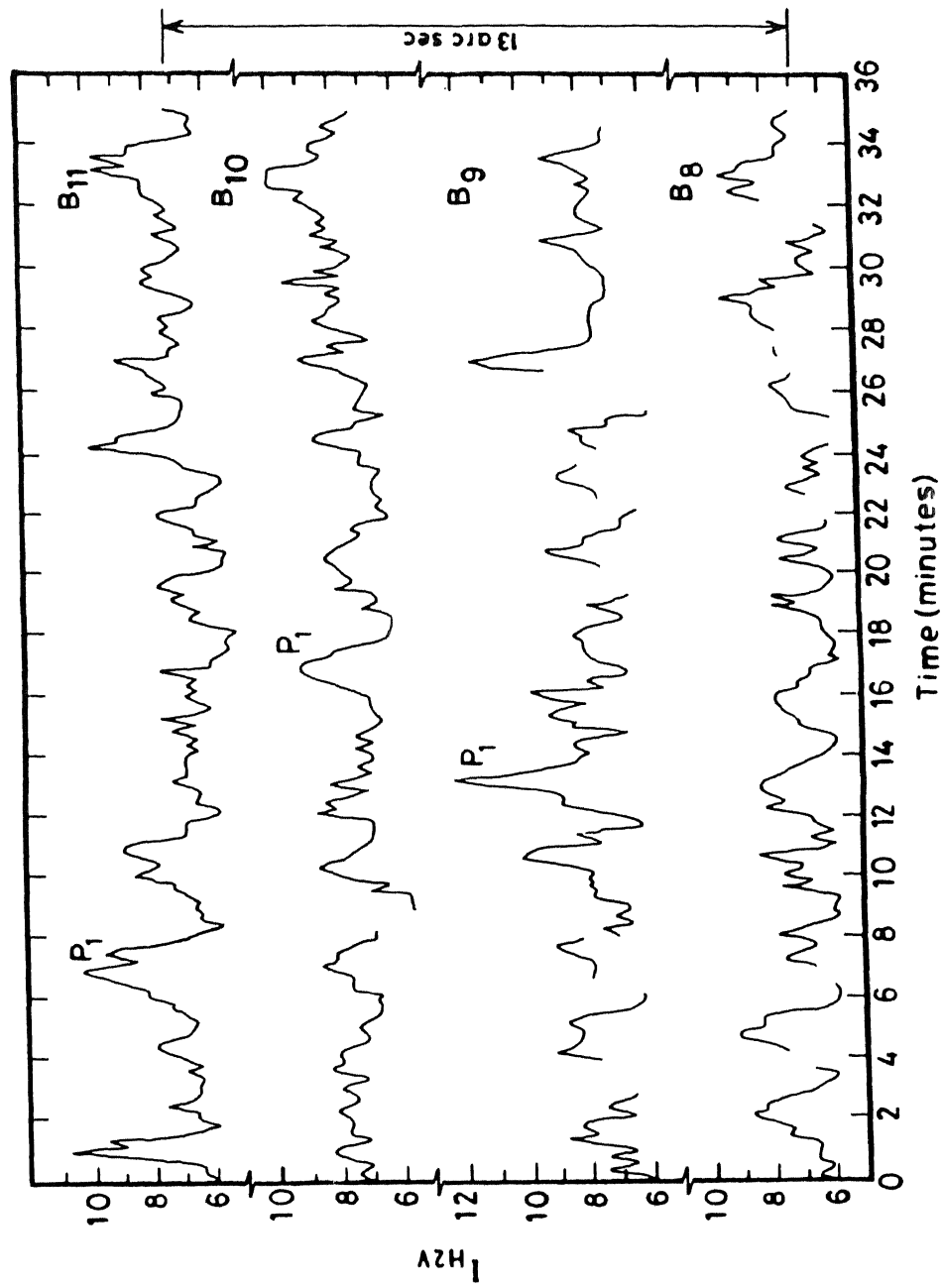
Fig. III.4 Light curves of the bright points B_8, B_9, B_{10} and B_{11}. The main impulse (P_1) is only 1.1 to 2.0 times the normal value in brightness. These bright points belong to Class III.

31

3.4   Similarities and Differences among the three classes of bright points

3.4.1   Similarities

3.4.1.1   Number of wave pulses that follow the main impulse

The plot of I_{H2v} versus time for the Class I bright points (e.g. B_{17} and B_{19}) in Fig. III.1 shows that the brightness enhancement is highest at the very start of the observations. The strong pulse in the train is designated as the "main impulse" and is indicated as P_1 in Figs. III.1 and III.2 for all the wave trains. Although the main impulse (P_1) is easily identifiable from a look at the I_{H2v} vs time curves (exceptions being B_2, B_3 of Fig. III.2 , B_{14} of Fig. III.3) it may be worth assigning an objective criterion for identifying the main impulse. On examination of the H-line profiles corresponding to the positions of P_1, it is seen that the ratio of the emission intensity is around 2 $(I_{H2V}/I_{H2R} \sim 2.0)$. Similarly in Class II, the bright point B_{12} shows maximum brightness at time t=1.7 minutes which is the main impulse(Fig. III.3). The amplitude of the main impulse of class II is much smaller than that of class I. In class III, the main impulse for the bright point B_9 (Fig. III.4) occurs at time t=13 minutes and is much weaker compared to that of class II.

The number of samples analysed here being large, there are instances where the main impulse is caught almost at the beginning of the observations (e.g. B_{17} and B_{19}) or the main impulse occurs almost at the tail end of the observations(e.g. B_5). These two extreme cases would enable us to estimate how many pulses are contained in the wave train preceding or following the main impulse. In the remaining cases, the main impulses have occurred almost at the middle of the observations (e.g. B_1) and so all the number of pulses that followed the main impulse do not appear in the observations . However

if the observations were to be made sufficiently long, one could expect to watch a main impulse followed by several pulses of decreasing amplitudes constituting the wave train, then another main impulse, followed by several smaller pulses, then next the main impulse and so on. One gets the same impression by pooling together the performances of all the bright points examined here. Thus a minimum of 8 to 10 follower pulses (this number could even be more) follow the main impulse of a bright point and this is an unmistakable characteristic feature of the bright points of class I. For the bright points of Class II and Class III (e.g. B_{12} and B_{13} in Fig. III.3 and B_8 and B_{11} in Fig. III.4) 4-6 follower pulses seems to be most common although there are a few expections like B_8, B_{11} and B_{12}. In B_8 most of the pulses have the same amplitude and so the main impulse P_1 is not easily identifiable. In B_{11} and B_{12} there are about 7 follower pulses. In the case of B_2 although there are 3 or 4 pulses of almost the same strength, we have called the strongest among these as the main impulse P_1. B_1 has two strong pulses preceding although the main impulse is unmistakably (P1). Most probably the main impulse is one of the earlier ones before P_1 but its amplitude is decreased, presumably because it might be out phase with the oscillations of the medium. Although there are variations, the most common feature is that the main impulse is followed by several (8-10 or more) pulses with decreasing amplitudes. Liu (1974) noticed only 3 to 5 pulses which may be due to the shorter duration of the time sequence he used and the smaller number of samples he analysed.

33

3.4.1.2   Period of oscillations

The main impulse as well as the follower pulses have a quasi-sinusoidal appearance.   The period of the pulses constituting a wave train has been evaluated.   This has been done as follows: The digitised values of the parameters, at intervals of 12 sec (which is the repetition rate of the frames) were fed to the computer and the minima on either side were located for each wave pulse.   The time interval between two successive minima was reckoned as the period.   In this way the periods for all the impulses for every bright point for the three classes were derived.   These have been plotted in the form of histograms.   The histograms for the five parameters are shown for the Class I bright points in Figs. III.17(a to e).   Similar histograms for the Class II and Class III samples are shown in Figs. III.18(a to e) and Figs. III.19(a to e) respectively.   The histograms show that the period of 190 ± 10 sec for the brightness oscillations is most common.   To confirm the distribution of periods a power spectrum analysis of the parameter I_{H2v} for the three classes was also done.   The power spectra are shown in Figs. III.20 to III.22.   They also show the 190 ± 10 sec period.   The period is the same for the pulses in the three classes and thus seems to be independent of the magnitude of the brightness enhancement and within a class the follower pulses have the same period as the main impulse irrespective of their brightness.

34
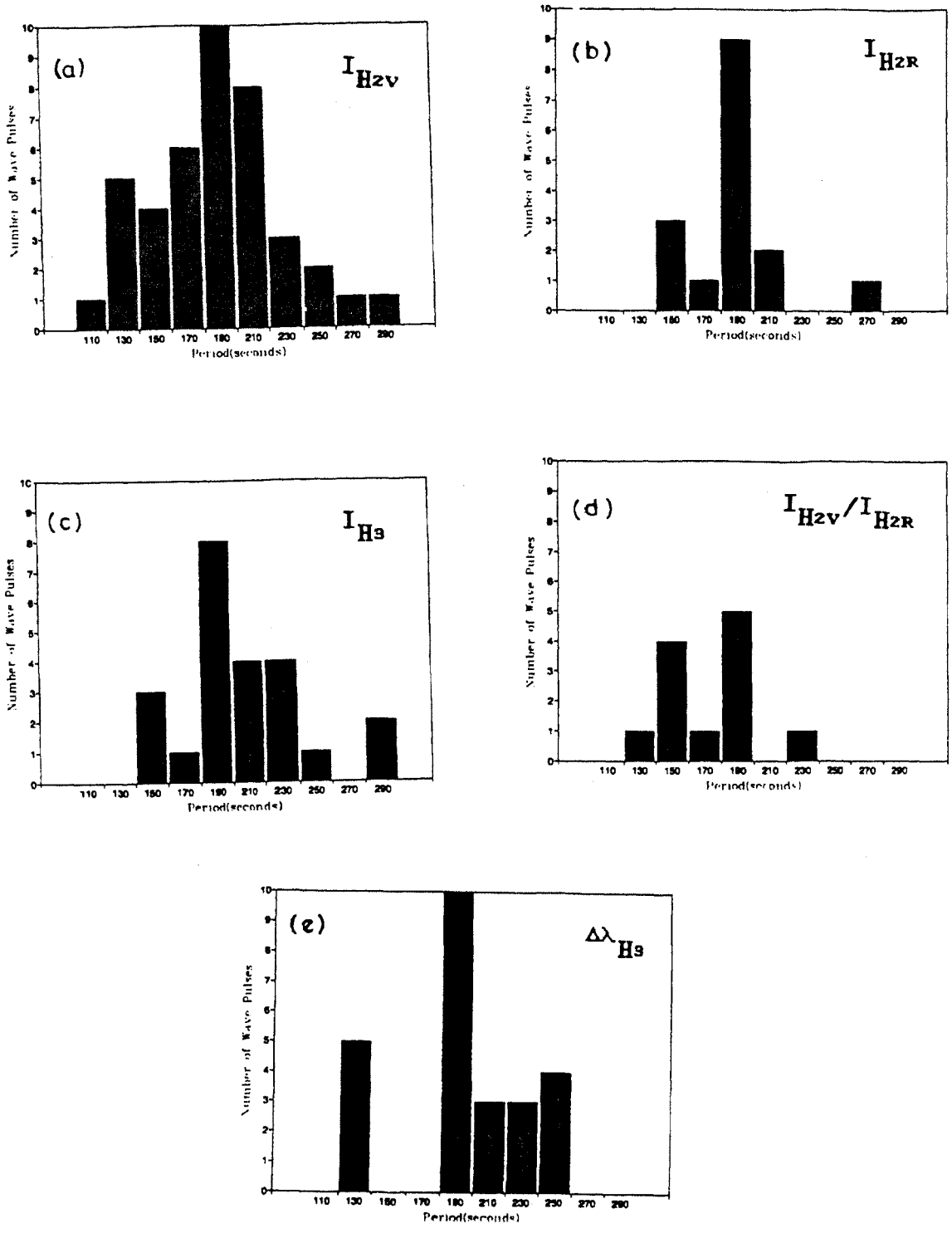
Fig.III.17 Histogram plots to illustrate the periodicity of oscillation for the five parameters of the H-line profile for Class I bright points. There is a sharp peak at 190 ± 10 sec in all the five parameters. (a) I_{H2v} (b) I_{H2R} (c) I_{H3} (d) I_{H2v}/I_{H2R} and (e) $\Delta\lambda_{H3}$.

35
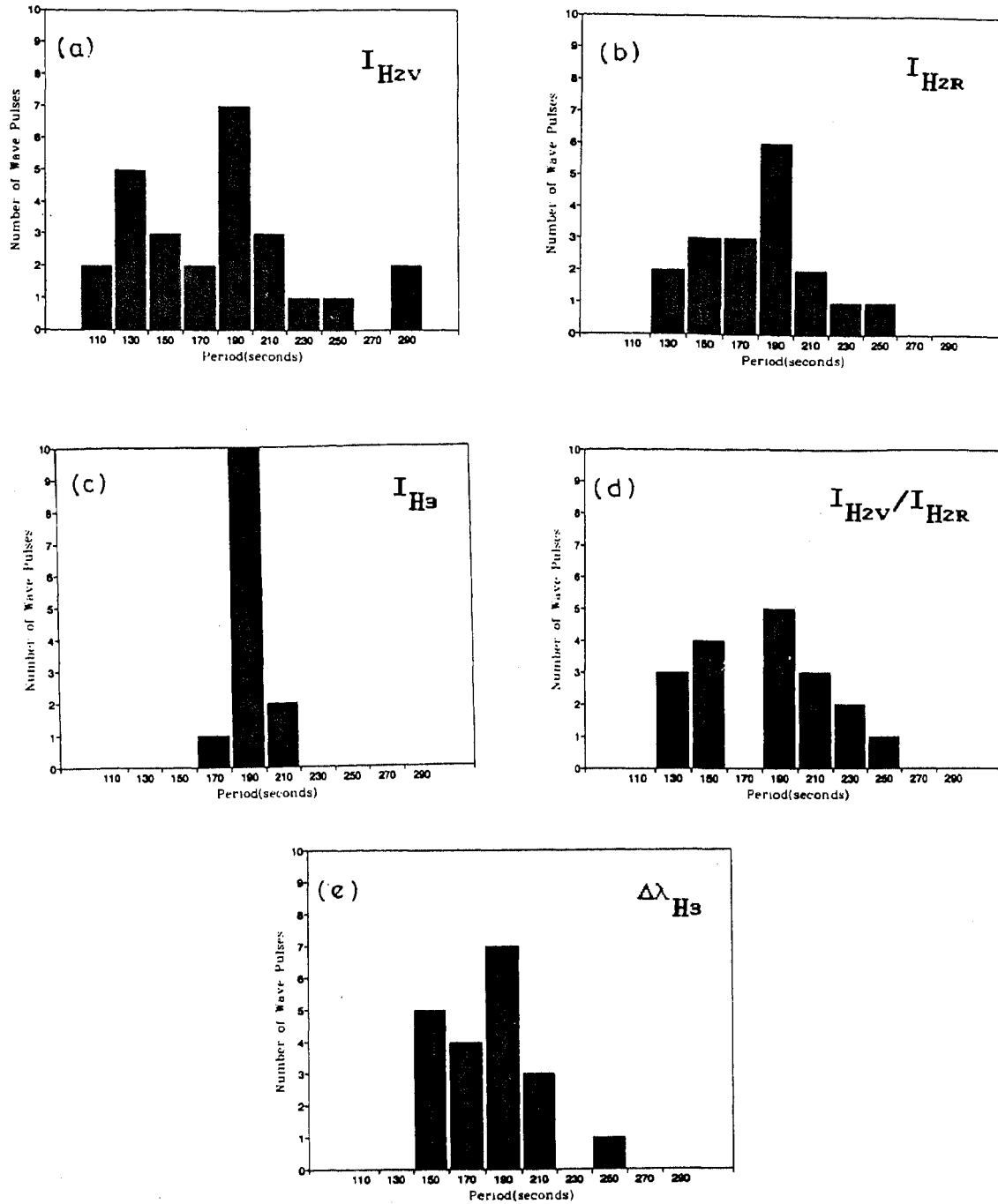
Fig. III.18 Distribution of the periodicity of oscillation for the five parameters of H-line profile of Class II bright points which show the 190 ± 10 sec periodicity conspicuously. (a) I_{H2v} (b) I_{H2R} (c) I_{H3} (d) I_{H2v}/I_{H2R} and (e) $\Delta\lambda_{H3}$.

36
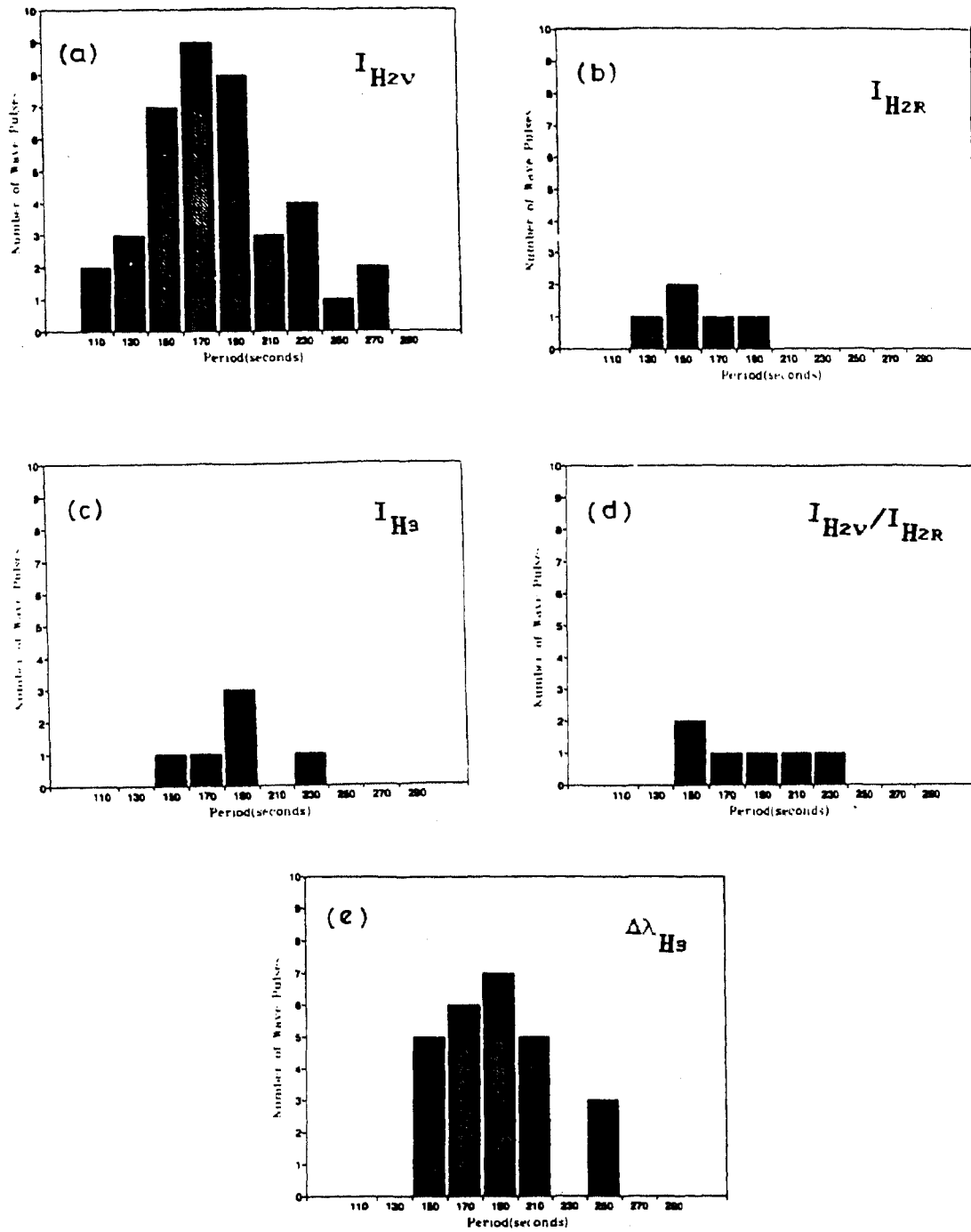
Fig. III.19 Distribution of the periodicity of oscillation for the five parameters of H-line profile of Class III bright points. The periods are not clear as in the classes I and II, although the 190 ± 10 sec periodicity is very significantly seen. (a) I_{H2v} (b) I_{H2R} (c) I_{H3} (d) I_{H2v}/I_{H2R} and (e) $\Delta\lambda_{H3}$.

37
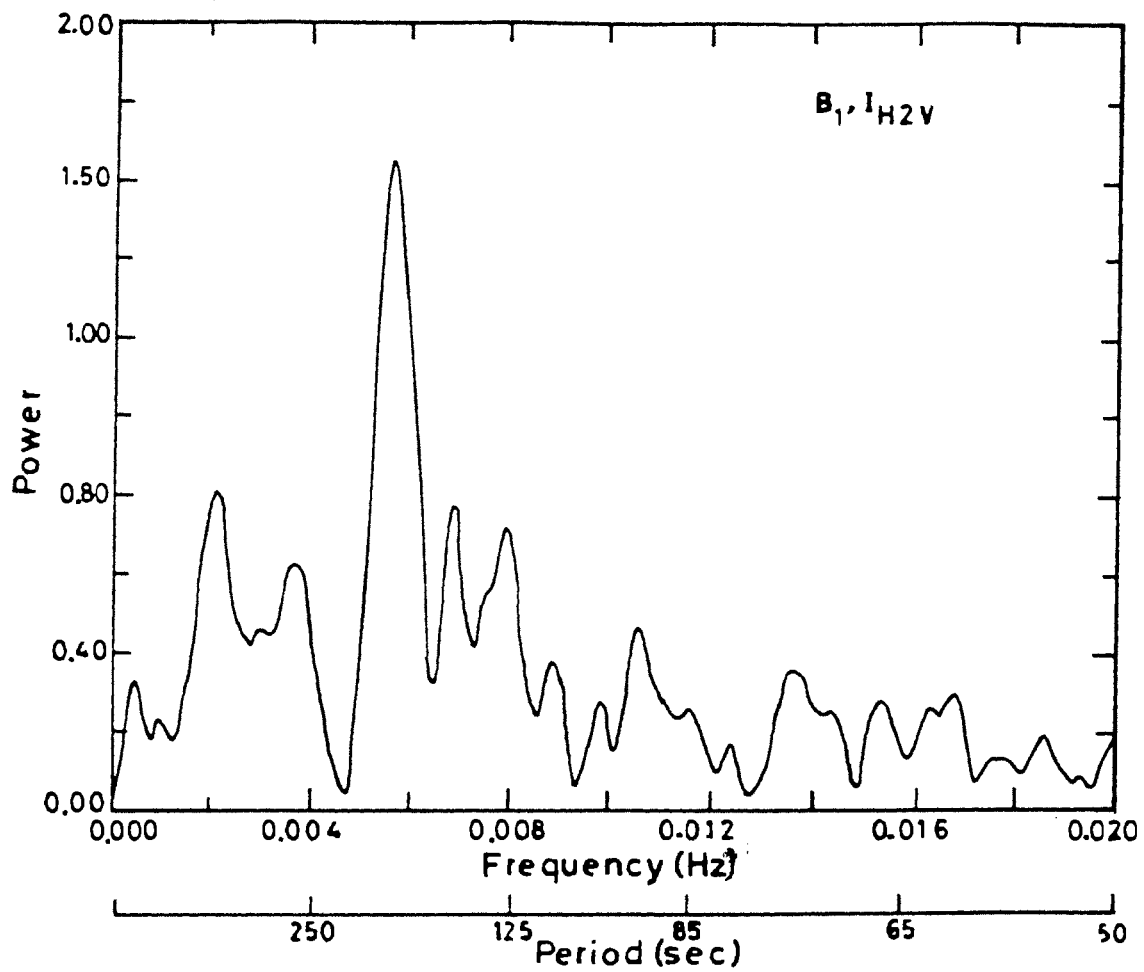
Fig. III.20 Power spectrum of the light curve of I_{H2v} Class I bright point B_1. Maximum power is concentrated in the region of ~ 190 sec.
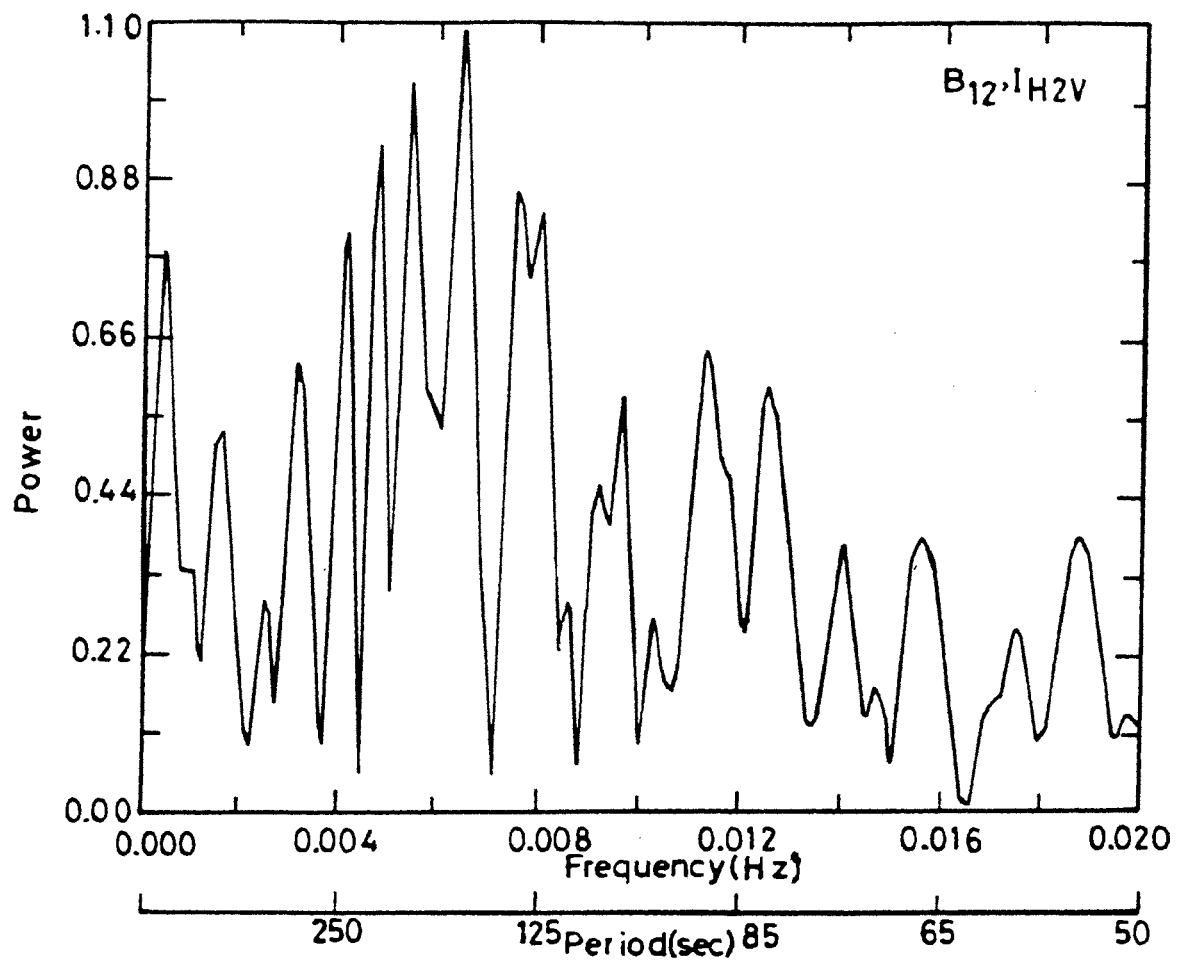
Fig. III.21 Power spectrum of the light curve of I_{H2v} Class II bright point B_{12}. The concentration of power around ~ 190 sec can be seen although other peaks are also present.
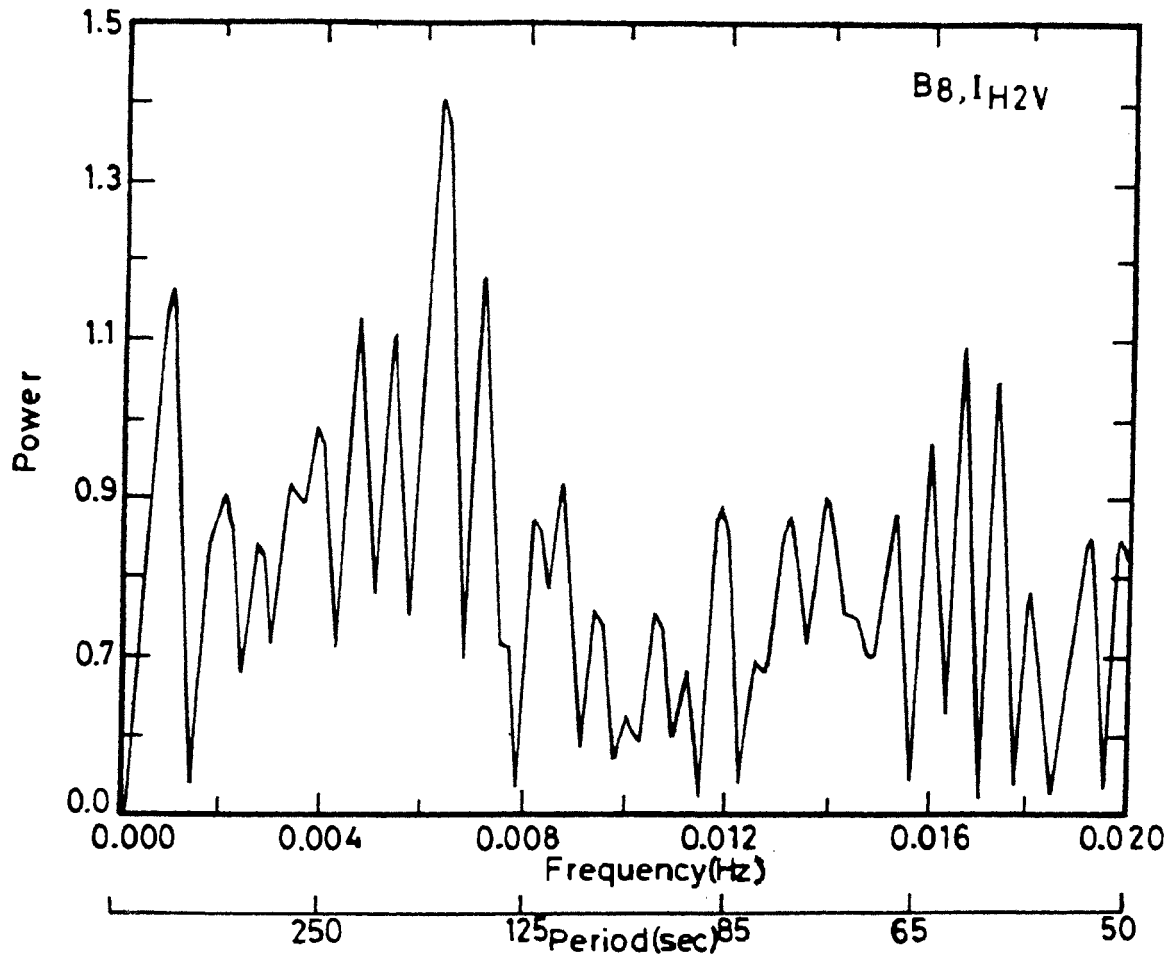
Fig. III.22 Power spectrum of the light curve of I_{H2v} Class III bright point. The peak around ~ 190 sec is clearly seen.

40

3.4.1.3 Amplitude of the follower pulses

The amplitude of the main impulse is the highest for class I bright points, lower for class II bright points and lowest for class III bright points. Similarly the amplitudes of the follower pulses also decrease from class I to class III. Although the amplitudes of the main impulse and of the follower pulses decrease from class I to class III the rate of decrease in amplitude of the pulses following the main impulse is more or less similar for all the three classes.

3.4.2 Differences

3.4.2.1 Amplitude of individual pulses

In the case of the class I bright points (Figs. III.1 and III.2) the main impulse shows a very large brightness enhancement in H_{2v} (I_{H2v}) during the brightest phase, which is 4 times or more compared to the normal value. Whereas in the case of Class II bright points (Fig. III.3) the main impulse shows an intensity enhancement of about 2.5 times the normal brightness value during the brightest phase and for the class III bright points (Fig. III.4) the main impulse shows an enhancement of 1.1 to 2.0 times the normal brightness value.

3.4.2.2 Asymmetries

The line profiles of the class I bright points become highly asymmetric in shape during the passage of the main impulse, whereas the

line profiles of the class II show less asymmetry compared to those of class I. The line profiles of class III bright points remain more or less symmetric during the passage of the impulse.

What causes this difference in behaviour in the bright points of the three classes? Sivaraman and Livingston(1982) have shown that the bright points have a one to one correspondence spatially with the arc sec inner network magnetic fields at the photospheric level. They have also shown that those bright points that increase in brightness many times the normal value are generally associated with magnetic elements with fields ~ 80 gauss and those bright points which reach lesser brightness correspond to weaker fields. This large field would correspond to the location of the bright point of class I classification. Similarly the main impulses of class II and class III would correspond to regions of lesser magnetic fields. From this comparison it is hypothesised that the magnitudes of the enhancements in brightness of the main impulses of each of the 3 classes are closely linked with the magnetic field associated with each bright point location. In other words the bright points located in a region of strong magnetic field will have the main impulse with strong intensity enhancement whereas the bright points located in a region of weaker fields will have the main impulse itself much weaker.

3.5 Phase relation between I_{H2V}/I_{H2R} versus $\Delta\lambda_{H3}$

In Figs. III.23 to III.25, the plot of the ratio of the intensities

42
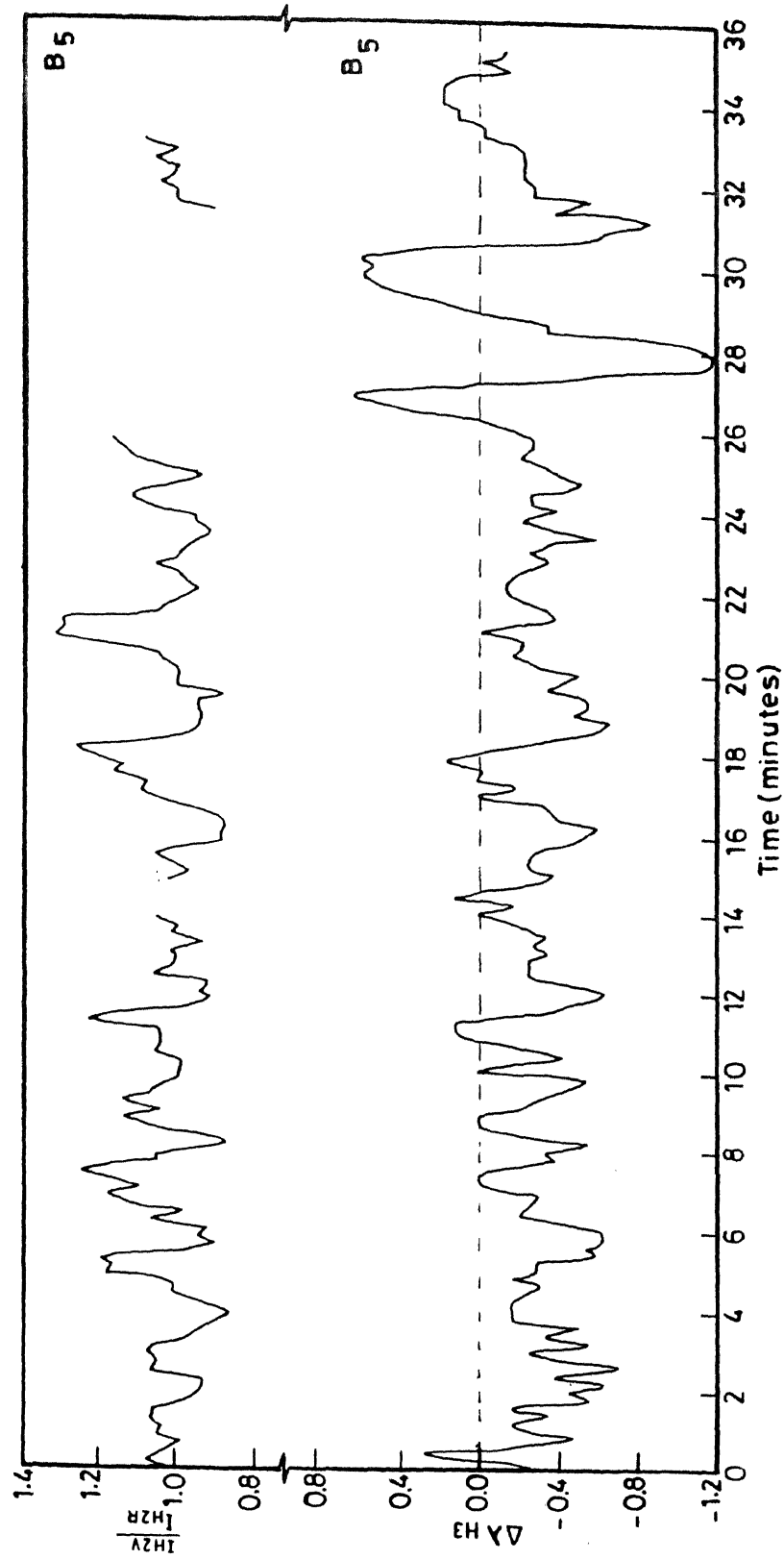
Fig.III.23 Phase relation between I_{H2V}/I_{H2R} and $\Delta\lambda_{H3}$ for the Class I bright point(B_5). The red shifts of λ_{H3} are correlated with $I_{H2V}/I_{H2R} > 1$ and violet shifts with $I_{H2V}/I_{H2R} < 1$.
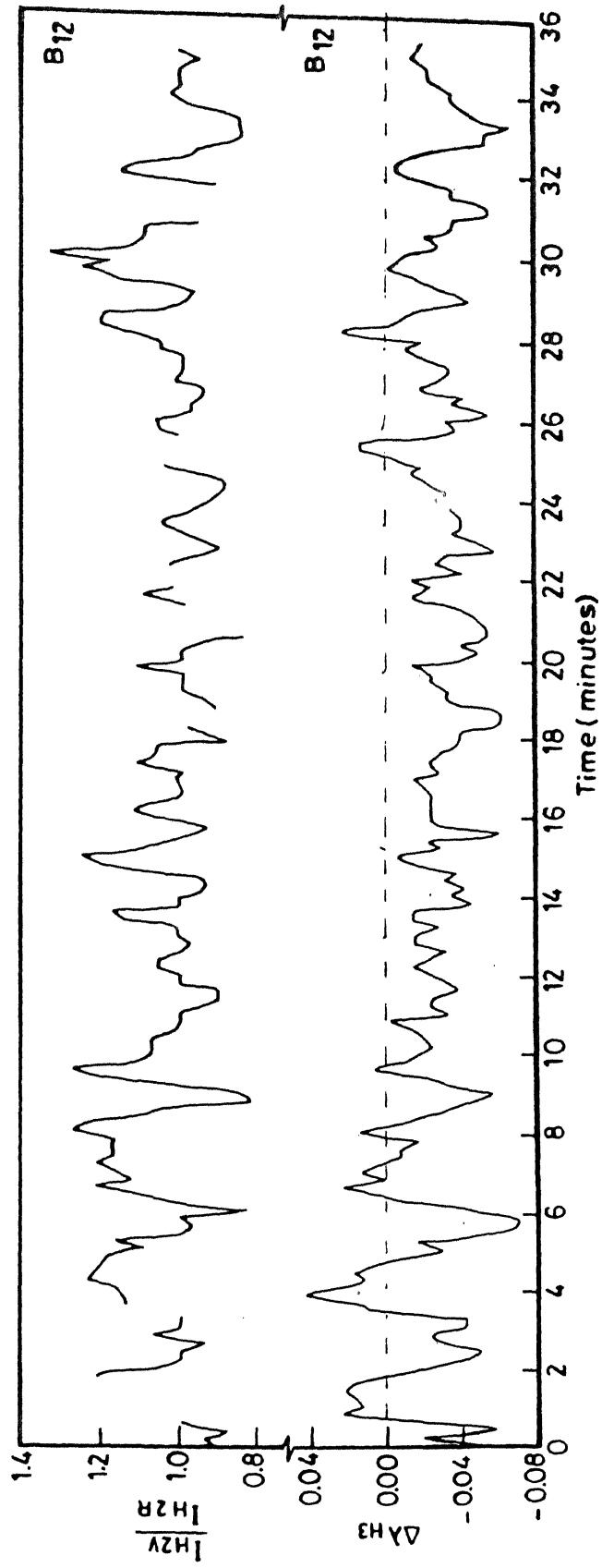
Fig.III.24 Phase relation between I_{H2V}/I_{H2R} and $\Delta\lambda_{H3}$ for the Class II bright point (B_{12}).

44
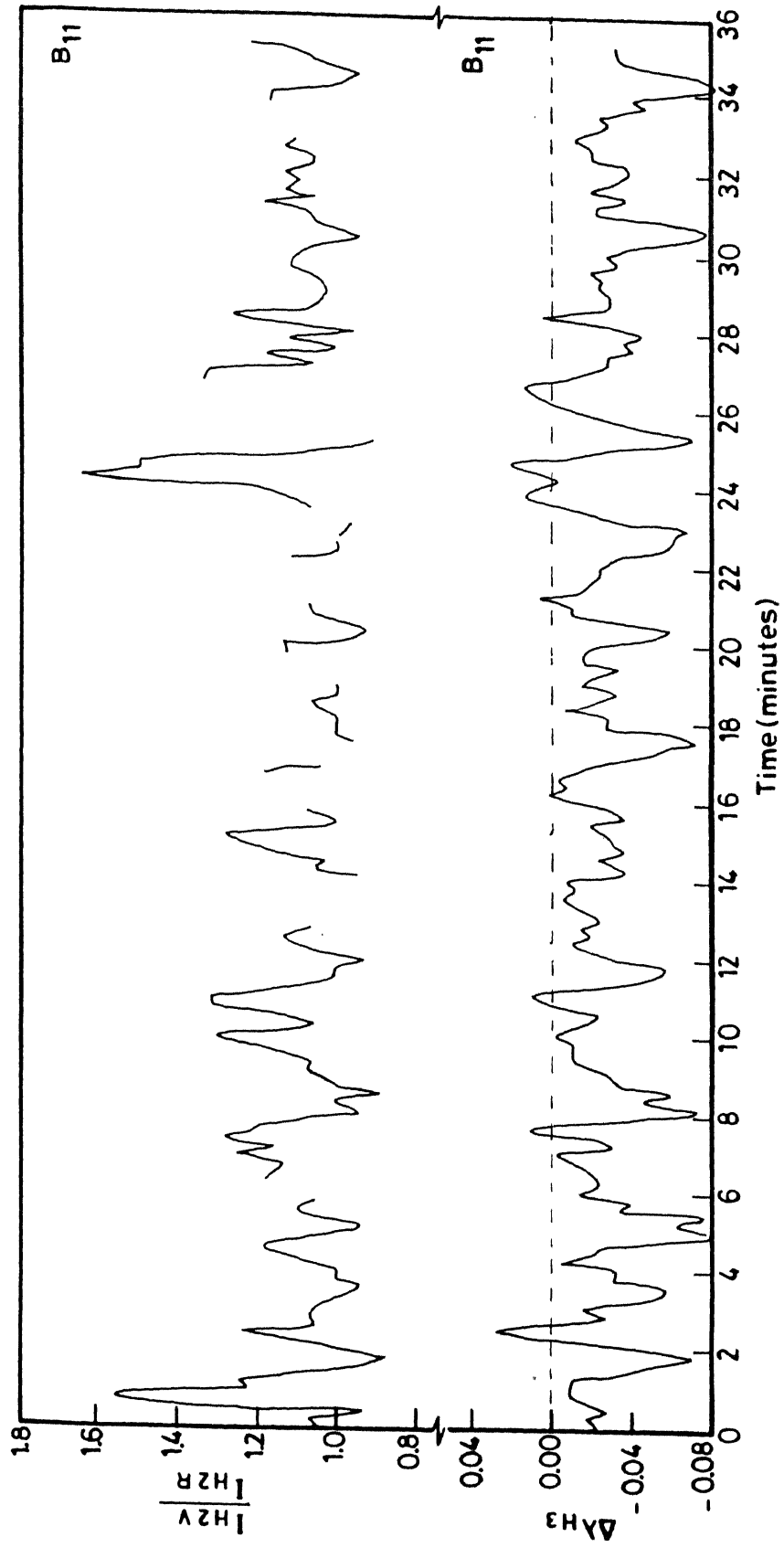
Fig.III.25 Phase relation between I_{H2V}/I_{H2R} and $\Delta\lambda_{H3}$ for the Class III bright point (B_{11}).

of H_{2V} and H_{2R} emission peaks (I_{H2V}/I_{H2R}) and also the Doppler displacements of H_3 absorption core $(\Delta\lambda_{H3})$ with reference to time are shown. Similar plots were obtained by Jensen and Orrall (1963)and by Orrall (1963) who brought out for the first time the oscillatory behaviour in the chromosphere using the CaII K line spectra. But their study, restricted to a few samples and exploratory in nature did not bring out the differences between one bright point to another. Fig.III.23 is for bright point B_5 (class I), Fig.III.24 is for B_{12} (class II) and Fig.III.25 is for B_{11} (class III). In class I, at the peak brightness phase, I_{H2V} is greatest while I_{H2R} is hardly recognisable. Hence on such occasions the value of I_{H2V}/I_{H2R} has not been derived. Simultaneous with the enhancement in brightness at the maximum phase in H_{2V} (I_{H2V}), the H_3 absorption core shows a large redward displacement which ranges from 5-6 km/sec. This obscures the emission in H_{2R} during this time, but when H_3 returns to its normal wavelength position, H_{2R} also regains its brightness. Knowing I_{H2V} and I_{H2R} for each of the profiles, the ratio of the emission (I_{H2V}/I_{H2R}) was derived. This ratio follows closely the pattern of oscillation of I_{H2V}. From Fig.III.23 it is seen that the Doppler shift in the H_3 absorption are well correlated with I_{H2V}/I_{H2R} i.e. the redward shifts in λ_{H3} are correlated with $I_{H2V}/I_{H2R} > 1$ and the violetward shifts of λ_{H3} are correlated with $I_{H2V}/I_{H2R} < 1$. These results are in conformity with those of Jensen and Orrall (1963) and Orrall (1966).

3.6 Close up view of the dynamical evolution of the line profile during the propagation of the main impulse

It would be interesting to have a close up view of the evolution of a bright point of Class I. The line profiles at the various epochs in the course of evolution of the bright point (e.g. B_5 of class I) presented in Fig.III.26 would help to illustrate the temporal evolution step by step.

The sequence of events can be described as follows:

i.   The profile at t=0 sec represents the profile in the undisturbed condition, which is the reference profile with H_{2V} and H_{2R} approximately of the same brightness levels.

ii.   At t=50 sec it does not look like the reference line profile any more. There is brightening in the far wings and the emission seen in H_{2V} or H_{2R} are submerged in the approaching brightness in the wings due the arrival of the impulse. Liu (1974) tentatively classified this as 'peculiar type' profile. It is seen that this type of profile occurs as a routine during the early stages of appearance of the travelling brightness enhancement.

iii.   At t=86 sec, the brightening has travelled towards H_{2V} and H_{2R} simultaneously.

iv.   At t=123 sec, the brightening has reached the H_2 level and H_3 shows a large redshift in wavelength. The emission in H_{2V} reaches the maximum brightness and the emission H_{2R} has been masked by the red shifted H_3 absorption and this results in a highly asymmetric profile.

47
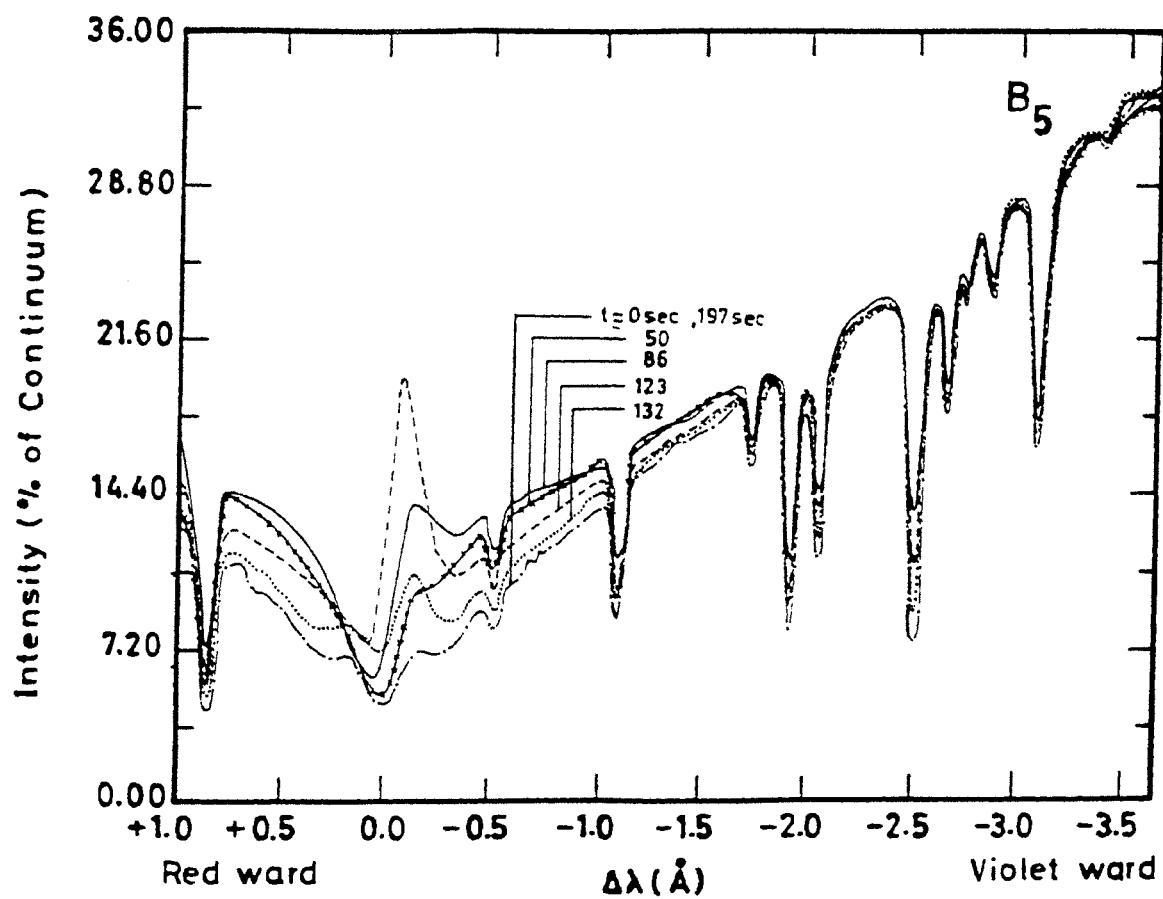
Fig. III.26 Close up view of the dynamical evolution of the H-line profile of Class I bright point (B_5) during the passage of the main impulse. See para 3.6, page 47 of text for description.

v.   At t=132 sec. the H_{2v} emission has faded and H_3 has returned to its normal wavelength position.   The dynamical phenomena described above has been observed by Punetha (1974); Liu (1974) and Cram and Dame (1983).

vi.   Finally at t=197 sec. the profile has returned to its undisturbed condition i.e. back to the reference profile as at t=0.   In many cases, the wing brightenings fade before the emission in the core (H_{2v} or H_{2R}) reaches its maximum brightness.

The bright points in Class II and Class III also exhibit similar phenomena but with reduced amplitudes of brightness enhancements.

The Doppler motions of the H_3, H_{2v} and H_{1v} during the passage of the main impulse have been measured and these are shown in Figs. III.27(a-c).   It can be seen from Fig. III.27(a) that as the H_{2v} emission (I_{H2v}) brightens during the passage of the main impulse, the core of H_3 shows systematically increasing redward shift ($\Delta\lambda_{H3}$) and attains a maximum value simultaneous with the maximum brightness phase of H_{2v} emission.   This Doppler motion quickly swings back to the normal wavelength position with the fall in brightness of H_{2v} emission, thus resembling a saw tooth pattern. H_{2v} emission peak itself exhibits a redward Doppler shift that mimics the Doppler shift in H_3 but with a lesser magnitude.   The maximum value of the redshifts in $H_3(\Delta\lambda_{H3})$ and H_{2v} ($\Delta\lambda_{H2v}$) are 7.7 km/sec and 5.3 km/sec respectively.   Whereas H_{1v} absorption shows a large violet shift (9.5 km/sec)during the passage of the impulse.   It can be argued that the asymmetries seen in the H_{2v} maxima and H_{1v} minima might give an illusion of a Doppler shift.
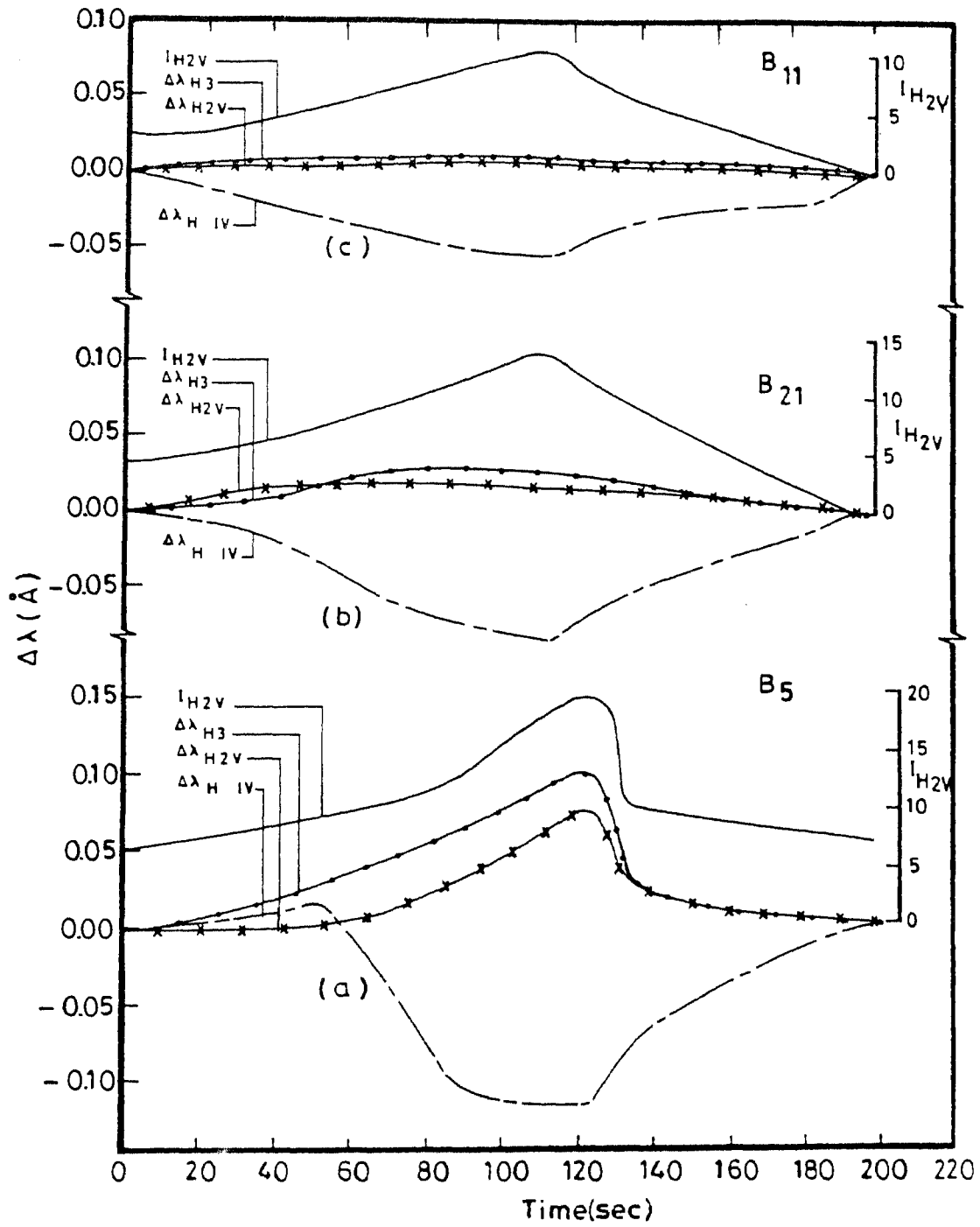
Fig. III. 27 Doppler motions in the wavelength positions of H_3, H_{2v} and H_{1v} during the passage of the main impulse for the three classes of bright points. (a)Class I (B_5) , (b)Class II (B_{21}) and (c)Class III (B_{11}). The redward displacements in H_3 and H_{2v} are simultaneous with the violet ward displacement in H_{1v}.

50

However, if one interprets the change in the position of the H_{2v} emission peak and H_{1v} minima as Doppler shifts, then the values for these shifts would be what are measured here. Looking at Fig. III.27(a) one gets the impression that the H line forming layers are compressed by the approaching layers H_3, H_2 and H_1. This would enhance the temperature and alter the opacity significantly compared to the ambient values. The same pattern of events also occur during the passage of the main impulse in the class II and class III bright points (shown in Figs. III.27(b) and III.27(c)). These occur with correspondingly smaller amplitudes.

3.7 The spatial and temporal coherence in the behaviour of the bright points

The plots of I_{H2V} versus time (Figs. III.2, III.3 and III.4) suggest that the intensity oscillations in the bright points (say B_3 & B_5 or B_1 & B_2) exhibit a certain amount of coherence. To examine this in detail, the correlation coefficients were worked out for a number of pairs of bright points using the digital data. The correlation coefficients were also computed by displacing the data chain of one bright point against the other (up to 5 steps) in steps of 12 secs which is the digitizing interval. The results are presented in Table 4. It is seen that there is a suggestion of a weak correlation (ranging from 20% to 40%) between the wave trains of two bright points that are within a distance of 8-10 arc sec, the exceptions being B_{16} & B_{22}

51

Table 4

Phase coherence and the correlation co-efficients of the bright points

Bright points	Dist. betn. in arc sec	Correlation co-efficient (r) Phase shift, Δt (sec)					
		0	12	24	36	48	60
B_{22} & B_{28}	200.00	0.10	0.20	**0.39**	0.30	0.20	0.10
B_{17} & B_{19}	76.00	0.1	0.15	0.30	0.28	**0.35**	0.20
B_{3} & B_{5}	20.85	0.10	0.11	**0.46**	0.25	0.15	0.09
B_{1} & B_{2}	3.00	0.25	**0.45**	0.25	0.28	0.20	0.30
B_{12} & B_{13}	3.05	**0.60**	0.10	0.25	0.10	0.15	0.10
B_{12} & B_{14}	7.10	0.25	0.12	0.15	**0.45**	0.20	0.20
B_{13} & B_{14}	3.05	0.22	0.20	**0.35**	0.10	0.10	0.20
B_{10} & B_{11}	5.70	0.20	0.32	**0.45**	0.28	0.21	0.15
B_{9} & B_{10}	3.70	0.18	0.20	**0.35**	0.30	0.20	0.18
B_{8} & B_{9}	3.00	0.20	**0.38**	0.30	0.22	0.18	0.10
B_{12} & B_{21} *	10.00	0.11	0.17	**0.23**	0.16	0.12	0.09
B_{15} & B_{16} *	2.86	0.41	**0.55**	0.35	0.28	0.20	0.13
B_{16} & B_{22} *	2.86	0.15	0.22	**0.40**	0.38	0.26	0.18
B_{22} & B_{29} *	11.44	0.11	0.18	0.22	0.35	0.48	**0.60**
B_{24} & B_{32} *	2.50	0.18	0.21	**0.38**	0.27	0.22	0.15
B_{25} & B_{17} *	2.14	0.08	0.12	0.13	0.20	0.26	**0.28**
B_{27} & B_{28} *	14.30	0.10	0.11	0.13	0.20	**0.38**	0.25
B_{29} & B_{23} *	4.30	0.10	0.15	0.18	0.30	**0.50**	0.35
B_{30} & B_{31}	2.50	0.·18	0.21	**0.38**	0.27	0.22	0.15

* The I_{H2V} plots of these bright points combination are not displayed here but the digitized values are used for calculating the correlation co-efficients.

; B_{25} & B_{17}; B_{29}& B_{23}. But there is no case of a bright point pair where the correlation is 20% or above when the distance between them is 10 arc sec or more. These results taken by themselves can not support unambiguously the existence of a coherence over a distance of 8-10 arc sec which is reminiscent of the mesogranular structure at the photospheric levels (Sivaraman,1973, November et al 1981,1982). But these results along with the evidence provided by Dame and Martic (1987) for the existence of such cells derived from the coherent behaviour of bright points using a long sequence of K-line filtergrams suggest that cells similar to the mesogranular cells possibly exist at these levels in the chromosphere.

3.8   Intensity oscillations in the network boundary regions

Among the 32 sample locations analysed, two (B_4 and B_{18}) lie on the network boundaries. The reduction of the line profiles for these locations were done exactly similar to that adopted for the inner network bright points. A plot of the line parameters derived for B_4 and B_{18} are shown in Figs. III.28 to III.32. The raw plots of I_{H2v} for B_4 and B_{18} show intensity fluctuations with periods approximately 0.5 to 1.5 min. Superposed on this is a quasi-sinusoidal pattern with a period 5-7 minutes. To uncover this period, a 5 point smoothing was applied to the raw data of the I_{H2v} plots of B_4 and B_{18}. The 5 to 7 minute oscillations then stand out. These are seen in these histogram
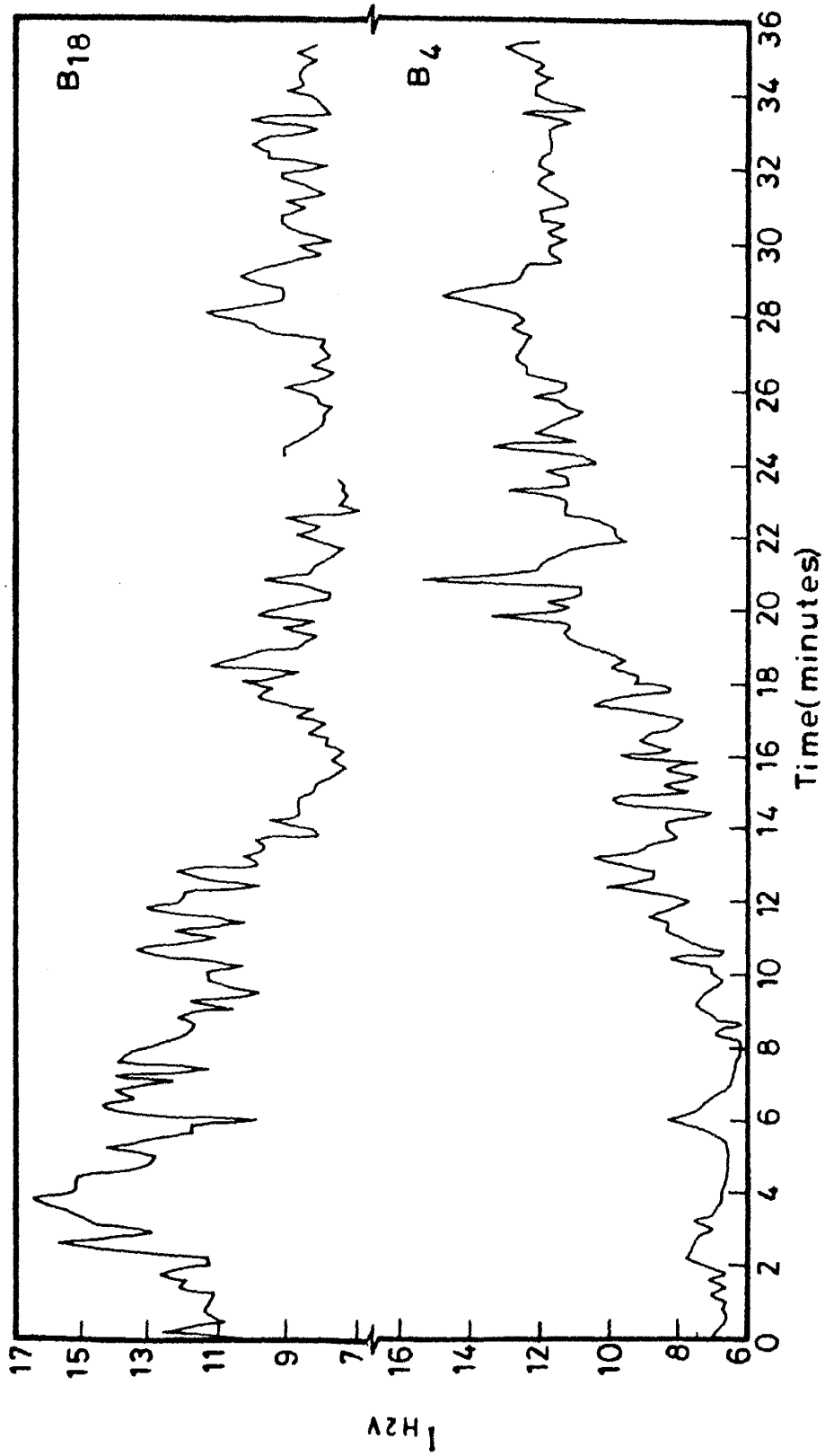
Fig.III.28 The temporal variations in I_{H2v} for the two locations on the network boundaries (B_4 and B_{18}).
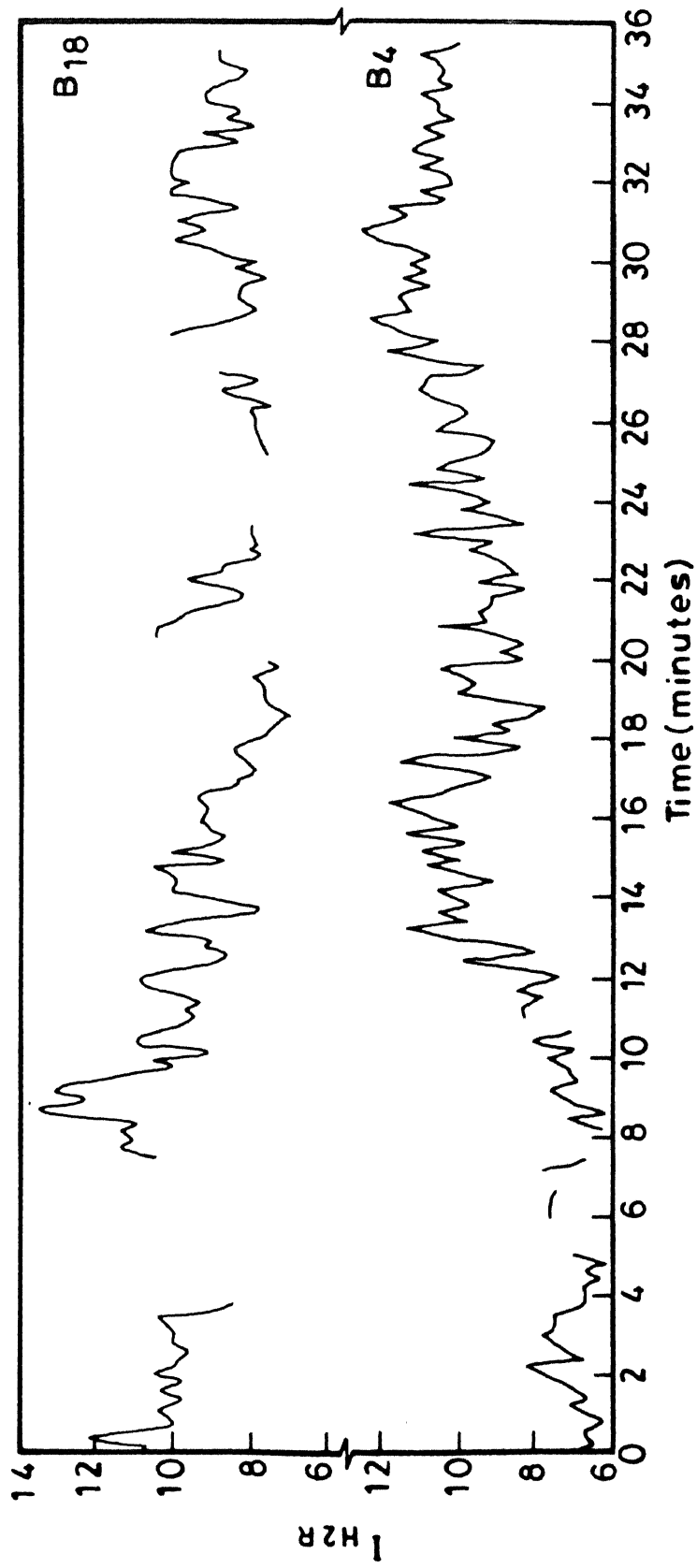
Fig.III.29 Temporal variations in I_{H2R} in the network boundary locations (B_4 and B_{18}).
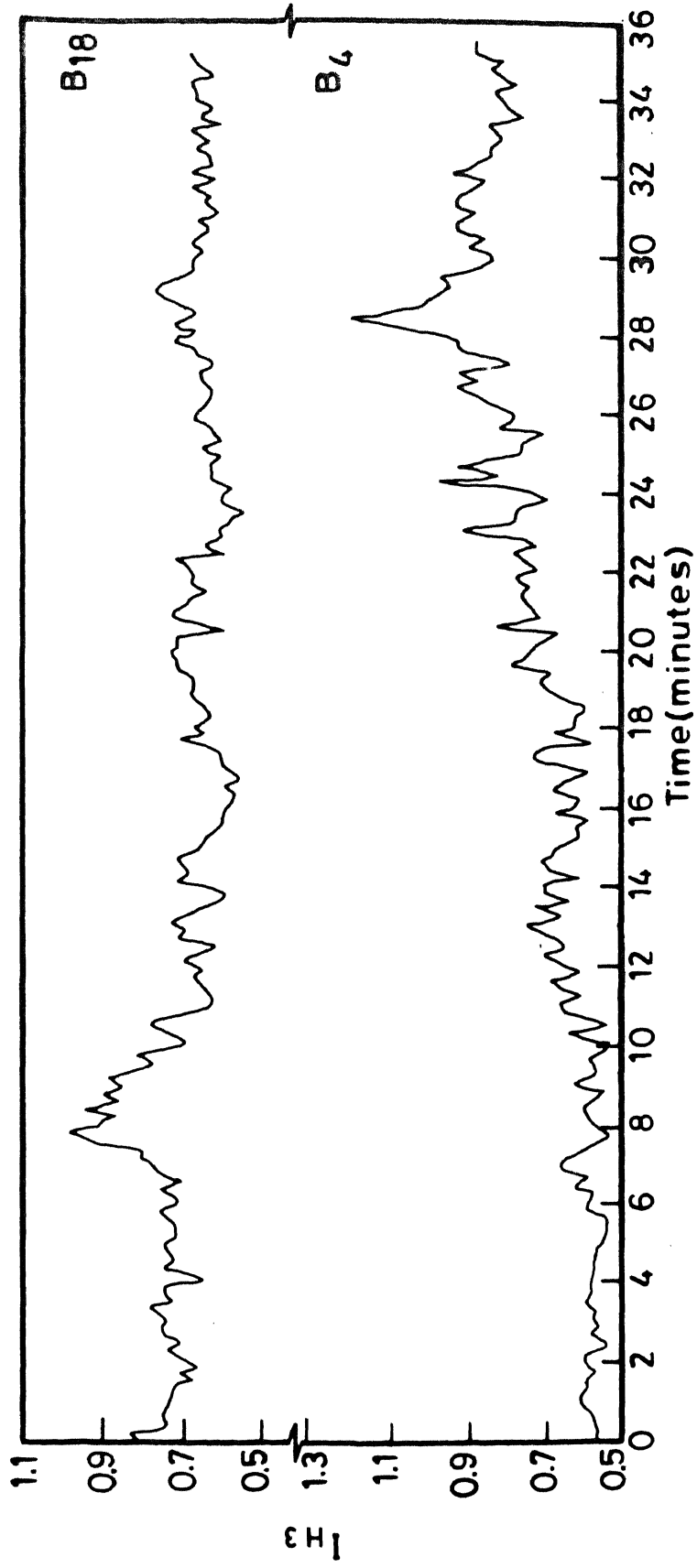
Fig. III.30 Temporal variations in I_{H3} in the network boundary locations (B_4 and B_{18}).
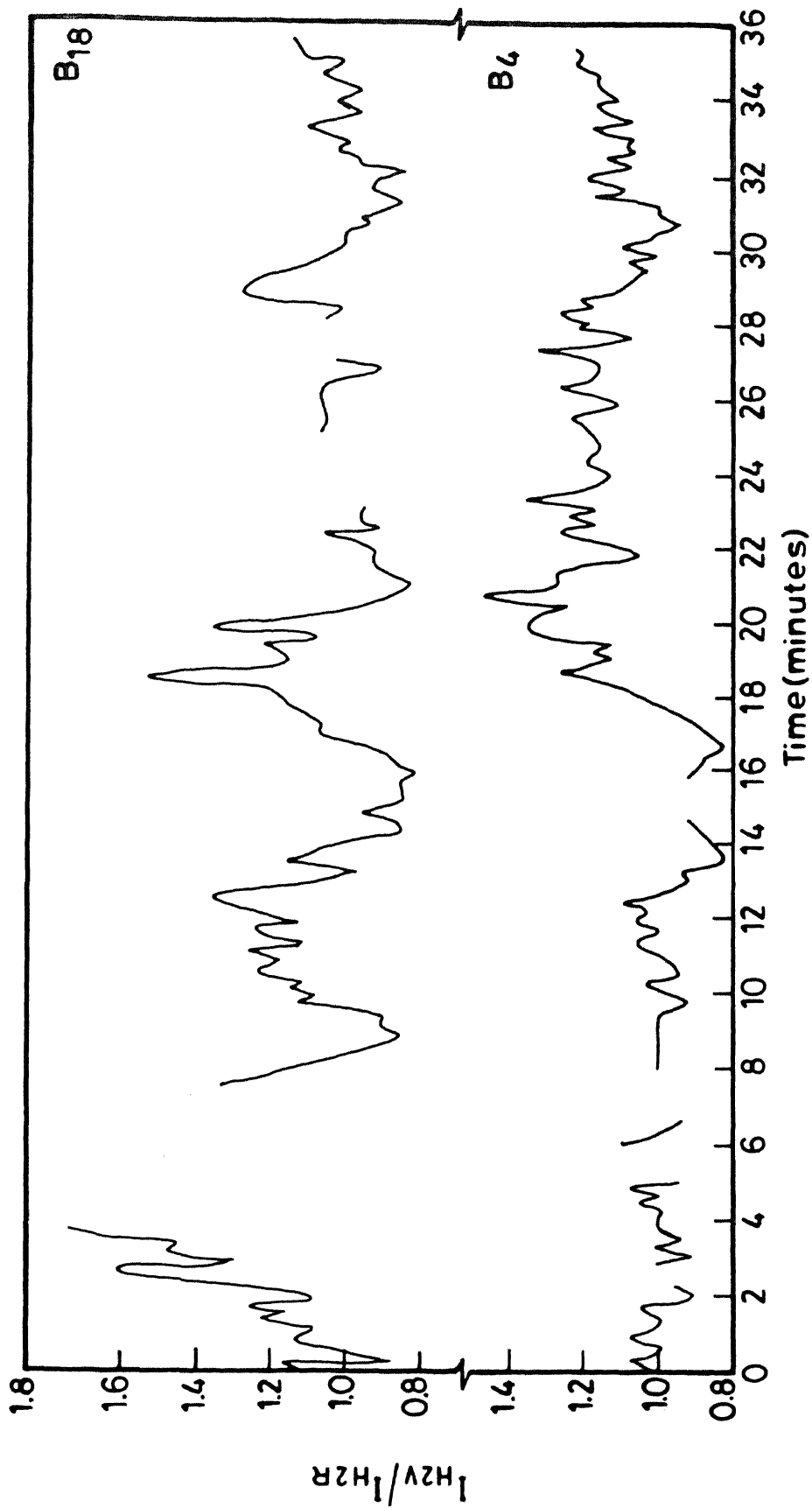
Fig.III.31 Temporal variations in I_{H2V}/I_{H2R} in the network boundary locations (B_4 and B_{18}).
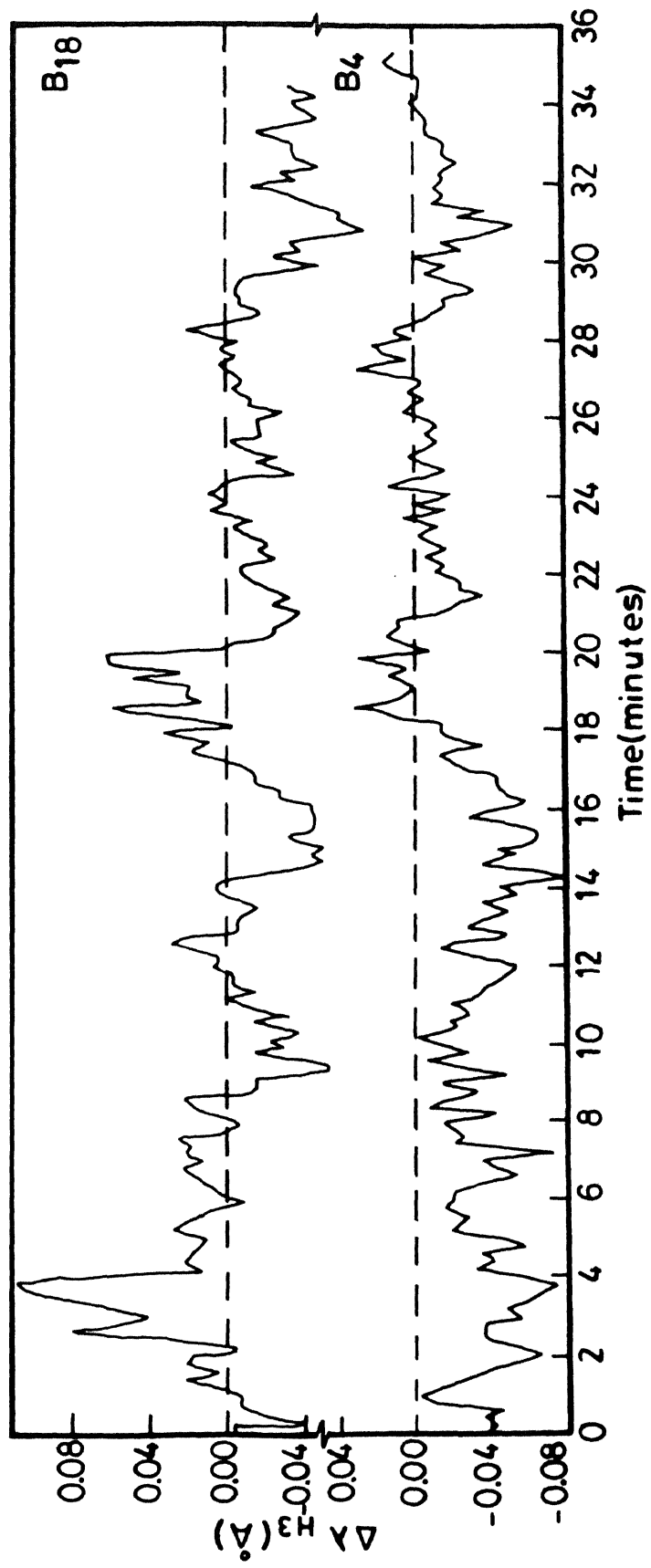
Fig.III.32 Temporal variations in $\Delta\lambda_{H3}$ in the network boundary locations (B_4 and B_{18}).
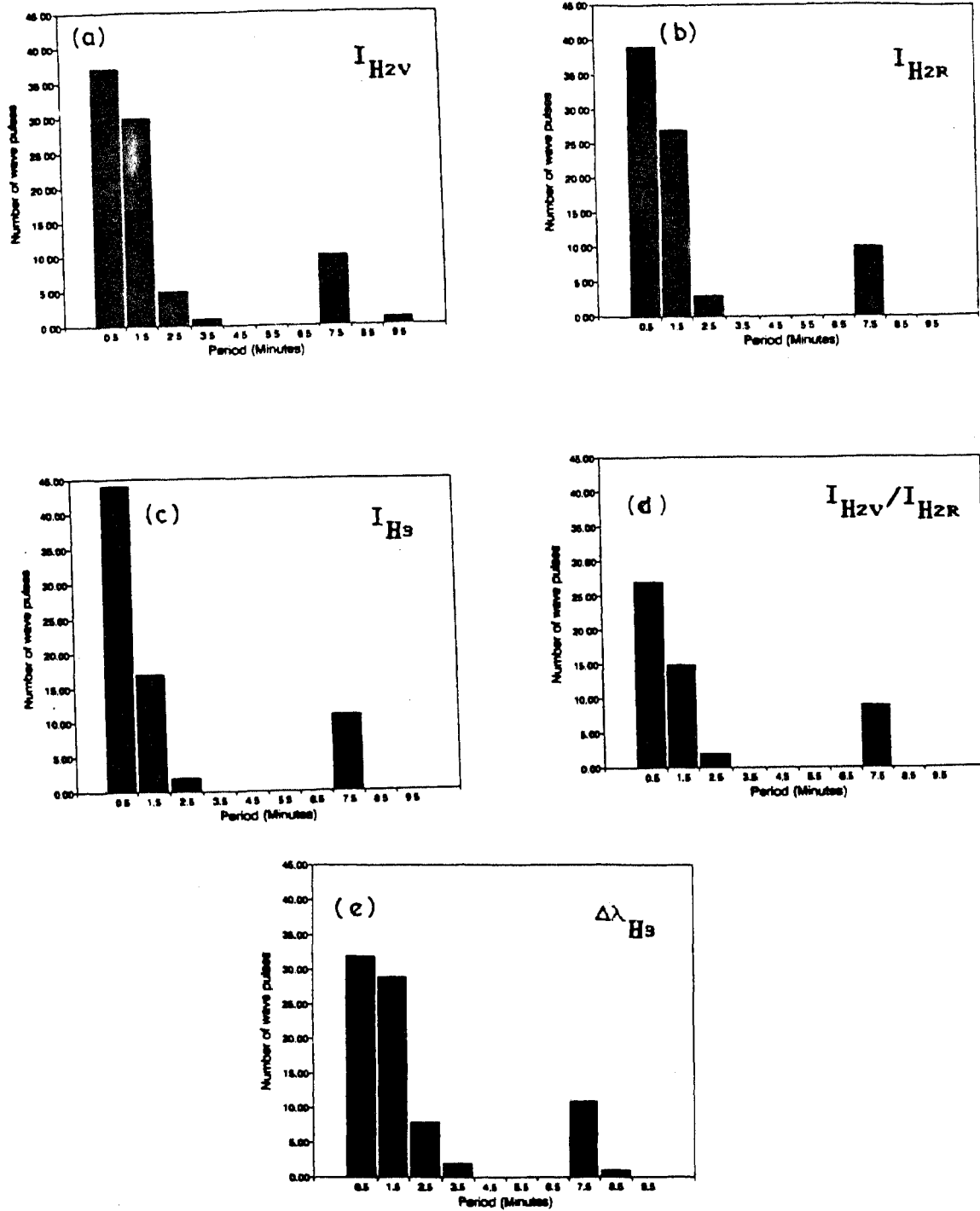
Fig.III.33 Histogram plots to illustrate the periodicity of oscillations for the five parameters of the H-line profile (a)I_{H2v}, (b)I_{H2R}, (c)I_{H3}, (d)I_{H2v}/I_{H2R} and (e)$\Delta\lambda_{H3}$ for the two network boundary locations. There are two sharp peaks in all the 5 parameters: one is around 1 minute and the other one is around 7 minutes.

plots (Fig. III.33) where the smaller period dominates because of their larger numbers. It is not clear whether these short excursions are real and if real whether they represent the ejections of spicules from the network boundaries. But the long period oscillations (5 to 7 min) appear to be characteristic of the network boundary elements. Similar periodicity is seen in the other parameters I_{H2R}, I_{H3}, I_{H2V}/I_{H2R} ,and $\Delta\lambda_{H3}$ also Figs. III.29 to III.32. Cram and Dame (1983) make a mention of the large period oscillations on the network boundaries. Thus the network boundaries also exhibit intensity oscillations like the bright points but with a periodicity much higher. This itself could be taken as an evidence to argue that the mechanism of heating in the two cases are dissimilar.

CHAPTER IV

PROPERTIES OF THE MAIN IMPULSE, FOLLOWER PULSES, ENERGY BUDGET FOR THE

HEATING OF THE CHROMOSPHERE

4.1 Properties of the main impulse and the follower pulses

In the previous chapter, the plots of I_{H2v} versus time (Figs. III 1 to III.4) show that the characteristic common to the bright points which have been examined is that there occurs a main impulse with an enhancement of brightness 4 or more times the normal level. This main impulse is the carrier of the energy and transports it upwards in the solar atmosphere. The main impulse is followed by several pulses , most commmonly 8 to 10 pulses for the energetic bright points. The amplitude of the main impulse is far higher than the amplitudes of the follower pulses in all the three classes, but the amplitude of the main impulse itself is highest for class I, lower for class II and lowest for class III bright points. An examination of the amplitudes of the follower pulses suggests an exponential decay. An exponential function has been fitted for B_1, B_5, B_{17}, B_{19} (Fig. IV.1). Similarly, exponential functions have been fitted for B_{15} and B_{21} of class II and B_9 and B_{11} of class III. These exponential function fits are presented in Table. 4.
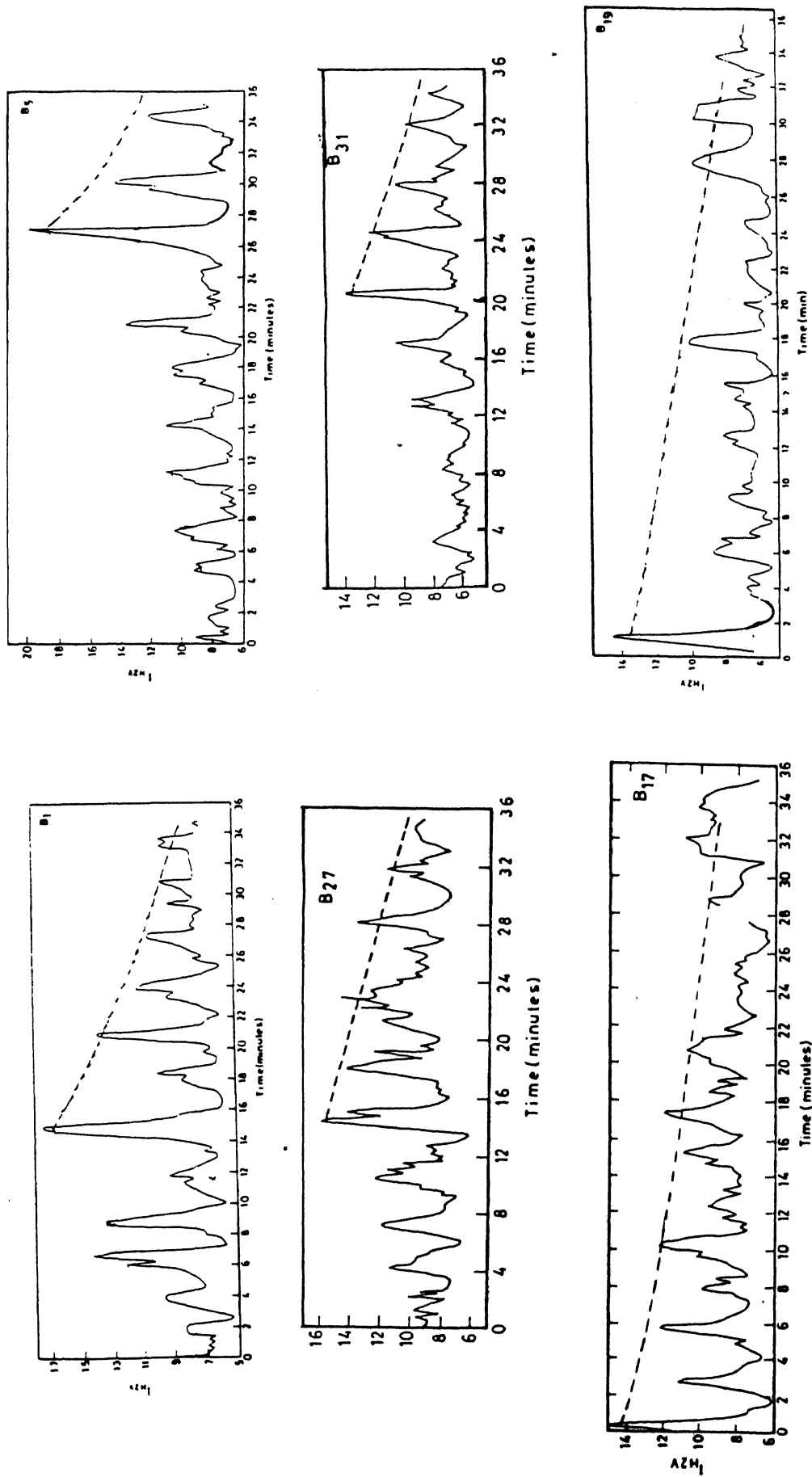
Fig.IV.1 An exponential function fitted for the brightness decay of the main impulse and the follower pulses for the bright points B_1 B_5, B_{27}, B_{31} B_{17} and B_{19}. The exponential equations are tabulated in Table4. The slopes are more or less the same.

61

Table 5

Exponential decay in the amplitudes of the follower pulses

Class	Bright point	Exponential Function $I(t)$
Class I	B_1	$16.69\ \mathrm{Exp}(-5.9 \times 10^{-4}t)$
	B_5	$18.89\ \mathrm{Exp}(-4.9 \times 10^{-4}t)$
	B_{17}	$14.63\ \mathrm{Exp}(-3.2 \times 10^{-4}t)$
	B_{19}	$13.66\ \mathrm{Exp}(-3.7 \times 10^{-4}t)$
	B_{22}	$15.21\ \mathrm{Exp}(-4.6 \times 10^{-4}t)$
	B_{27}	$15.84\ \mathrm{Exp}(-3.3 \times 10^{-4}t)$
	B_{28}	$19.87\ \mathrm{Exp}(-3.5 \times 10^{-4}t)$
	B_{31}	$13.58\ \mathrm{Exp}(-4.9 \times 10^{-4}t)$
Class II	B_{12}	$11.78\ \mathrm{Exp}(-3.2 \times 10^{-4}t)$
	B_{15}	$11.48\ \mathrm{Exp}(-5.6 \times 10^{-4}t)$
	B_{21}	$12.44\ \mathrm{Exp}(-2.4 \times 10^{-4}t)$
Class III	B_9	$12.20\ \mathrm{Exp}(-4.7 \times 10^{-4}t)$
	B_{11}	$10.90\ \mathrm{Exp}(-3.9 \times 10^{-4}t)$

It is seen that their slopes are nearly the same for the bright points in the 3 classes and it is possible to represent the exponential decay in the amplitudes reasonably well for the 3 classes by one parameter namely 4.14×10^{-4}, which is the mean slope of all the values. Liu's (1974) plots (his Figures 6b and 6c) also show the main impulse and the exponential decay of the follower pulses. An exponential fit done to his data from his Figures 6b & 6c, turn out to be 3.6×10^{-4} and is comparable to the values presented in Table 5. This suggests that the main impulse (with a period $190 \stackrel{+}{-} 10$ sec) is the perturbing disturbance which throws the medium into resonating mode seen as the follower pulses with identical period as the exciting impulse itself. The main impulse has a quasi-sinusoidal appearance, but when examined in detail, shows a saw tooth shape. The follower pulses also tend to show a saw tooth shape although this becomes less apparent after a few pulses. The main impulse of bright points (B_1 and B_5 ; Fig. IV.3) are plotted on a large scale to bring out the slow rising time and fast falling time. It is also clear that the main impulses of class II and class III do not have a saw tooth shape ; even in the class I the saw tooth shape becomes measurable only when the main impulse is very energetic i.e. has a large amplitude of intensity enhancement (e.g. B_1 and B_5). The main impulses of B_{17} and B_{19} are not very energetic and do not show this. Liu's plots (Figures 6b and 6c) also shows that the main impulse has a saw tooth shape. The rise time and the fall time for the bright points (B_1, B_5, B_{28}, B_{12}, B_{13}, B_8 and B_{10}) are presented in Table. 6.
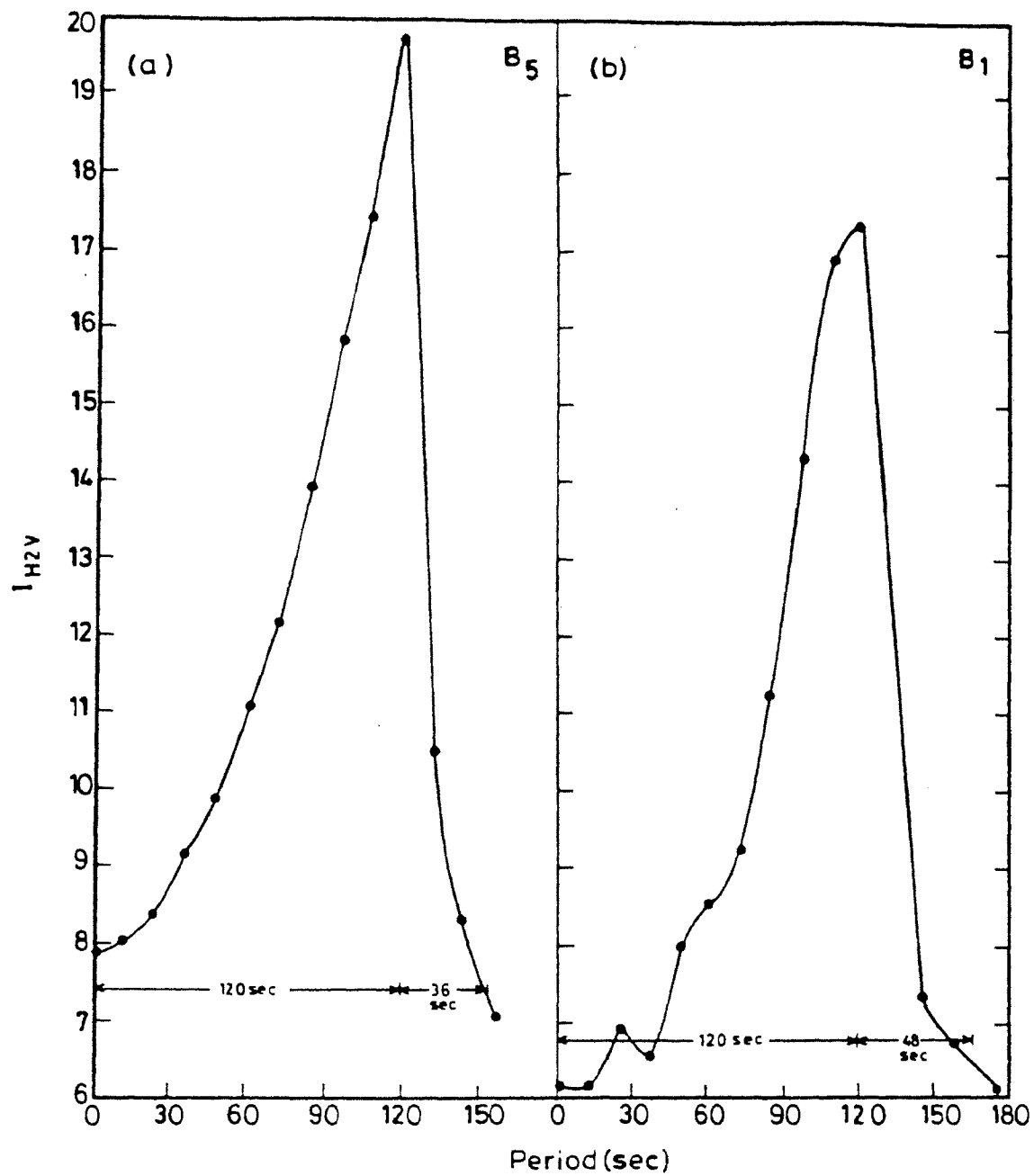
Fig. IV.2   Saw tooth nature of an energetic main impulse of the bright points B_1 and B_5.   The rising time is more compared to the falling time.   The rising and falling times are 120 sec and 48 sec for B_1 and 120 sec and 36 sec for B_5.

Table.5

The rising and falling times of the main impulse to
illustrate the saw tooth nature

Class	Bright point	Rising time (sec)	Falling time (sec)
ClassI	B_1	120	48
	B_5	120	36
	B_{28}	84	60
ClassII	B_{12}	72	72
	B_{13}	96	96
ClassIII	B_8	72	72
	B_{10}	84	84

It is also obvious that although all the main impulses of class I
bright points are not of the same amplitudes, they have the same
periods namely 190 ± 10 sec. Also for the follower pulses the
amplitudes decrease exponentially, but still the periods for all of
them cluster around the value of 190 ± 10 sec. This is true for the
main impulses and the follower pulses of the other two classes also.
Thus the period is nearly constant and is independent of the amplitudes
of the pulses.

4.2 Energy budget and the heating of the solar chromosphere

It is obvious that the main impulse is the carrier of the energy.
The extra energy delivered by the main impulse over the energy flux of
the background has been computed by the two methods described below:

Method 1.   The area covered by the main impulse was evaluated from the I_{H2v} plots.   These I_{H2v} plots are themselves in percent of the continuum.   The flux value of 4.49×10^{10} ergs/cm^2/A/sec for the smoothed continuum at 3950A was adopted from Labs and Neckel (1968) to express these flux values in absolute flux units (ergs/cm^2/sec).   The normal value of the flux of H_{2v} averaged over a region shown as NN[1] (Fig. IV. 3) was then subtracted from the flux calculated for the main impulse.   This difference is the extra energy carried by the main impulse.   The energy flux values thus evaluated for many bright points are presented in Table. 6.

Table. 6

Energy flux in the main impulses

Class	Bright point	Energy flux $\times 10^9$ ergs/cm^2/sec	
		Method 1	Method 2
ClassI	B_1	1.91	2.26
	B_2	1.75	1.85
	B_5	2.30	2.40
ClassII	B_{13}	1.11	1.21
	B_{14}	1.12	1.25
ClassIII	B_9	1.35	1.22
	B_{11}	0.59	0.49
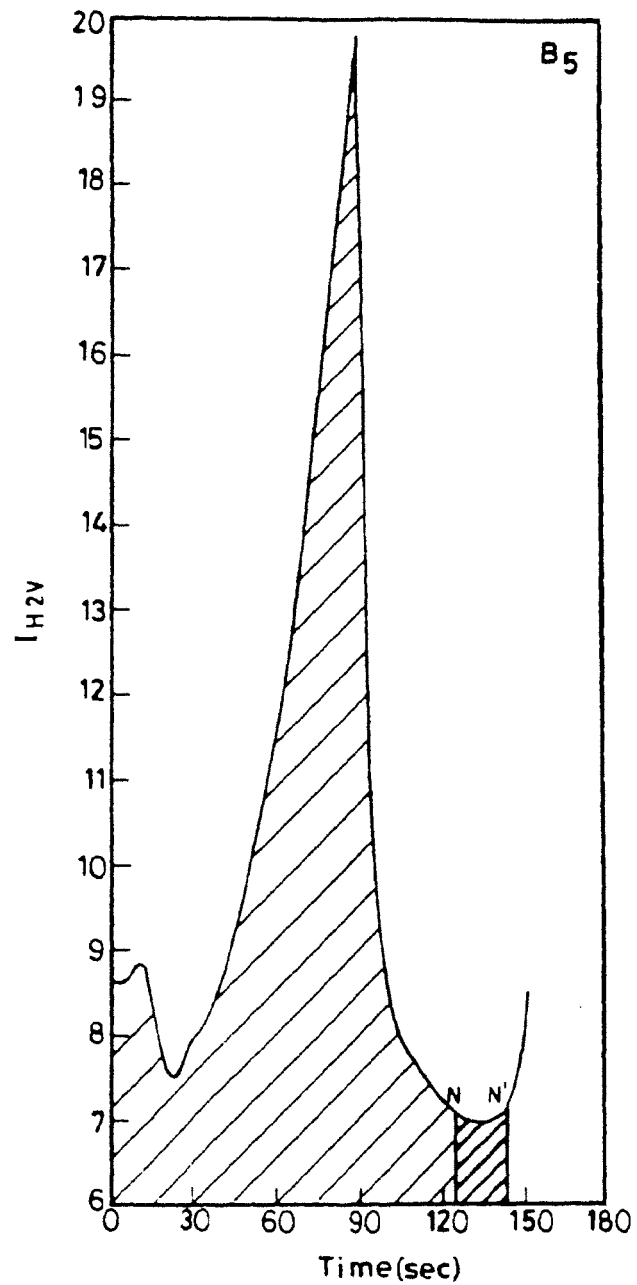
Fig. IV.3 The I_{H2v} curve of the main impulse of the bright point B_5. The shaded region is the area measured to calculate the energy flux above the reference profile. NN^1 is a small region that represents the reference profile.

67

Method 2. The area enclosed by the H-line profile (when H_{2v} is at its peak brightness) was evaluated over a 1A pass band. These profiles have their intensities expressed in terms of the continuum. This can be called as the 1A H-index (Fig. IV.4). This area was then converted in to energy flux (ergs/cm^2/sec) by using the Labs and Neckel (1968) flux values. The energy contained in a reference profile was evaluated in the same way. The difference between the two was reckoned as the energy transported by the main impulse. The values of the energy flux so obtained from several profiles are also tabulated in Table.6.

The energy flux values derived from the two methods match well. Cram and Dame (1983) derived energy flux values similar to our method.2 with a difference. They determined the energy emitted from the difference between the average profile of all their observations and the average profile of the lowest decile. This is incorrect as the main impulse is the carrier of the energy and the follower pulses are only the resonant oscillations of the medium.

The energy delivered by all the bright points over the entire visible hemisphere of the sun was estimated as follows:

The number counts of the bright points over a large number of networks was made from an excellent spectroheliogram obtained at the Mc Math telescope of the Kitt Peak National Observatory. It is seen that on an average within each network there are 9 to 10 bright points and these are distributed approximately in equal numbers among the three classes. These numbers agree well with the number counts made from the

68
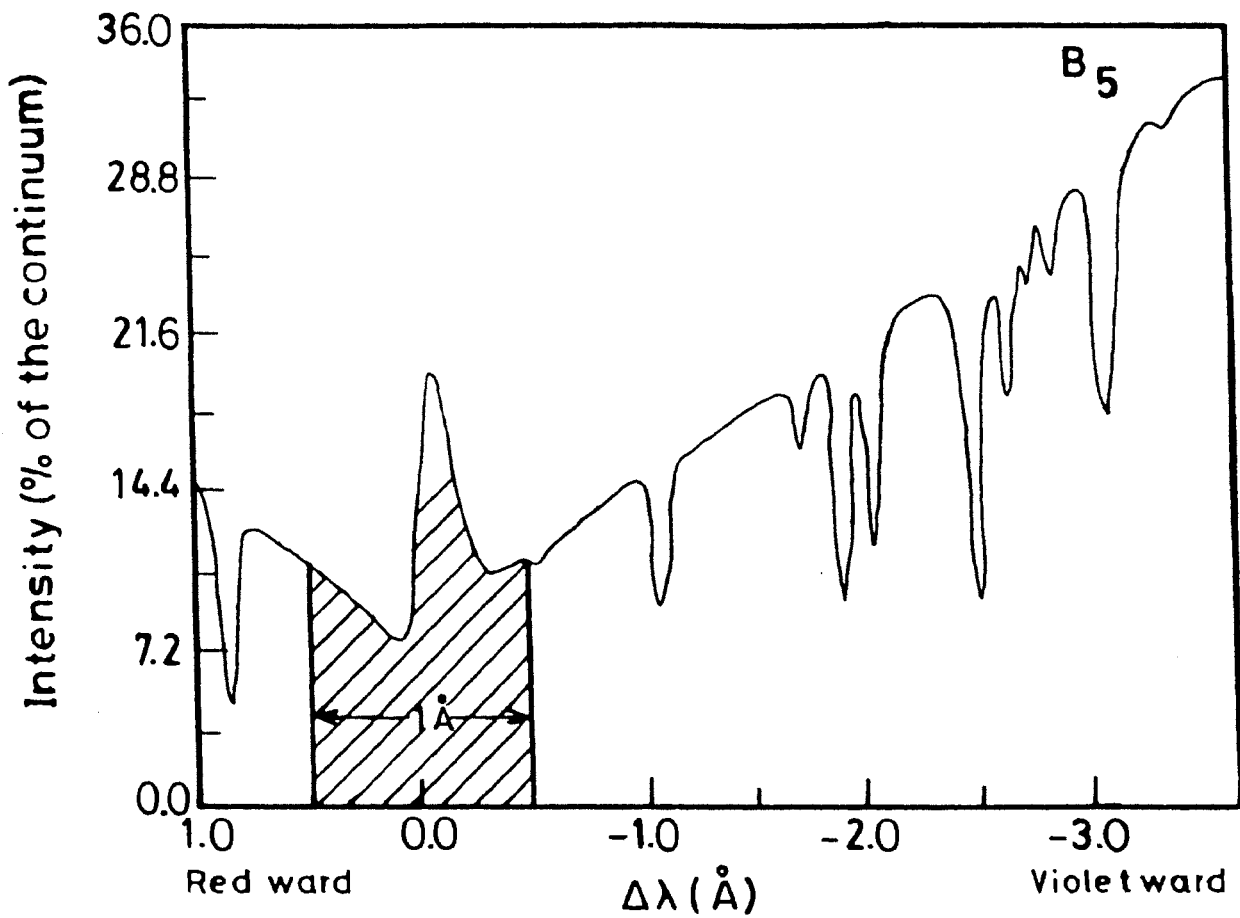
Fig. IV.4 H-line profile of the bright point(B_5) when the energetic main impulse reached the H_{2v} level. The shaded region represents the flux in the 1Å pass band in terms of the continuum brightness. The energy flux contained in the 1Å pass band (1Å H index) is the excess energy in shaded area over a reference profile.

spectroheliogram in 1600A continuum obtained by the NRL group (Bonnet et al 1982).

The mean energy per bright point,belonging to any of the three classes is $= 10^9$ ergs/cm^2/sec approximately. By assuming that the size of a bright point = 1.5 arc sec.

Energy associated with one bright point $= 10^9 \times \pi \times (1.5)^2/4$ ergs/sec.

Number of bright points over the entire solar surface $\sim 10^4$.

$E_{\text{Total for all bright points}}$ $= 10^{13} \times \pi (1.5)^2/4$ ergs/sec.

This energy when smeared over the area of the visible hemisphere of the sun would give the energy in ergs/cm^2/sec on the sun contributed by all the bright points.

Area of the visible hemisphere of the sun $= 2\pi \times (31 \times 60)^2/4$ arc sec.

The total energy from all the bright points when smeared over the area of the visible hemisphere of the sun,

$$= 10^{13} \times (1.5)^2/2(31 \times 60)^2$$
$$= 32.5 \times 10^5 \text{ ergs/cm}^2/\text{sec.}$$

The estimates of the energy in the bright points may seem to be optimistic, as all the 10^4 bright points do not deliver energy simultaneously and all the time. Only when they are in the main impulse phase do they radiate energy. Thus the number of bright points which participate in delivering energy at any one time would be less than the number used here. However only the average value of the energy per bright point has been used here although the most energetic ones deliver as much as 2-3 times this average energy value. To make the estimate still conservative, we may suppose that at any one time only about 1/4 th of the total number will deliver the energy.

Thus the energy delivered by all the bright points in the H-line

$$=8.1 \times 10^5 \text{ ergs/cm}^2/\text{sec}.$$

Since a similar amount of energy is delivered by these bright points in the K-line also, the total energy radiated = $1.6 \times 10^6 \text{ergs/cm}^2/\text{sec}.$

The total energy delivered by the network elements in temperature minimum (T_{min}) region is estimated to be ~ $7.5 \times 10^6 \text{ergs/cm}^2/\text{sec}$ (Cook and Ewing, 1990). If it is assumed that only about 1/4 of this energy will be delivered by the H and K lines together, the contribution from the network elements would be = $1.8 \times 10^6 \text{ergs/cm}^2/\text{sec}.$

Thus the total amount of energy carried by the bright points and the network together = $3.4 \times 10^6 \text{ergs/cm}^2/\text{esc}.$ This matches well with the model calculations by Anderson and Athay (1989b) according to which $3.8 \times 10^6 \text{ergs/cm}^2/\text{sec}$ is the energy dissipated by the CaII ions. Thus the bright points are the sites where substantial heating takes place and the main impulses transport this energy. The energy in the bright points provide half the energy necessary to maintain the quiet chromosphere and the other half is contributed by the network elements. The detailed calculations of Anderson and Athay (1989a and 1989b) show that this energy exactly balances the radiative losses in the chromosphere by CaII ions.

Liu (1974) estimated the energy flux in the wave from the r.m.s velocity amplitude and the phase speed of the waves which the intensity enhancements propagate through the atmosphere. He then assumed that

71

the waves were acoustic and calculated the group velocity and the energy flux. This fell short of the flux estimated by the empirical model of Vernazza, Avrett and Loeser (1981) by a factor of 2. The energy estimates made here fully satisfy the energy requirements for the heating of the quiet chromosphere.

The chromosphere is highly structured and can be identified with the atmosphere inside the bright points. With their association with magnetic fields, these can be considered as magnetic flux tubes. The main impulse is a sort of compressional wave that propagates vertically along the flux tube and carries the energy to the chromosphere and provides the energy for its heating. In the case of the class I bright points the value of the magnetic fields are high and most likely to be in the range of 40 to 80 gauss spread over a linear scale size of ~ 2 arc sec. The observations are seeing limited and so the fields would definitely be more when the real linear size of a bright point is less (~ 1 arc sec or even less) as can be seen from the UV spectroheliograms.

The 3-minute oscillations exhibited by the bright points have been interpreted as the visible manifestation of the 3-minute waves which heat up the chromosphere. It has been shown in this study that the bright points provide 50% of the energy budget required for the chromospheric heating. The remaining half is provided by the network boundaries (Cook and Ewing 1991). There is general agreement that the waves in the bright points are acoustic (Kalkofen, 1989) and the

theoretical models aim at explaining how these long period waves can travel in the chromosphere. Kalkofen (1989) has put forward several arguments in support of this idea. Many of these models are hydrodynamic in nature and ignore the point that the bright point can have magnetic fields and hence influence the propagation characteristics. The phase velocity (V_o) of propagation of the main impulse has been calculated from the time lapse between the appearances of the brightening at the levels of H_{1v} and H_{2v} knowing the difference in the heights between these two levels. The difference in the heights of H_{1v} and H_{2v} from the model of Vernazza, Avrett and Loeser (1981) is 575 km and the time lag measured from our spectra is 24 sec.

This gives us a value of $V_o=24$ km/sec.

Now if V_A is the Alfven velocity and C_s is the sound speed then $V_A^2=V_o^2-C_s^2$ (Priest, 1982). If it is assummed that the temperature of the region of formation of the H_2 line is $6000^{\circ}K$ (Vernazza, Avrett and Loeser, 1981), then C_s turns out to be 7.06 km/sec using the relation $C_s= KT/m_H$ (Preist, 1982 and Anderson and Athay, 1989). Inserting the values of V_o and C_s in $V_A^2= V_o^2-C_s^2$ it is found that $V_A =22.2$ km/sec.

Now assuming that the magnetic field of a bright point of class I is ~ 80 gauss (Sivaraman and Livingston, 1982) and using the above value of 22.20 km/sec for V_A in the relation $V_A^2 = B^2/4\pi\rho$ (Gibson, 1972 and Zirin, 1988), the density turns out to be $\rho = 1.04 \times 10^{-10} gm/cm^3$. This density is ~ 3 times the value of the model of Vernazza, Avrett and Loeser (1981). But it must be emphasised that the Vernazza, Avrett and Loeser (1981) model is only a mean model for the chromosphere and does not describe the medium within a bright point or a flux tube. Thus it turns out that inside the bright points (or flux tubes) at least of class I, it is a combination of Alfven and

acoustic waves with a predominance of the Alfven wave that propagates whereas when the magnetic fields become weaker (as in class II and particularly class II bright points) the propagation is mainly by acoustic waves.

CHAPTER V

SUMMARY OF THE RESULTS AND CONCLUSIONS

In this work the time sequence spectra in the CaII H line is analysed to examine the characteristics in the course of evolution of the bright points within the network regions. This spectra was obtained on September 13, 1971 at the Vacuum Tower Telescope (VTT) of the Sacramento Peak Observatory, New Mexico under high spatial and temporal resolution and pertain to a quiet region at the centre of the solar disc.

From the 5664 line profiles the H line parameters for 30 bright points and 2 network boundary regions were dervied. These were plotted versus time for the 35 minutes duration of the sequence. The results arrived at from the analysis of these profiles can be summarised as follows:

1). The plot of I_{H2v} (intensity of the H_{2v} emission) versus time (Fig.III 1-4) show that there occurs a main impulse which is followed by several impulses of smaller amplitudes. Based on the pattern of the main impulse and the follower pulses, the bright points can be classified into three classes.

Class I. Those bright points that show very large intensity enhancement in H_{2v} (I_{H2v}) at their brightest phase (the main impulse) as high as 4 to 5 times the normal value (Figs.III.1 and III.2).

Class II. Those bright points that show moderate (2-3 times the

75

normal value) intensity enhancement in H_{2v} (I_{H2v}) at the maximum brightness phase (Fig. III. 3).

Class III. Those bright points that show only a marginal increase in intensity in H_{2v} (I_{H2v}) at the brightest phase (Fig. III. 4).

2). The 'main impulse' is followed by 8-10 smaller pulses with exponentially decreasing brightness. It is seen that there are similarities and differences among the three classes. There are about 8 to 10 follower pulses in the case of class I whereas for class II and class III 4 to 6 follower pulses are seen to be most common. It has been customary to describe one cycle of the chromospheric oscillation in terms of a 'typical profile' (Punetha ,1974 ;Liu ,1974 and Durrant ,Grossmann-Doerth, and Kneer ,1976). But it is seen from this study that there is no single typical profile of a bright point that can describe the evolution fully; there are more than one variety of profiles. This study shows that the large variety of profiles can be brought broadly under the three classes described above.

3). The plot of I_{H2v} versus time (Figs. III(1-4) and their histograms (Figs. III. 17-19 and power spectra (Figs. III(20-22) show that the bright points exhibit oscillations in brightness with a period of 190 $\pm$ 10 sec. These are the well known 3-min chromospheric oscillations. The period of the brightness oscillations is 190 $\pm$ 10 secs in all the three classes (Figs. III. 17-19) and thus is independent of the magnitude of the brightness enhancement. The main impulse and the following pulses have the same periods.

4). The energetic main impulses have a saw tooth shape (Fig. IV. 35). The follower pulses also tend to show a saw tooth shape although this becomes less apparent after a few pulses. The less energetic of the main impulses tend to become sinusoidal and so are the pulses following them.

The period is nearly constant and is independent of the amplitudes of the pulses.

5). The rate of decrease in amplitude of the pulses following the main impulse are more or less similar for all the three classes and it is found that a common exponential fit can describe all of them fairly well.

6). The main impulse which propagates upward is the carrier of the energy for the heating of the chromosphere and the bright points are the sites where intense heating takes place.

7). It is hypothesised that the magnitudes of the enhancements in brightness of the main impulses of the 3 classes are closely linked with the magnetic field associated with each bright point location i.e. the bright points located in a region of strong magnetic field will have the main impulse with high intensity enhancement whereas the bright points located in a region of weaker fields will have the main impulse itself much weaker.

8).   The study of the Doppler motions of H_3, H_{2v} and H_{1v} of the line profiles during the passage of the main impulse gives the impression that the H line forming layers are compressed by the approaching layers H_3, H_2 and H_1 (Figs. III.27).   This would enhance the temperature and alter the opacity significantly compared to the ambient values.   The same pattern of events are seen in Class II and class III with correspondingly smaller amplitudes.

9).   The temporal variations in the brightness at the network boundary regions exhibit oscillations of longer periods of the order of 5 to 7 minutes (Fig. III.28-33).   Thus the network boundaries also exhibit intensity oscillations like the bright points but with longer periods. This itself could be taken as an evidence to argue that the mechanism of heating in the two cases are dissimilar.

10).   The total energy contained in the bright points was estimated by two methods and this energy flux together with that contributed by the network elements (3.4×10^6 ergs/cm^2/sec) match well with the energy estimated in the model calculations by Anderson and Athay (1981) which is 3.8×10^6 ergs/cm^2/sec for CaII ions.   Thus the bright points are the sites where substantial heating takes place and the main impulses transport this energy.   It is shown in this work that the bright points provide 50% of the energy budget required for the chromospheric heating.   The remaining half is provided by the network boundaries (Cook and Ewing ; 1991).

11). From the time lag between the appearance of the main impulse at the H_{1V} and H_{2V} levels and the differences in their heights in the chromosphere it is seen that the phase velocity (V_o) is ~ 24 km/sec. The estimation of phase velocity (V_o), the Alfven velocity (V_A) and the sound speed (C_S) within a bright point shows that V_A is very large (22.20 km/sec) for class I bright point where the magnetic fields are high. For class II and class III , V_A would decrease with a corresponding increase in C_S. This leads to picture that inside the class I bright points which have higher magnetic fields there is a combination of Alfven and acoustic waves with a predominance of the Alfven wave whereas when the magnetic fields become weaker (as in class II and particularly class III bright points) the propagation is mainly by acoustic waves.

What more needs to be done?

The results presented in this thesis pertain to the heating of the chromosphere by wave train at the sites of the bright points which form

a fundamental entity in the solar (and stellar) chromosphere(s). Some of the interesting questions that can be asked now are :

i.   How are the main impulses seen in the bright point generated? Are they from exploding granules or is there a piston action from below which injects energy and drives it upward through these magnetic pipes?

ii.   To answer these, one should know before hand where are the foot points of these bright points anchored in the photosphere? How are they located in reference to the photospheric granulation? For these high quality spectral observations lasting for 2 to 3 hours would be required in the H or K line region and with simultaneous granulation pictures and velocity measurements at the photospheric levels. Such long duration observation would call for the use of the C.C.D. cameras at the focal plane in the place of photographic film. This would give data with better signal to noise ratio and higher dynamical range.

iii.   It would be worth while to ascertain the causal relation between the bright points and the inner network photospheric magnetic fields. Again the use of a C.C.D. camera for obtaining the narrow band filtergrams in H_{2v} or K_{2v} emission and simultaneous magnetic observations would help to establish this relation.

iv.   It would be necessary to choose a larger sample for the network locations (as done for the bright points) and examine the intensity oscillations in them so that their properties can uniquely be understood the way it has been done for the bright points.

v.   Another feature that should be studied to the same detail is the dark whiskers.   Are these new features or only the unresolved background chromosphere? Can a bright point occur at a site previously occupied by a whisker?

Answer to these questions have to be sought for a fuller understanding of the quiet chromosphere of the sun and the late type of stars.

REFERENCES

Anderson, L.S. and Athay, R.G. 1989a, Ap.J. **336**, 1089.

Anderson, L.S. and Athay, R.G. 1989b, Ap.J. **346**, 1010.

Athay, R.G. 1963, The solar spectrum, ed. C.de Jager (Dordrecht, Holland, D.Reidel Publ. Co.), p.151.

Athay, R.G. 1985, In Chromospheric Diagnostics and Modelling ,ed. B.W.Lites (NSO),P67.

Babcock, H.W. and Babcock, H.D., 1955, Ap. J. **121**, 349.

Bappu, M.K.V. and Sivaraman, K.R., 1971, Solar Phys. **17**, 316.

Beckers, J.M., 1968, Solar Phys. 3, 367.

Beckers, J.M., Mauter, H.A. Mann, G.R.and Brown,D.R.: 1972, Solar Phys. **25**, 81.

Biermann, L., 1946, Naturwiss, **33**, 118.

Biermann, L., 1948, Zs.f.Ap., **25**,161.

Bonnet,R.M.,Bruner,M.,Acton,L..,Brown,W.A.,Decaudin,M,and Foing,B.:1982, Atron.Astrophys. **111**,125.

Cook, J.W. and Ewing J.A. 1990, Ap.J. **355**, 719.

Cook, J.W. and Ewing J.A. 1991, Ap.J. **371**, 804.

Cram, L.E. and Dame', L., 1983, Ap. J. **272**, 355.

D'Azambuja, L. 1930, Ann. Obs. Paris, Meudon **8**, Part 2.

Dame', L. and Martic, M. 1988, IAU Symposium No.123, p433.

Durrant,C.J ,Grossmann-Doerth,U. and Kneer,F.J. 1976, Astr.Ap. **51**,95.

Edmonds Jr.F.N.,Michard,R. and Servajaean, R. 1965, Ann. Astrophys. **28**,534.

Evans,J.W. and Michard,R. 1962, Ap.J. **136** ,493.

Gibson, E.G.,1972,The Quiet Sun ,NASA,P212.

Hale, G.E. and Lilerman, F. 1904, Ap.J. **19**, 41.

Jager,C.de and Kuperus, M. 1961, Bull. Astron. Inst. Neth. **16** ,71.

Jensen, E. and Orrall, F.Q. 1963, Ap.J. **138**,252.

Kalkofen, W. 1989a, Ap. J. (Letters), **346**, L37.

Kalfofen, W., 1989b, Proc. IAU Symposium No.142, Basic Plasma processes on the sun, 1989, ed. E.R. Priest and V.Krishan, Kluwer Academic publfcations, P.197.

Kurerpus, M. 1965, Recherches Astronomiques de L' Observatoire D' Utrecht, XVII.

Kuperus, M. 1969, Astrophysics Space Sci. Rev. 9 ,713.

Labs,D. and Neckel,H. 1968, Zs.f.Ap. 69,1.

Leighton, R.B., 1961, Nuovo Cimento Suppl. **22**, 321.

Leighton, R.B., Noyes, R.W. and Simon, G.W., 1962, Ap. J. **135**, 474.

Lighthill, M.J. 1952, Proc. R. Soc. London **A211**, 564.

Lighthill, M.J. 1954, Proc. R. Soc. London **A222**, 1.

Lighthill, M.J. 1967, Aerodynamic Phenomena in Stellar Atmospheres I.A.U. Symposium No.**28**, p429.

Liu, S.Y., 1974, Ap. J. **189**, 359.

Mitchell,S.A.,1935 ,Columbia University Press, New York, p142.

Moore, D.W., and Spiegel, E.A. 1964, Ap.J. **139**, 48.

November, L.M., Toomre, J. Gebbie, K.B. and Simon, G.W. 1981, Ap. J. (Letters), **245**, L23.

November, L.M., Toomre, J. Gebbie, K.B. and Simon, G.W., 1982, Ap. J. **258**, 846.

Orrall,F.Q.,1966, Ap.J. **143** ,917.

Osterbrock, D.E. 1961, Ap.J. **134**, 347.

83

Priest, E. R. 1982, Solar Magnetohydrodynamics (Dordrecht: Reidel Publ. Co.).

Proudman, I. 1952 , Proc. R. Soc. London **A214** , 119.

Punetha, L.M. 1974, Bull. Astron. Inst. Czechoslovakia, **25**, 207.

Schatzman, E. ,1949, Ann.Astrophys. **12**,203.

Schwarzchild, M. , 1948, Ap.J. **107**, 1.

Sivaraman, K.R., 1972, Ph.D. Thesis , University of Kerala.

Sivaraman, K.R., 1973, Sol. Phys. **33**, 333.

Sivaraman, K.R. and Livingston, W.C., 1982, Solar Phys. **80**, 227.

Simon, G.W. and Leighton, R.B. 1964, Ap. J. **140**, 1120.

Skumanich, A.; Smythe, C. and Frazier, E.N., 1975, Ap. J. **200**. 747.

Smith, E. v.p. 1960, Ap. J. **132**, 202.

Stein, R.F. 1967, Sol. Phys. **2** ,385.

Stein, R.F. 1968, Ap.J. **154**, 297.

Stein, R. F. and Leibacher, J, 1981, In : The Sun as a star, ed. S.D. Jordan (NASA : Monograph Series on Nonthermal Phenomena in Stellar Atmospheres, p289.

Thomas, R. 1957, Ap. J. **125**, 260.

Title, A.M. 1966, Selected Spectroheliograms, Caltech, Pasadena, Calif.

Title A.M.,Shine R.A. Tarbell T.D. Topka K.P. and Scharmer G.B. IAU Symposium No.138 ,Solar Photosphere:Structure,Convection and Magnetic Fields Ed.Stenflo,J.O., Kluwer Academic Publishers ,P49.

Ulmschneider, P. 1986, Adv. Space Res. **6**, No.8 ,39.

Ulmschneider, P. 1989, Astron. & Astrophys.

Vernazza, J.E., Avrett,E.H. and Loeser,R. 1981,Ap. J. Suppl.**45**, 635.

Whitaker, W.A. 1963, Ap.J. **139** ,914.

White, O.R. and Suemoto, Z. 1968, Solar Phys. 3, 523.

Zirin, H. 1988,Astropysics of the Sun, Cambridge University Press,P48.

Appendix I

The plots of the CaII H line parameters I_{H2R} ,I_{H3} , I_{H2V}/I_{H2R} and $\Delta\lambda_{H3}$ for the three classes Figs. III.5 to III.16.
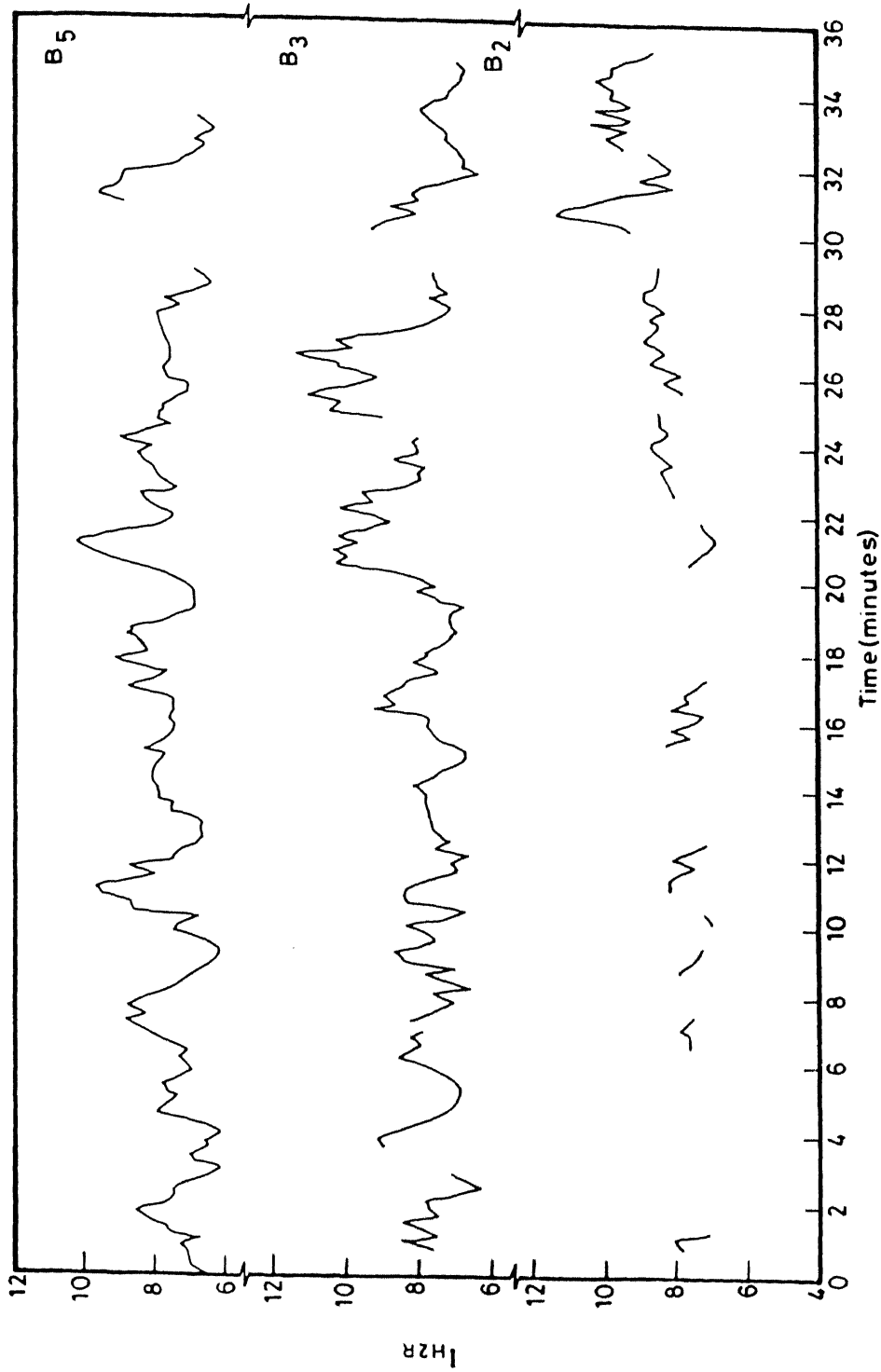
Fig.III.5 Temporal variation in the intensity of H_{2R} emission peak (I_{H2R}) for Class I bright points. On occasions when the redward shifts of H_3 absorption are large the H_{2R} emission is not recognisable. The break in the curves indicate the H_{2R} is not measurable in the profile.
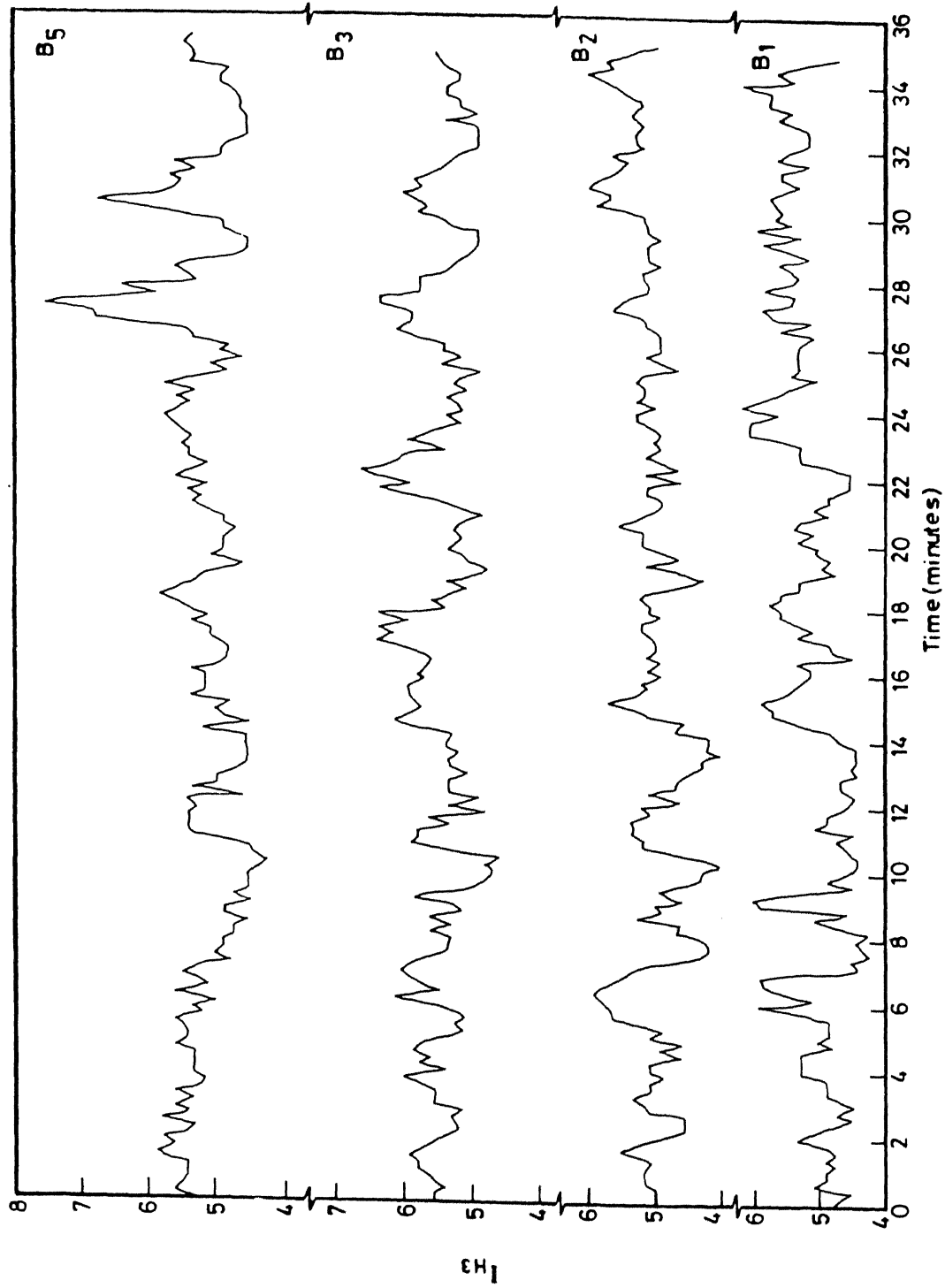
Fig.III.6 Temporal variation in the intensity of H_3 (I_{H_3}) absorption core for Class I bright points. The 190 sec intensity oscillations are identical to the oscillations in H_{2v} (Fig.III.2).
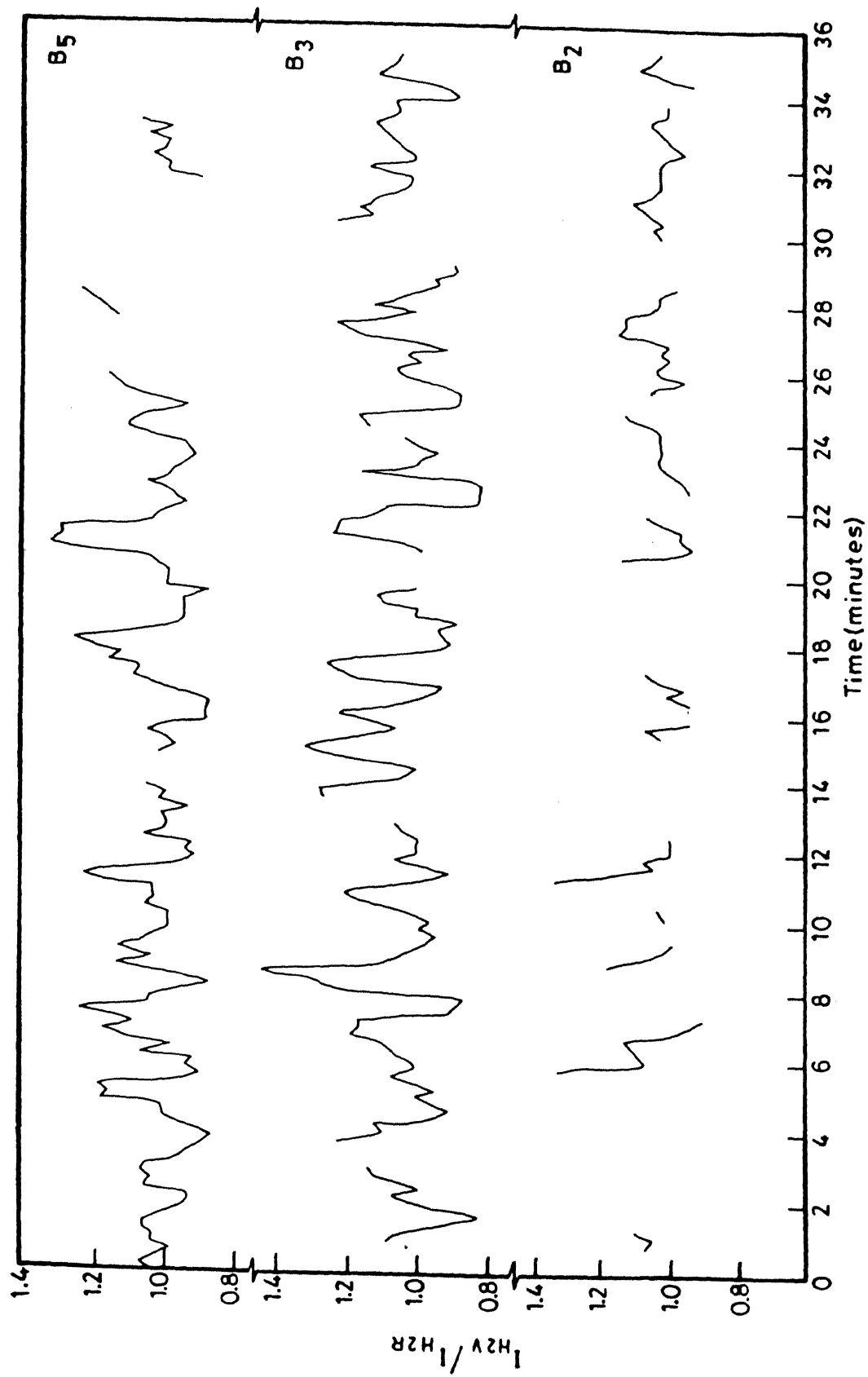
Fig.III.7 Temporal variation of the ratio of the emissions in H_{2v} and H_{2R} (I_{H2V}/I_{H2R}) for Class I bright points.
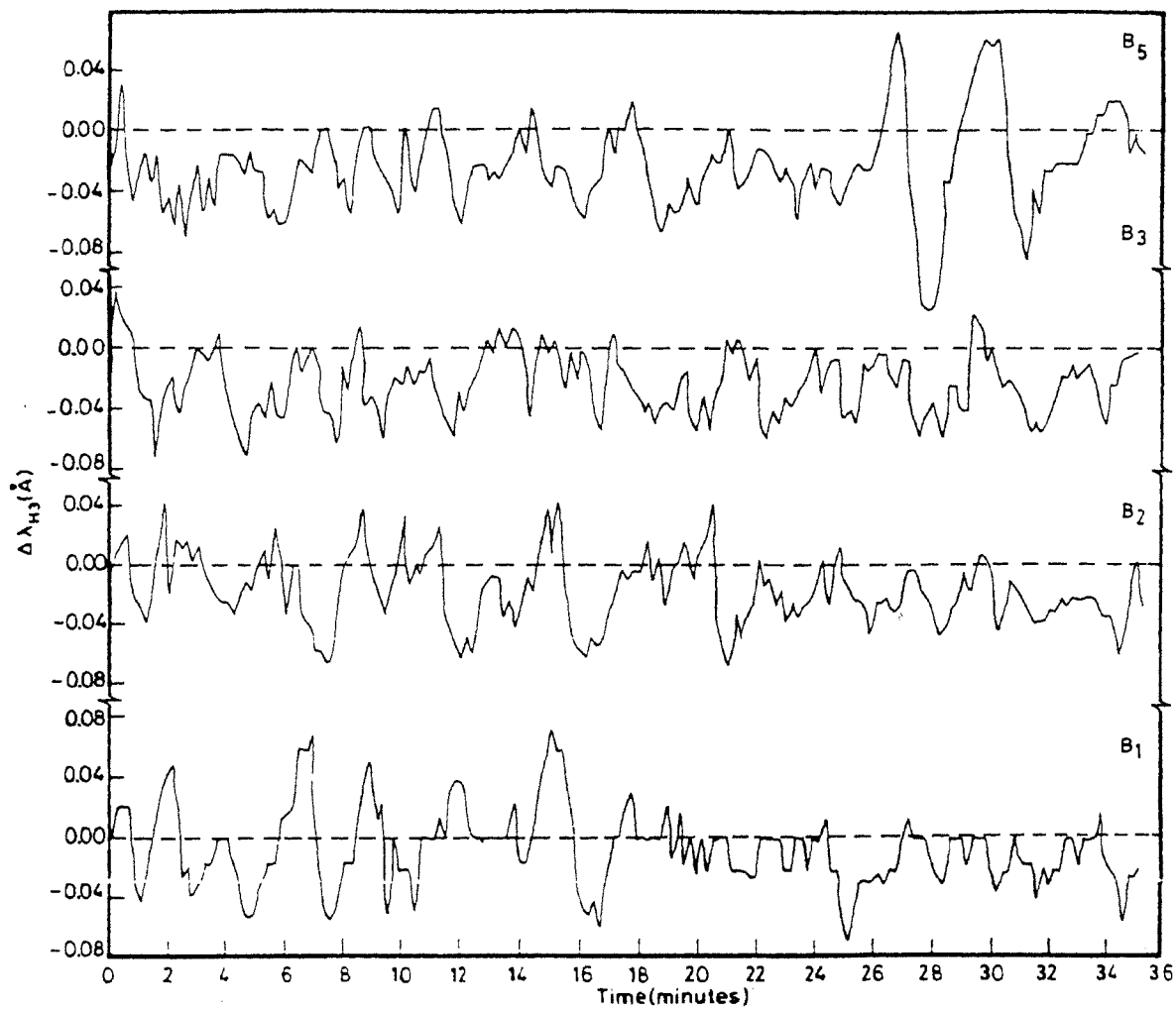
Fig. III.8 Temporal variation in the Doppler shift of H_3 ($\Delta\lambda_{H3}$) absorption core for Class I bright points. The 190 sec oscillations are seen in all the bright points.

90
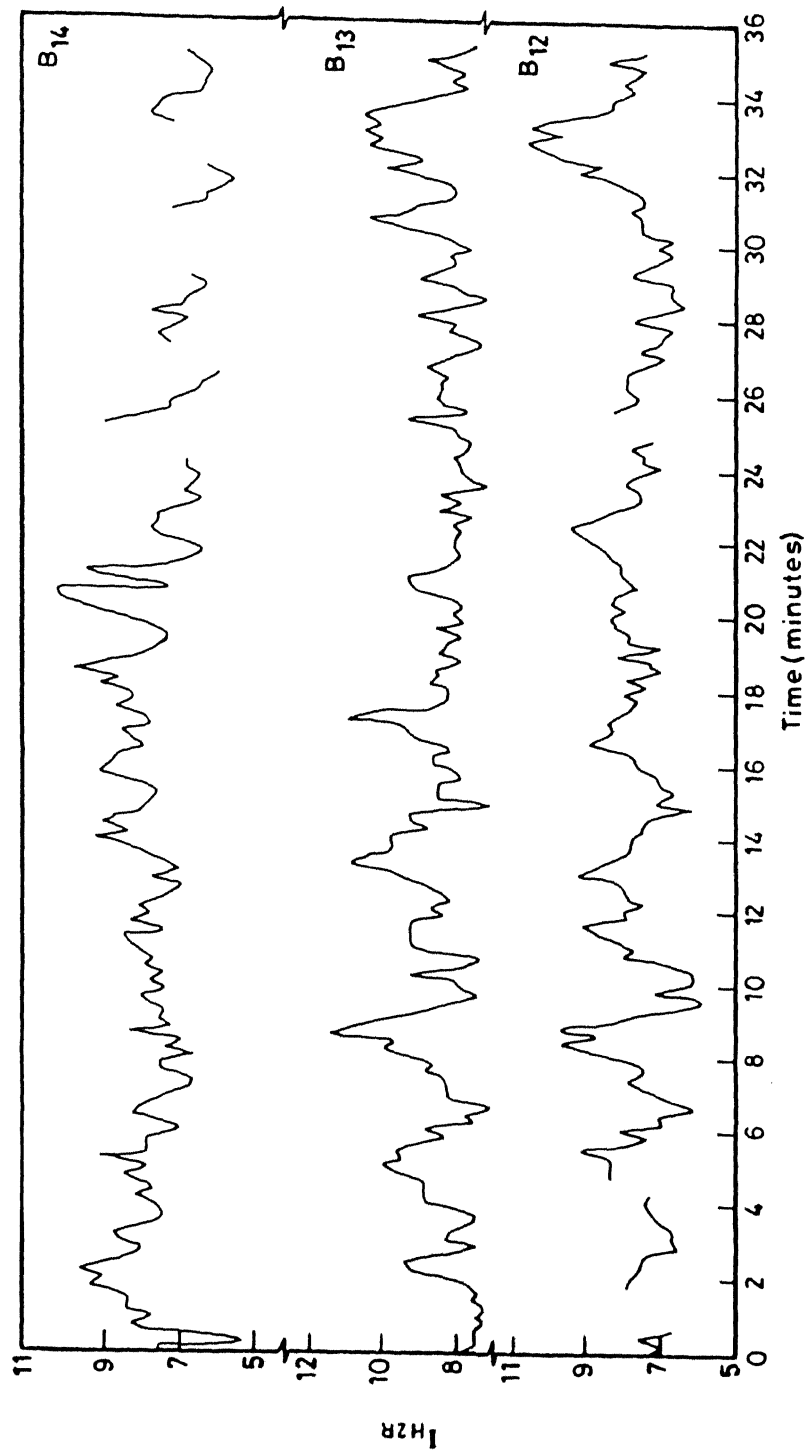
Fig.III.9 Temporal variation in I_{H2R} of Class II bright points. This is identical to the I_{H2V} plot except for the amplitudes.
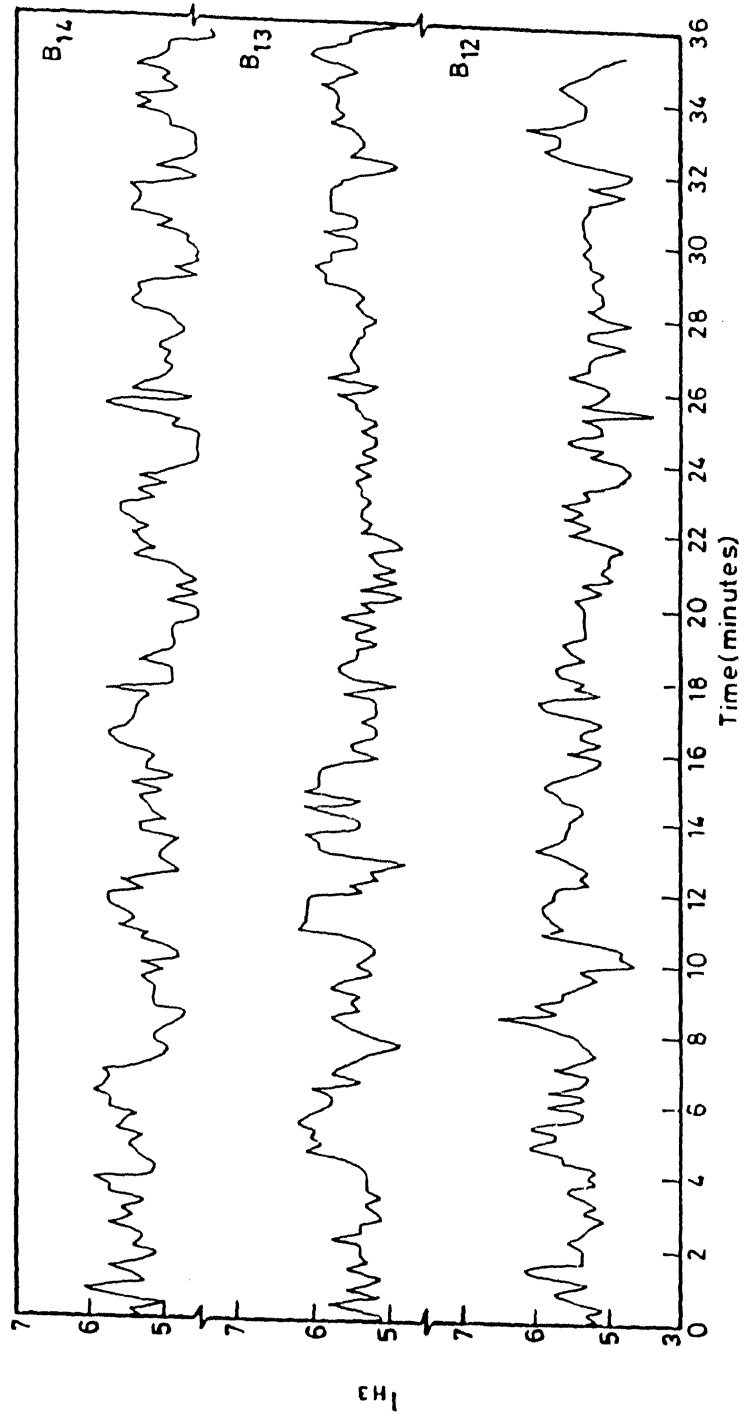
Fig.III.10 Temporal behaviour of I_{H3} of Class II bright points.
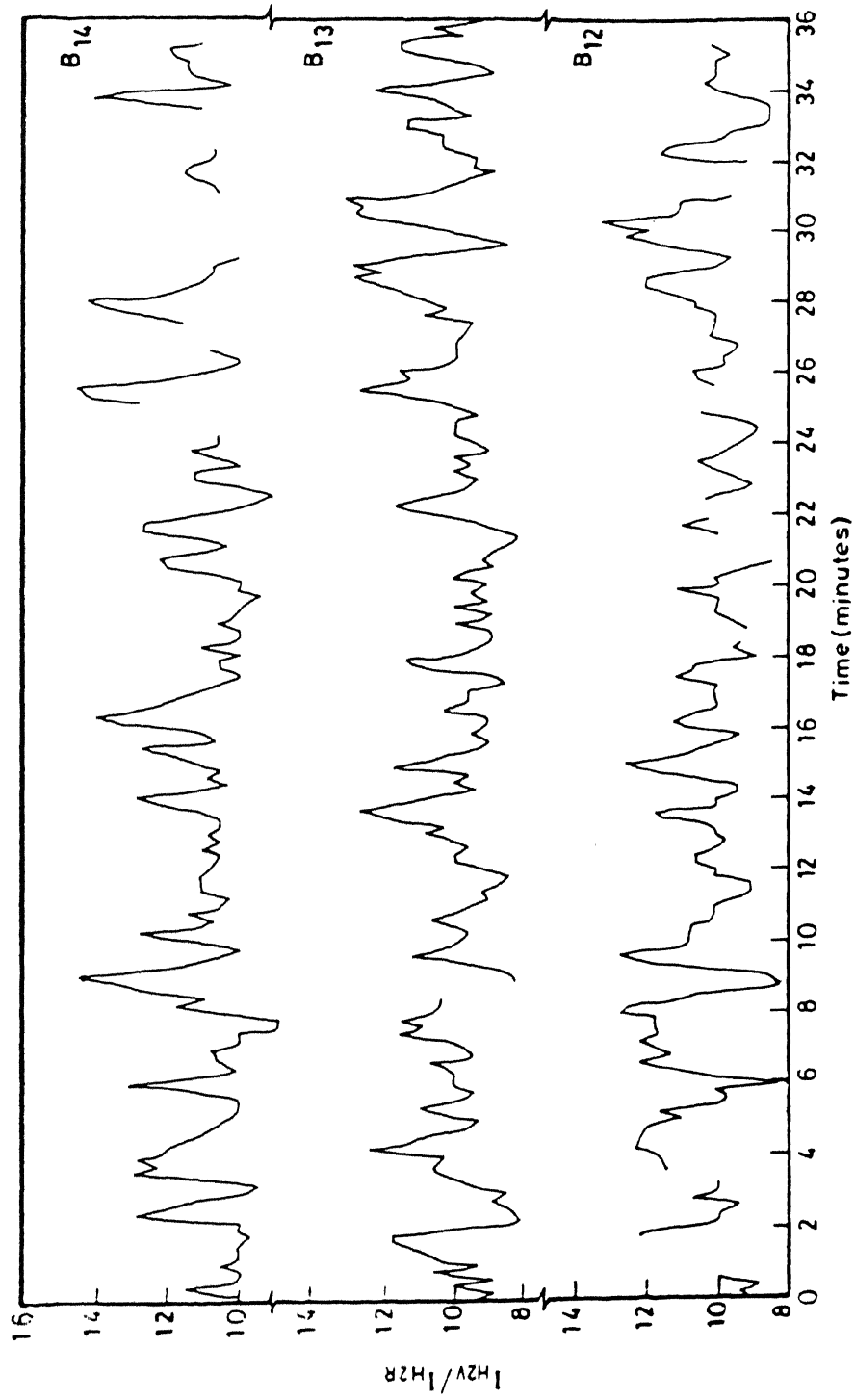
Fig.III.11 Temporal behaviour of I_{H2V}/I_{H2R} of Class II bright points. The 190 sec period of oscillation in all the bright points.

93
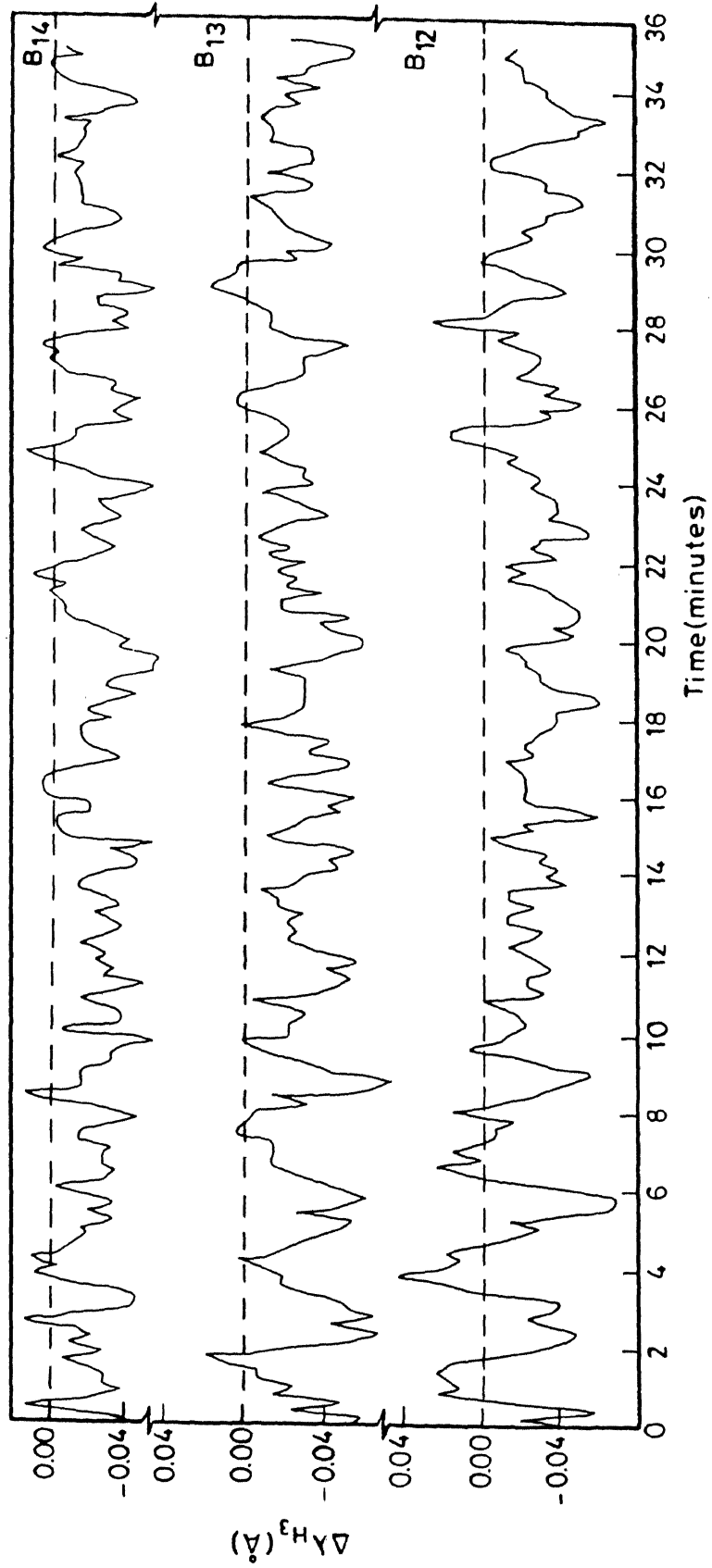
Fig.III.12 Temporal behaviour of Doppler shift of H_3 absorption core of Class II bright points.
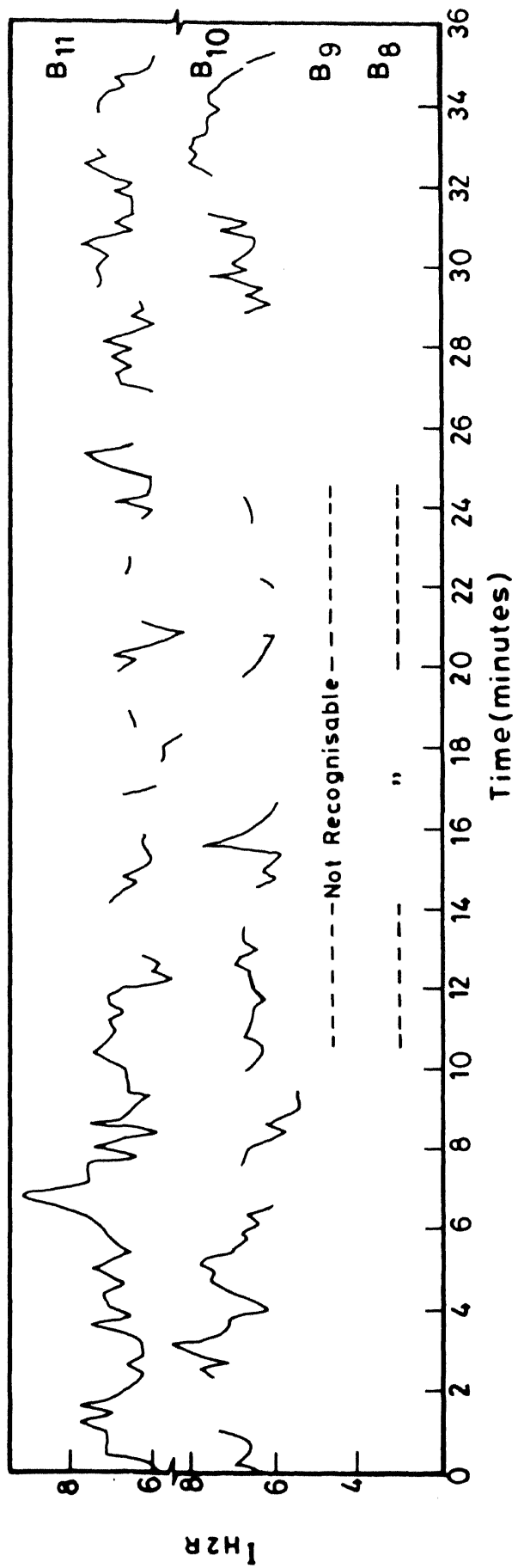
Fig.III.13 Temporal variation of I_{H2R} of Class III bright points. The bright points B_8 and B_9 does not show any intensity enhancements. The break in the curve shows that the H_{2R} is not recognisable in the profile at that particular time of evolution.
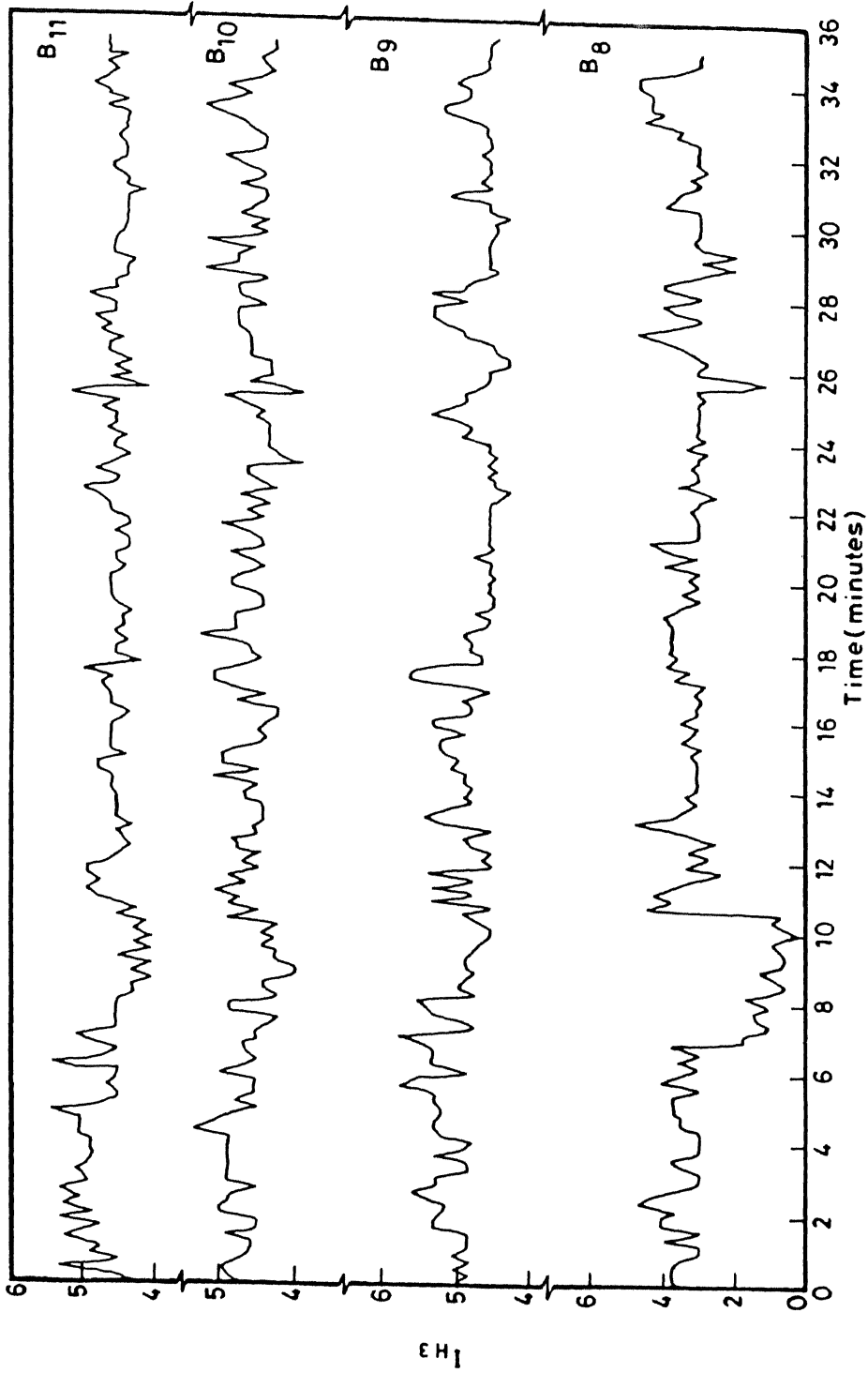
Fig.III.14 Temporal variation of I_{H3} of Class III bright points which show 190 sec period of oscillation.
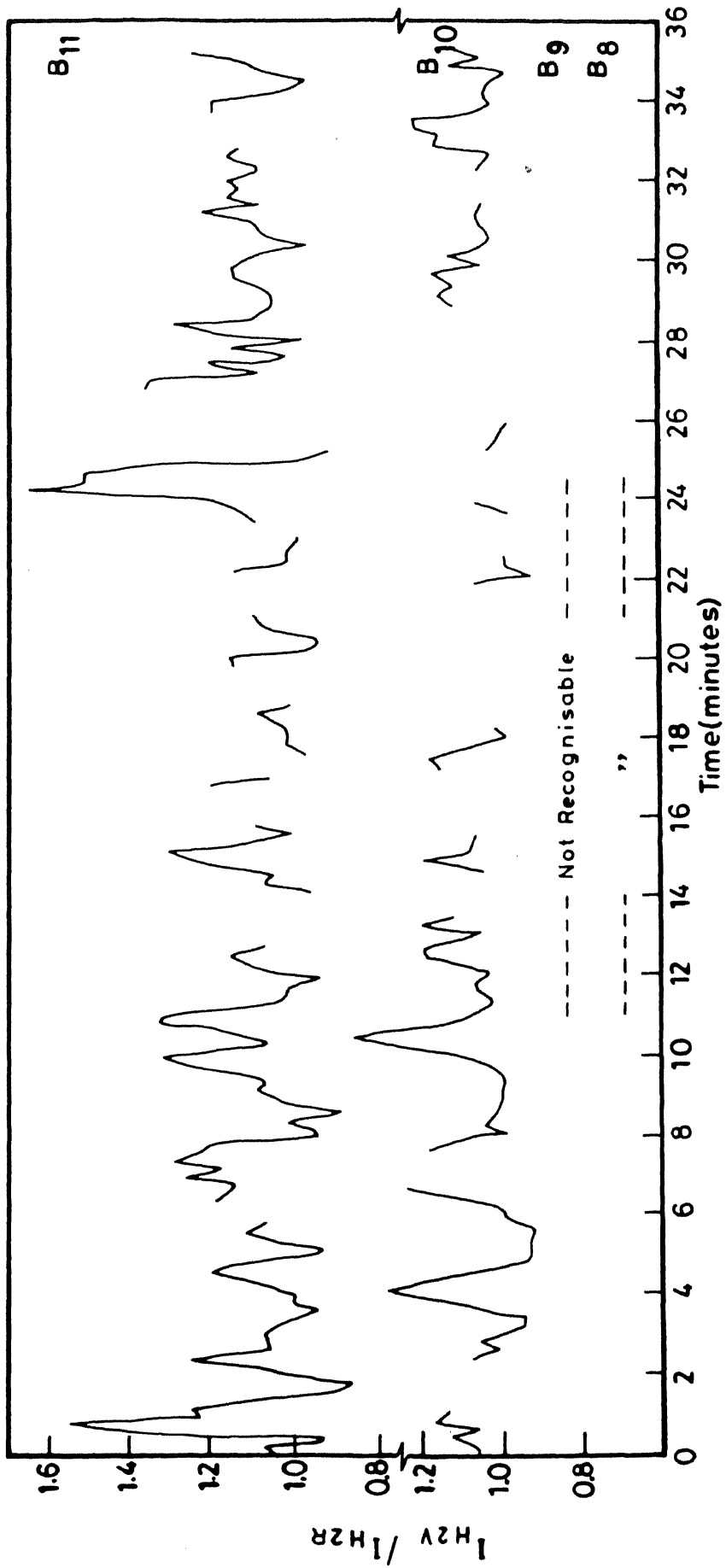
Fig.III.15 Temporal variation of I_{H2V}/I_{H2R} of Class III bright points. Since the H_{2R} is not recognisable in the bright points B_8 and B_9, the ratio is not worked out.
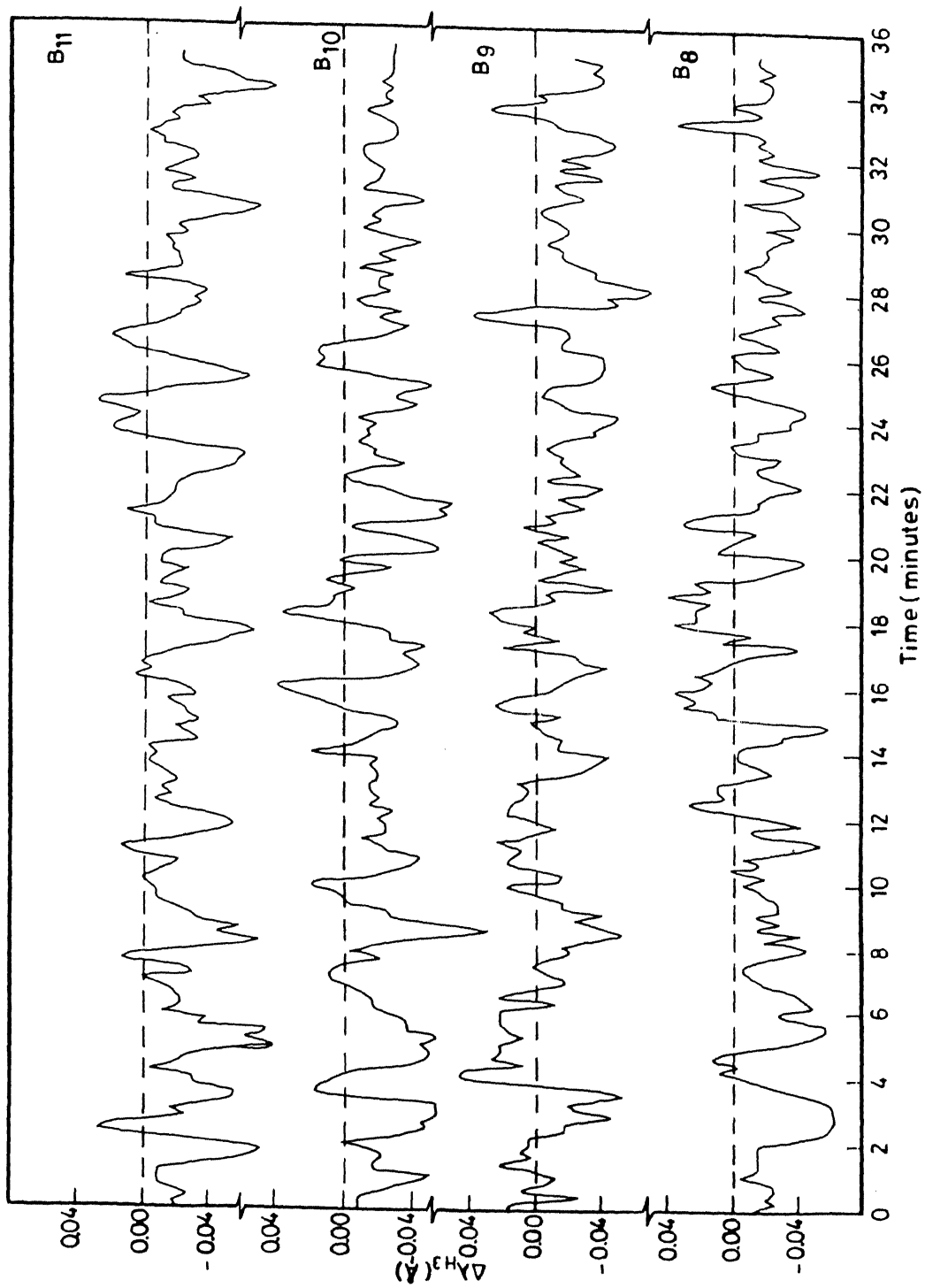
Fig.III.16   Temporal variation of $\Delta\lambda_{H3}$ of Class III bright points.